โครงสร้างของแบริออนในแบบจำลองควาร์กเชิงไคแรลเพอร์เทอร์เบชัน

นายชูหยาง หลิว

STRUCTURE OF BARYONS IN

PERTURBATIVE CHIRAL QUARK MODEL

Xuyang Liu

A Thesis Submitted in Partial Fulfillment of the Requirements for the

Degree of Doctor of Philosophy in Physics

Suranaree University of Technology

Academic Year 2013

STRUCTURE OF BARYONS IN

PERTURBATIVE CHIRAL QUARK MODEL

Suranaree University of Technology has approved this thesis submitted in partial fulfillment of the requirements for the Degree of Doctor of Philosophy.

Thesis Examining Committee

_____

(Assoc. Prof. Dr. Puangratana Pairor)

Chairperson

_____

(Prof. Dr. Yupeng Yan)

Member (Thesis Advisor)

_____

(Dr. Khanchai Khosonthongkee)

Member

_____

(Dr. Kem Pumsa-ard)

Member

_____

(Dr. Sorakrai Srisuphaphon)

Member

_____

(Dr. Ayut Limphirat)

Member

_____   _____

(Prof. Dr. Sukit Limpijumnong)   (Assoc. Prof. Dr. Prapun Manyum)

Vice Rector for Academic Affairs   Dean of Institute of Science

ชูหยาง หลิว : โครงสร้างของแบริออนในแบบจำลองควาร์กเชิงไคแรลเพอร์เทอร์เบชัน
(STRUCTURE OF BARYONS IN PERTURBATIVE CHIRAL QUARK MODEL)
อาจารย์ที่ปรึกษา : ศาสตราจารย์ ดร.ยูเป็ง แยน, 90 หน้า

แบบจำลองควาร์กเชิงไคแรลเพอร์เทอร์เบชันได้ถูกนำมาใช้เพื่อศึกษาคุณสมบัติอิเล็กโทร
วีค ของแบริออนชุดแปด โดยแบริออนถูกพิจารณาว่าเป็นสถานะกักกันของเวเลนซ์ควาร์กเชิง
สัมพัทธภาพจำนวนสามควาร์ก ในขณะที่กลุ่มหมอกของสเกลาร์มีซอนเทียมถูกพิจารณาว่าเป็น
ทะเลของควาร์กที่ถูกกระตุ้นซึ่งถูกเพิ่มขึ้นเพื่อให้เป็นไปตามข้อกำหนดของความสมมาตรเชิง
ไคแรลแบบจำลองซิกมาแบบไม่เชิงเส้นในแบบจำลองควาร์กเชิงไคแรลเพอร์เทอร์เบชันประสบ
ผลสำเร็จในการใช้อธิบายอันตรกิริยาระหว่าง ควาร์กและมีซอน เพื่อที่จะปรับปรุงแบบจำลองค
วาร์กเชิงไคแรลเพอร์เทอร์เบชัน ฟังก์ชันคลื่นของควาร์กเชิงสัมพัทธภาพได้ถูกขยายภายในฐาน
หลักสมบูรณ์ของฟังก์ชันสเตอร์เมียน และสัมประสิทธิ์การขยายสามารถคำนวณได้จากการเทียบผล
ที่ได้เชิงทฤษฎีของฟอร์มแฟกเตอร์เชิงประจุของโปรตอนเทียบกับผลการทดลอง จากนั้นทำการ
ประยุกต์แบบจำลองควาร์กเชิงไคแรลเพอร์เทอร์เบชันด้วยฟังก์ชันคลื่นของควาร์กที่ถูกกำหนดไว้
ล่วงหน้า ในการศึกษาฟอร์มแฟกเตอร์เชิงแกน และ ฟอร์มแฟกเตอร์เชิงแม่เหล็กไฟฟ้าของแบริออน
ชุดแปด เช่นเดียวกับการคำนวณค่าโมเมนต์แม่เหล็ก รัศมีประจุ รัศมีแม่เหล็ก และประจุเชิงแกน ผล
การคำนวณสรุปได้ว่าแบบจำลองควาร์กเชิงไคแรลเพอร์เทอร์เบชัน บนพื้นฐานของการกำหนด
ฟังก์ชันคลื่นของควาร์กไว้ล่วงหน้า ได้ผลที่สอดคล้องเป็นอย่างดีกับข้อมูลที่ได้จากการทดลอง

สาขาวิชาฟิสิกส์   ลายมือชื่อนักศึกษา_____

ปีการศึกษา 2556   ลายมือชื่ออาจารย์ที่ปรึกษา_____

                                          ลายมือชื่ออาจารย์ที่ปรึกษาร่วม_____

XUYANG LIU : STRUCTURE OF BARYONS IN PERTURBATIVE
CHIRAL QUARK MODEL. THESIS ADVISOR : PROF.
YUPENG YAN, Ph.D. 90 PP.

PCQM/FORM FACTORS/STURMIAN FUNCTIONS/OCTET BARYONS

The perturbative chiral quark model (PCQM) is used to study the electroweak properties of octet baryons, where baryons are considered as the bound states of three relativistic valence quarks while a cloud of pseudoscalar mesons, as the sea-quark excitations, is introduced for chiral symmetry requirements. The interactions between quarks and mesons are achieved by the nonlinear σ model in the PCQM. To improve the PCQM, the relativistic quark wave function is expanded in the complete basis of Sturmian functions and the expansion coefficients are extracted by fitting the theoretical results of the proton charge form factor to experimental data. We apply the PCQM with the predetermined quark wave function to study the electromagnetic and axial form factors of octet baryons as well as magnetic moments, charge and magnetic radii and axial charge. It is concluded that the PCQM results, based on the predetermined quark wave function, are in good agreement with experimental data.

School of Physics	Student's Signature _____
Academic Year 2013	Advisor's Signature _____
	Co-Advisor's Signature _____

ACKNOWLEDGEMENTS

CONTENTS

CONTENTS (Continued)

CONTENTS (Continued)

LIST OF TABLES

LIST OF FIGURES

LIST OF FIGURES (Continued)
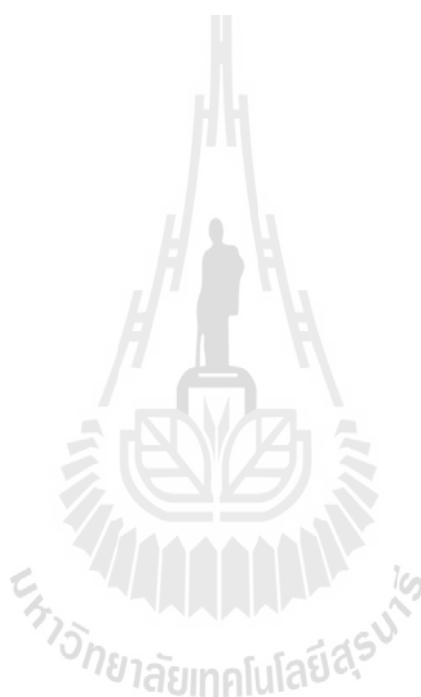
CHAPTER I

INTRODUCTION

Form factors play an extremely important role in hadron physics since they contain the information of the structure of hadrons, in particular their shape and size. In addition, form factors describe the distributions of charge and current in momentum space, which are intimately related to the internal structure of hadrons: the constituents of hadron, their interaction and their wave functions. Therefore, form factors are also significant touchstones for any model in hadron physics. Among all form factors, the nucleon electromagnetic and axial form factors have received much attention since they supply necessary information on the electroweak nucleon structure, and also help us understand electromagnetic and weak interactions. Until very recently, the nucleon electromagnetic and axial form factors have been measured experimentally with high precision.

Experimentally, the proton charge $G_E^p(Q^2)$ and magnetic $G_M^p(Q^2)$ form factors have been measured directly in the unpolarized ep elastic scattering using the Rosenbluth separation technique (Rosenbluth, 1950). Experimental data from such measurements were in high precision for $G_E^p(Q^2)$ with the squared momentum transfer $Q^2 \in [0.01, 2]$ GeV^2 (Berger et al., 1971; Price et al., 1971; Hanson et al., 1973; Bartel et al., 1973; Borkowski et al., 1974; Murphy et al., 1974; Borkowski et al., 1975; Andivahis et al., 1994; Walker et al., 1994) and $G_M^p(Q^2)$ for $Q^2 \in [0.1, 30]$ GeV^2 (Berger et al., 1971; Price et al., 1971; Hanson et al., 1973; Bartel et al., 1973; Borkowski et al., 1974; Borkowski et al., 1975; Arnold et al., 1986; Bosted et al., 1992; Andivahis et al., 1994; Walker et al., 1994). However,

the uncertainties on $G_E^p(Q^2)$ grow rapidly as the squared momentum transfer Q^2 increases. More precise data on the ratio of $G_E^p(Q^2)/G_M^p(Q^2)$ were extracted by the polarizations of the beam electron and either the proton target $\vec{p}(\vec{e}, e'p)$ (Milbrath et al., 1998; Gayou et al., 2002; Ron et al., 2011; Zhan et al., 2011) or the scattered proton $p(\vec{e}, e'\vec{p})$ (Jones et al., 2006; Crawford et al., 2007), in which the uncertainties are much smaller than those from unpolarization measurements. The data obtained from polarization measurements clearly show that the ratio of $G_E^p(Q^2)/G_M^p(Q^2)$ decreases linearly with increasing the squared momentum transfer Q^2.

Owing to the lack of free neutron, the data on the neutron charge $G_E^n(Q^2)$ (Platchkov et al., 1990) and magnetic $G_M^n(Q^2)$ (Anklin et al., 1994; Anklin et al., 1998; Kubon et al., 2002; Lachniet et al., 2009) form factors were obtained from quasi-elastic scattering off the deuteron. As in the case of proton electromagnetic form factors, the polarized measurement technique was applied to extract more accurate data on the ratio of $G_E^n(Q^2)/G_M^n(Q^2)$ from scattering polarized electrons on polarized ^{3}He (Herberg et al., 1999; Zhu et al., 2001; Warren et al., 2004; Glazier et al., 2005; Plaster et al., 2006), although experimental data of $G_E^n(Q^2)$ is still small and less precise in general.

For the axial form factor of the nucleon, two methods are mainly applied, namely (anti)neutrino scattering off protons (Ahrens et al., 1987) or nuclei (Kustom et al., 1969) and charged pion electroproduction (Amaldi et al., 1970; Nambu and Yoshimura, 1970; Amaldi et al., 1972; Bloom et al., 1973; Brauel et al., 1973; Read, 1974; Guerra et al., 1976; Esaulov et al., 1978). For more details on the nucleon electromagnetic and axial form factors, we refer to Refs. (Arrington et al., 2007; Bernard et al., 2002).

Except for the nucleon N, there is no direct experimental data for light

hyperons (Σ, Λ and Ξ) electromagnetic and axial form factors. However, the magnetic moments and axial charge of the octet baryons (the electromagnetic and axial form factors at zero recoil) have been measured experimentally (Beringer et al., 2012) and evaluated in Lattice QCD (Erkol et al., 2010). Recently, the charge radius of the Σ^- has also been determined (Eschrich et al., 2001). These data supply the primary information of the light hyperon form factors at low momentum transfer and inspire theoretical studies on octet baryon form factors.

It is widely believed that Quantum Chromodynamics (QCD) is the right dynamics of strong interaction and has been extremely well tested in the high-energy region, i.e., in the perturbative QCD regime. In the confinement regime where the momentum transfer is low, however, the strong coupling constant α_s is large (Beringer et al., 2012) and multi-loop perturbative calculations are needed. Therefore, traditional perturbative approaches may not be applicable in solving QCD confinement problems. Due to the fact that QCD may be is non-perturbative at low energy, various approaches were employed to study properties of baryons such as:

- Lattice QCD (Wilson, 1974): Lattice QCD is based on the first principles of QCD to solve non-perturbative QCD problems. In lattice QCD, quark fields are located at discrete space and time lattice sites, while gluon fields link the neighboring sites. The continuum QCD is recovered when the spacing of lattice sites is reduced to zero. Lattice QCD has already made successful contact with many experiments, and it has also given some predictions, in which lattice QCD calculations fully depend on computer power.

- Chiral perturbation theory (ChPT) (Scherer, 2003): The ChPT is an effective field theory at hadronic level. In the ChPT, the Lagrangian is constructed with all the physical symmetries, including the chiral symmetry.

The parameters of the Lagrangian can be determined by fitting theoretical results to experimental data. The ChPT is a powerful tool for nuclear physics, even for hadron physics at the low energy regime, but it is not suitable for revealing the internal structure of hadrons at the quark level.

- Effective quark model: Models are based on constituent (valence) quarks, for example, three quarks for a baryon, two (quark and antiquark) for a meson. The gluonic degrees of freedom are usually replaced by effective interactions. In general, models are established with phenomenological assumptions, which lead to a variety of versions.

In this thesis, we focus on the perturbative chiral quark model (PCQM) (Lyubovitskij et al., 2001b; Lyubovitskij et al., 2001c; Lyubovitskij et al., 2002a) to study the octet baryon electromagnetic and axial form factors at the low energy region.

Historically, MIT bag model (Chodos et al., 1974a; Chodos et al., 1974b; DeGrand et al., 1975), proposed in 1974 by A. Chodos et al, provided a phenomenological description of quarks being confined inside hadrons. The basic idea of the model is to confine three relativistic massless quarks to a spherical cavity, the so-called "bag". Inside the bag, quarks are treated as non-interacting particles, which implies asymptotic freedom. The theoretical works in this model were in good agreement with experimental data. Unfortunately, the MIT bag model necessarily violated the chiral symmetry, which was considered to be one of the best symmetries of the strong interaction.

Subsequently, two types of quark models were developed through introducing the pion cloud to the MIT bag model for the sake of restoring the chiral symmetry. One was cloudy bag model (Théberge et al., 1980; Thomas et al., 1981; Thomas, 1984) which was extended to include the interaction of the confined quarks with the pion fields on the bag surface. The pion cloud was treated

perturbatively based on the MIT bag, and pionic effects generally improved the description of nucleon observables. Nevertheless, the cloudy bag model still adhered to "bag". Later, the other model named chiral quark model was developed where the rather unphysical sharp bag boundary was replaced by a finite surface thickness of the quark core. Chiral quark models (Chin, 1982; Oset et al., 1984; Gutsche and Robson, 1989) have played an important role in the description of low-energy nucleon physics. Confinement is introduced through a static quark potential of general form with adjustable parameters. The perturbative technique allows a fully quantized treatment of the pion field up to a given order in accuracy.

Perturbative chiral quark model(PCQM) (Lyubovitskij et al., 2001a; Lyubovitskij et al., 2001b; Lyubovitskij et al., 2001c; Lyubovitskij et al., 2002a; Lyubovitskij et al., 2002b; Pumsa-ard et al., 2003; Cheedket et al., 2004; Khosonthongkee et al., 2004; Faessler et al., 2008) as a further development of chiral quark models with a perturbative treatment of the pion cloud, is realized by relativistic quark wave functions and static potential for confinement as well as the chiral symmetry requirements. In the PCQM, baryons are considered as bound states of valence quarks surrounded by not only the pion cloud but also other pseudoscalar meson cloud, as imposed by chiral symmetry requirements. The interaction of quarks with the pseudoscalar octet mesons (π, K, and η-meson) is introduced on the basis of the nonlinear σ-model (Lyubovitskij et al., 2001b). The confinement of the quarks is achieved by a static potential, where the lorentz covariance is not implied. The PCQM is one of the effective approaches to study the structure and interactions of baryons in low-energy physics.

Compared to the previous similar models, the PCQM contains several new features: (i) generalization of the phenomenological confining potential, (ii) SU(3) extension of the chiral symmetry to include meson cloud contributions, (iii) con-

sistent formulation of perturbation theory both on the quark and baryon level by using renormalization techniques and by taking into account excited quark states in the meson loop diagrams, (iv) fulfillment of the constraints imposed by the chiral symmetry (low-energy theorems), and (v) possible consistency with the ChPT (Lyubovitskij et al., 2002a).

As an improvement to the PCQM, a manifestly Lorentz covariant approach (Faessler et al., 2005; Faessler et al., 2006a; Faessler et al., 2006b; Faessler et al., 2006c) is considered by Pumsa-ard et al. The Lorentz covariant quark model is motivated by the ChPT, where high order chiral corrections of p^4 are included and the quark operators are dressed by the chiral fields. In a similar way to the PCQM, the dressed quark operators are projected onto the baryonic level in order to obtain hadronic matrix elements. By adjusting Low Energy Constants, the physical observables are obtained. In Refs. (Faessler et al., 2005; Faessler et al., 2006c), electromagnetic form factors of nucleons are studied with including vector-meson contributions. Electromagnetic properties of hyperons and $N \to \Delta\gamma$ transition are investigated in Refs (Faessler et al., 2006a; Faessler et al., 2006b). The theoretical results are in good agreement with experimental data both at very low momentum transfer and high energies.

The PCQM has been applied to study low-energy meson-baryon scatterings (Lyubovitskij et al., 2001c), electromagnetic excitations of nucleon resonances (Pumsa-ard et al., 2003), nucleon polarizabilities (Dong et al., 2006) and neutron electric dipole form factor (Dib et al., 2006), etc. In Refs. (Lyubovitskij et al., 2001a; Cheedket et al., 2004; Faessler et al., 2008) and Ref. (Khosonthong-kee et al., 2004), electromagnetic form factors of the baryons and axial form factor of the nucleon are derived in the PCQM, and the theoretical results are in good agreement with experimental data only at very low momentum transfer. It is

noted that these works have employed a variational Gaussian ansatz for the quark wave function,

$$u_0(\vec{x}) = N_0 \exp\left(-\frac{\vec{x}^2}{2R^2}\right) \begin{pmatrix} 1 \\ i\rho\frac{\vec{\sigma}\cdot\vec{x}}{R} \end{pmatrix} \chi_s \chi_f \chi_c, \qquad (1.1)$$

where N_0 is a normalization constant; χ_s, χ_f and χ_c are the spin, flavor and color quark wave functions, respectively. R is the dimensional parameter and ρ is the dimensionless parameter. As mentioned before, the internal structure of hadrons dominates the form factors, and therefore we believe that it is the Gaussian-type wave function of baryons which leads to the theoretical predictions for the form factors of baryons consistent well with experimental data only at very low momentum transfer. In this work we attempt to extract a more reasonable quark wave functions in the PCQM. We expand the general quark wave function in a completed basis of Sturmian functions (Rotenberg, 1970) with expansion parameters determined by fitting the theoretical results of proton charge form factor to experimental data. The electromagnetic and axial form factors of octet baryons are studied in the PCQM with the fitted quark wave function.

This thesis is organized as follows. In Chapter II, we describe the details of the PCQM and Sturmian completed basis. The theoretical expressions of electromagnetic form factors of octet baryons are given in Chapter III. We determine the quark wave function and derive numerical results for the electromagnetic form factors of octet baryons in this chapter. In Chapter IV, the axial form factors of octet baryons are presented in the PCQM with the quark wave function fitted in Chapter III. Finally, conclusions and discussions are given in Chapter V.

CHAPTER II

PERTURBATIVE CHIRAL QUARK MODEL

The Perturbative Chiral Quark Model (PCQM) employed in this thesis is a relativistic quark model, including relativistic quark wave functions, confinement and chiral symmetry requirements. The valence quarks move in a self-consistent field (static potential) $V_{\text{eff}}(r) = S(r) + \gamma^0 V(r)$, with $r = |\vec{x}|$, providing confinement, which are supplemented by a cloud of Goldstone bosons (π, K, and η). Goldstone fields are treated as small fluctuations around the three-quark (3q) core. The effective of the PCQM can be given by

$$\mathcal{L}_{\text{eff}}(x) = \mathcal{L}_{\text{inv}}(x) + \mathcal{L}_{\chi\text{SB}}(x), \tag{2.1}$$

with $\mathcal{L}_{\text{inv}}(x)$ being the chiral invariant Lagrangian

$$\mathcal{L}_{\text{inv}}(x) = \bar{\psi}(x)\left\{ i\slashed{\partial} - \gamma^0 V(r) - S(r)\left[\frac{U + U^\dagger}{2} + \gamma^5 \frac{U - U^\dagger}{2} \right] \right\}\psi(x)$$

$$+ \frac{F^2}{4}\text{Tr}\left[\partial_\mu U \partial^\mu U^\dagger \right], \tag{2.2}$$

and $\mathcal{L}_{\chi\text{SB}}(x)$ breaking the chiral symmetry explicitly

$$\mathcal{L}_{\chi\text{SB}}(x) = -\bar{\psi}(x)\mathcal{M}\psi(x) - \frac{B}{2}\text{Tr}\left[\hat{\Phi}^2(x)\mathcal{M} \right], \tag{2.3}$$

where $\psi(x)$ is the triplet of the u, d, and s quark fields taking the form

$$\psi(x) = \begin{pmatrix} u(x) \\ d(x) \\ s(x) \end{pmatrix}, \tag{2.4}$$

and the eight Goldstone bosons are most conveniently summarized in the matrix $U \in SU(3)$ represented by the exponential parameterization

$$U = \exp\left[i\frac{\hat{\Phi}}{F}\right] \simeq 1 + i\frac{\hat{\Phi}}{F} + \frac{1}{2}\left(i\frac{\hat{\Phi}}{F}\right)^2 + \cdots . \tag{2.5}$$

In the above equations $\hat{\Phi}$ is the octet matrix of pseudoscalar mesons

$$\hat{\Phi} = \sum_{i=1}^{8} \Phi_i \lambda_i = \begin{pmatrix} \pi^0 + \frac{1}{\sqrt{3}}\eta & \sqrt{2}\pi^+ & \sqrt{2}K^+ \\ \sqrt{2}\pi^- & -\pi^0 + \frac{1}{\sqrt{3}}\eta & \sqrt{2}K^0 \\ \sqrt{2}K^- & \sqrt{2}\bar{K}^0 & -\frac{2}{\sqrt{3}}\eta \end{pmatrix}. \tag{2.6}$$

$\mathcal{M} = \text{diag}\{m_u, m_d, m_s\}$ is the mass matrix of current quarks, restricted to the isospin symmetry limit $m_u = m_d = \hat{m}$. F and B are respectively the pion decay constant in the chiral limit and the quark condensate constant. In our calculation, we employ the following set of QCD parameters: $\hat{m} = 7$ MeV, $m_s/\hat{m} = 25$, $F = 88$ MeV and $B = -\langle 0|\bar{u}u|0\rangle = -\langle 0|\bar{d}d|0\rangle = 1.4$ GeV. To the leading order of the chiral expansion, the masses of the pseudoscalar mesons take the values,

$$M_\pi^2 = 2\hat{m}B, \qquad M_K^2 = (\hat{m} + m_s)B, \qquad M_\eta^2 = \frac{2}{3}(\hat{m} + 2m_s)B. \tag{2.7}$$

Note that the masses in Equation (2.7) satisfy the "Gell-Mann-Oakes-Renner" relation and the "Gell-Mann-Okubo" relation as well

$$M_\pi^2 + 3M_\eta^2 = 4M_K^2. \tag{2.8}$$

With the unitary chiral rotation $\psi \to \exp\left[-i\gamma^5\hat{\Phi}/(2F)\right]\psi$, the Lagrangian in Equation (2.2) transforms into a Weinberg-type form $\mathcal{L}^W$ containing the axial-vector coupling and the Weinberg-Tomozawa term

$$\mathcal{L}^W(x) = \mathcal{L}_0(x) + \mathcal{L}_I^W(x) + o(\Phi_i^2), \tag{2.9}$$

where

$$\mathcal{L}_0(x) = \bar{\psi}(x)\big[i\slashed{\partial} - \gamma^0 V(r) - S(r)\big]\psi(x) - \frac{1}{2}\Phi_i(x)\big(\Box + M_\Phi^2\big)\Phi^i(x), \quad (2.10)$$

and

$$\mathcal{L}_I^W(x) = \frac{1}{2F}\partial_\mu\Phi_i(x)\bar{\psi}(x)\gamma^\mu\gamma^5\lambda^i\psi(x) + \frac{f_{ijk}}{4F^2}\Phi_i(x)\partial_\mu\Phi_j(x)\bar{\psi}(x)\gamma^\mu\lambda_k\psi(x)$$

$$(2.11)$$

is the quark-meson interaction Lagrangian, f_{ijk} are the totally antisymmetric structure constants of $SU(3)$, and $\Box = \partial^\mu\partial_\mu$.

We expand the quark field $\psi(x)$ on the basis of the potential eigenstates

$$\psi(x) = \sum_\alpha \left(b_\alpha u_\alpha(\vec{x})\, e^{-i\mathcal{E}_\alpha t} + d_\alpha^\dagger v_\alpha(\vec{x}) e^{i\mathcal{E}_\alpha t}\right), \quad (2.12)$$

where b_α and $d_\alpha^\dagger$ are the single quark annihilation and antiquark creation operators. In the above expansion $u_\alpha(\vec{x})$ and $v_\alpha(\vec{x})$ are respectively the single quark and antiquark wave functions and $\mathcal{E}_\alpha$ are the single quark/antiquark energy, which are derived from the Dirac equation

$$\Big[-i\gamma^0\vec{\gamma}\cdot\vec{\nabla} + \gamma^0 S(r) + V(r) - \mathcal{E}_\alpha\Big]u_\alpha(\vec{x}) = 0. \quad (2.13)$$

In previous works (Lyubovitskij et al., 2001a; Cheedket et al., 2004; Khoson-thongkee et al., 2004; Faessler et al., 2008), Gaussian ansatz is applied to the quark wave function, as shown in Equation (1.1). It is noted, however, that Gaussian-type quark wave function of baryons results in the theoretical predictions for the form factors of baryons consistent well with experimental data at very low momentum transfer Q^2. In principle, one could solve Equation (2.13) for a certain potential numerically or by expanding the quark wave function in any complete

basis. In this work, we study the form factors of baryons by employing a properly adapted numerical method based on Sturmian functions.

The ground state quark wave function $u_0(\vec{x})$ may, in general, be expressed as

$$u_0(\vec{x}) = \begin{pmatrix} g(r) \\ i\vec{\sigma} \cdot \hat{x} f(r) \end{pmatrix} \chi_s \chi_f \chi_c, \tag{2.14}$$

where χ_s, χ_f and χ_c are the spin, flavor and color quark wave functions, respectively. In our calculations, the quark wave function is projected from the quark level to the baryon level, and the wave functions of octet baryons with the SU(3) flavor, SU(2) spin and SU(3) color symmetries take the form as in (Close, 1979). The radial quark wave functions $g(r)$ and $f(r)$, the upper and the lower components in the ground state, are expanded in the complete set of the Sturmian functions $S_{nl}(r)$

$$g(r) = \sum_n A_n \frac{S_{n0}(r)}{r}, \tag{2.15}$$

$$f(r) = r \sum_n B_n \frac{S_{n0}(r)}{r}, \tag{2.16}$$

where

$$S_{nl}(r) = \left[\frac{n!}{(n+2l+1)!} \right]^{\frac{1}{2}} (2br)^{l+1} e^{-br} L_n^{2l+1}(2br), \tag{2.17}$$

and $L_n^{2l+1}(x)$ are Laguerre polynomials. The details of Sturmian functions are given in Appendix A. The expansion coefficients A_n and B_n, length parameter b of Sturmian functions are determined by fitting theoretical results of proton charge form factor to experimental data in Chapter III.

The calculation technique in the PCQM is based on the Gell-Mann and Low theorem (see Appendix B), in which the expectation value of an operator $\hat{O}$

can be calculated from

$$\langle \hat{O} \rangle = {}^{B}\langle \phi_0 | \sum_{n=0}^{\infty} \frac{i^n}{n!} \int d^4 x_1 \cdots \int d^4 x_n T[\mathcal{L}_I^W(x_1) \cdots \mathcal{L}_I^W(x_n) \hat{O}] |\phi_0\rangle_c^B, \qquad (2.18)$$

where the state vector $|\phi_0\rangle^B$ corresponds to the unperturbed three-quark states projected onto the respective baryon states, which are constructed in the framework of the $SU(6)$ spin-flavor and $SU(3)$ color symmetry. The subscript c in Equation (2.18) refers to contributions from connected graphs only. $\mathcal{L}_I^W(x)$ is the quark-meson interaction Lagrangian as given in Equation (2.11).

By applying Wick's theorem and appropriate propagators for quarks and mesons, Equation (2.18) can be evaluated in a straightforward manner. In our work the quark propagator $iG_\psi(x, y)$ is given by

$$
\begin{aligned}
iG_\psi(x, y) &= \langle \phi_0 | T\{\psi(x)\bar{\psi}(y)\} | \phi_0 \rangle \\
&= u_\alpha(\vec{x})\bar{u}_\alpha(\vec{y}) \exp[-i\mathcal{E}_\alpha(x_0 - y_0)]\theta(x_0 - y_0). \qquad (2.19)
\end{aligned}
$$

For the meson field, however, we use the free Feynman propagator

$$
\begin{aligned}
i\Delta_{ij}(x - y) &= \langle 0 | T\{\Phi_i(x)\Phi_j(y)\} | 0 \rangle \\
&= \delta_{ij} \int \frac{d^4 k}{(2\pi)^4 i} \frac{\exp[-ik(x - y)]}{M_\Phi^2 - k^2 - i\epsilon}, \qquad (2.20)
\end{aligned}
$$

where M_Φ is the meson mass.

CHAPTER III

ELECTROMAGNETIC FORM FACTORS

AND MODEL PARAMETERS

3.1 Electromagnetic Form Factors of Octet Baryons

In the framework of the PCQM, the charge and magnetic form factors of octet baryons in the Breit frame are defined by

$$
\chi^{\dagger}_{B_{s'}} \chi_{B_s} G_E^B(Q^2) = {}^B\langle\phi_0| \sum_{n=0}^{n} \frac{i^n}{n!} \int \delta(t) d^4x d^4x_1 \cdots d^4x_n \mathrm{e}^{-iq\cdot x}
$$
$$
\times T[\mathcal{L}_I^W(x_1)\cdots\mathcal{L}_I^W(x_n)j^0(x)]|\phi_0\rangle_c^B, \qquad (3.1)
$$

$$
\chi^{\dagger}_{B_{s'}} \frac{i\vec{\sigma}\times\vec{q}}{m_B+m_{B'}} \chi_{B_s} G_M^B(Q^2) = {}^B\langle\phi_0| \sum_{n=0}^{n} \frac{i^n}{n!} \int \delta(t) d^4x d^4x_1 \cdots d^4x_n e^{-iq\cdot x}
$$
$$
\times T[\mathcal{L}_I^W(x_1)\cdots\mathcal{L}_I^W(x_n)\vec{j}(x)]|\phi_0\rangle_c^B. \qquad (3.2)
$$

Here, $G_E^B(Q^2)$ and $G_M^B(Q^2)$ are the charge and magnetic form factors of octet baryons with the space-like squared momentum transfer Q^2, which is carried out by the electromagnetic current. In the Breit frame, the initial momentum of the baryons is $p_i = (E, -\vec{q}/2)$, the final momentum is $p_f = (E, \vec{q}/2)$, and the four-momentum of the photon is $q = (0, \vec{q})$. Thus, $Q^2 = -q^2 = \vec{q}^2$. m_B is the mass of baryons. χ_{B_s} and $\chi^{\dagger}_{B_{s'}}$ are the baryon spin wave functions in the initial and final states, $\vec{\sigma}$ is the baryon spin operator, $\mathcal{L}_I^W(x)$ is the quark-meson interaction Lagrangian in Equation (2.11), and $j^\mu(x)$ is the electromagnetic current

$$
j^\mu = j_\psi^\mu + j_\Phi^\mu + j_{\psi\Phi}^\mu + \delta j_\psi^\mu, \qquad (3.3)
$$

which contains the quark current $j_\psi^\mu(x)$, the charged pseudoscalar mesons current $j_\Phi^\mu(x)$, the quark-meson coupling current $j_{\psi\Phi}^\mu(x)$, and $\delta j_\psi^\mu(x)$, a current arising from the counterterm. The currents in the above equation take the forms,

$$j_\psi^\mu = \bar{\psi}\gamma^\mu Q\psi = \frac{2}{3}\bar{u}\gamma^\mu u - \frac{1}{3}\bar{d}\gamma^\mu d - \frac{1}{3}\bar{s}\gamma^\mu s, \tag{3.4}$$

$$j_\Phi^\mu = \left[f_{3ij} + \frac{f_{8ij}}{\sqrt{3}}\right]\Phi_i\partial^\mu\Phi_j$$

$$= \left[\pi^-i\partial^\mu\pi^+ - \pi^+i\partial^\mu\pi^- + K^-i\partial^\mu K^+ - K^+i\partial^\mu K^-\right], \tag{3.5}$$

$$j_{\psi\Phi}^\mu = \left[f_{3ij} + \frac{f_{8ij}}{\sqrt{3}}\right]\frac{\Phi_j}{2F}\bar{\psi}\gamma^\mu\gamma^5\lambda_i\psi, \tag{3.6}$$

$$\delta j_\psi^\mu = \bar{\psi}\big(Z - 1\big)\gamma^\mu Q\psi$$

$$= \frac{1}{3}\Big[2(\hat{Z} - 1)\bar{u}\gamma^\mu u - (\hat{Z} - 1)\bar{d}\gamma^\mu d - (\hat{Z}_s - 1)\bar{s}\gamma^\mu s\Big], \tag{3.7}$$

where Q is the quark charge matrix $Q = \text{diag}\{2/3, -1/3, -1/3\}$, and the renormalization constants $\hat{Z}$ and $\hat{Z}_s$ are defined as

$$\hat{Z} = 1 - \frac{3}{4(2\pi F)^2}\int_0^\infty dk k^4 F_{II}^2(k)\left[\frac{1}{\omega_\pi^3(k^2)} + \frac{2}{3\omega_K^3(k^2)} + \frac{1}{9\omega_\eta^3(k^2)}\right], \tag{3.8}$$

$$\hat{Z}_s = 1 - \frac{1}{(2\pi F)^2}\int_0^\infty dk k^4 F_{II}^2(k)\left[\frac{1}{\omega_K^3(k^2)} + \frac{1}{3\omega_\eta^3(k^2)}\right], \tag{3.9}$$

with $\omega_\Phi(k^2) = \sqrt{M_\Phi^2 + k^2}$ and the vertex function $F_{II}(k)$ for the $qq\Phi$ system taking the form

$$F_{II}(k) = 2\pi\int_0^\infty dr\int_0^\pi d\theta r^2(g(r)^2 + f(r)^2\cos 2\theta)\sin\theta e^{ikr\cos\theta}. \tag{3.10}$$

In accordance with the interaction Lagrangian $\mathcal{L}_I^W(x)$ in Equation (2.11) and the electromagnetic current $j^\mu(x)$ in Equations (3.4)-(3.7), there are five Feynman diagrams, as shown in Figure 3.1, contributing to the electromagnetic
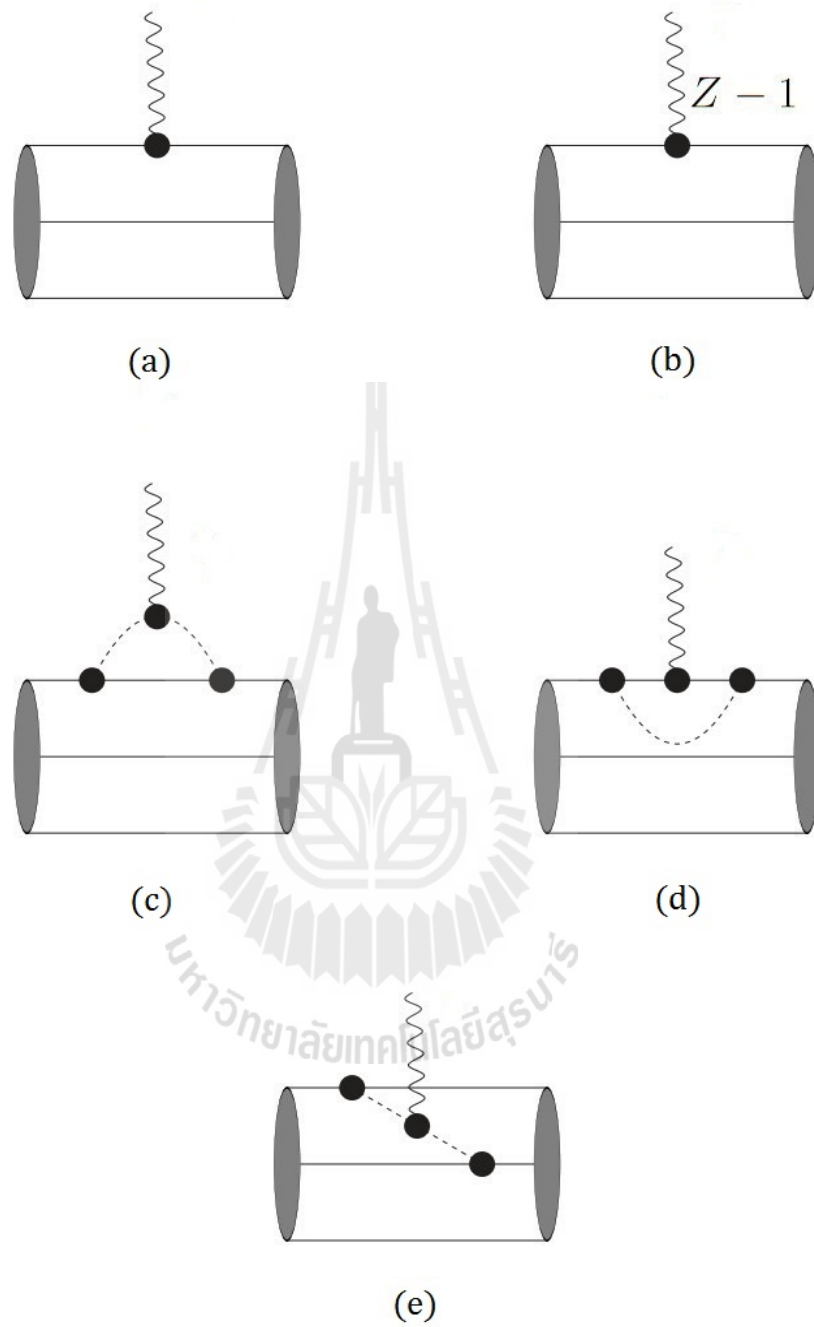
Figure 3.1 Diagrams contributing to the electromagnetic form factors: 3q-core leading order diagram (a), 3q-core counterterm diagram (b), meson cloud diagram (c), vertex correction diagram (d), and meson-in-flight diagram (e).

form factors to the one-loop order. Detailed calculations, as shown in Appendix C and Appendix D, lead to the contributions of these diagrams as follows:

(a) Three-quark core leading-order diagram (LO)

$$G_E^B(Q^2)\big|_{LO} = a_1^B G_E^p(Q^2)\big|_{LO}, \qquad (3.11)$$

$$G_M^B(Q^2)\big|_{LO} = b_1^B \frac{m_B}{m_N} G_M^p(Q^2)\big|_{LO}, \qquad (3.12)$$

where

$$G_E^p(Q^2)\big|_{LO} = 2\pi \int_0^\infty dr \int_0^\pi d\theta r^2 \sin\theta [g(r)^2 + f(r)^2] e^{iQr\cos\theta}, \qquad (3.13)$$

$$G_M^p(Q^2)\big|_{LO} = \frac{4\pi i m_N}{Q} \int_0^\infty dr \int_0^\pi d\theta r^2 \sin(2\theta) g(r) f(r) e^{iQr\cos\theta}. \qquad (3.14)$$

(b) Three-quark core counterterm (CT)

$$G_E^B(Q^2)\big|_{CT} = \left[a_2^B(\hat{Z} - 1) + a_3^B(\hat{Z}_s - 1) \right] G_E^p(Q^2)\big|_{LO}, \qquad (3.15)$$

$$G_M^B(Q^2)\big|_{CT} = \left[b_2^B(\hat{Z} - 1) + b_3^B(\hat{Z}_s - 1) \right] \frac{m_B}{m_N} G_M^p(Q^2)\big|_{LO}. \qquad (3.16)$$

(c) Meson-cloud diagram (MC)

$$G_E^B(Q^2)\big|_{MC} = \frac{1}{2(2\pi F)^2} \int_0^\infty dk \int_{-1}^1 dx k^2 (k^2 + kQx)$$

$$\times F_{II}(k) F_{II}(k_+) t_E^B(k^2, Q^2, x)\big|_{MC}, \qquad (3.17)$$

$$G_M^B(Q^2)\big|_{MC} = \frac{5m_B}{6(2\pi F)^2} \int_0^\infty dk k^4 \int_{-1}^1 dx (1 - x^2)$$

$$\times F_{II}(k) F_{II}(k_+) t_M^B(k^2, Q^2, x)\big|_{MC}, \qquad (3.18)$$

where

$$t_E^B(k^2, Q^2, x)\big|_{MC} = a_4^B C_\pi(k^2, Q^2, x) + a_5^B C_K(k^2, Q^2, x), \tag{3.19}$$

$$t_M^B(k^2, Q^2, x)\big|_{MC} = b_4^B D_\pi(k^2, Q^2, x) + b_5^B D_K(k^2, Q^2, x), \tag{3.20}$$

$$C_\Phi(k^2, Q^2, x) = \frac{1}{\omega_\Phi(k^2)\omega_\Phi(k_+^2)[\omega_\Phi(k^2) + \omega_\Phi(k_+^2)]}, \tag{3.21}$$

$$D_\Phi(k^2, Q^2, x) = \frac{1}{\omega_\Phi^2(k^2)\omega_\Phi^2(k_+^2)}, \tag{3.22}$$

$$k_\pm = \sqrt{k^2 + Q^2 \pm 2k\sqrt{Q^2}x}. \tag{3.23}$$

(d) Vertex-correction diagram (VC)

$$G_E^B(Q^2)\big|_{VC} = \frac{1}{4(2\pi F)^2} \int_0^\infty dk\, k^4 F_{II}^2(k) G_E^p(Q^2)\big|_{LO}$$

$$\times \left[\frac{a_6^B}{\omega_\pi^3(k^2)} + \frac{a_7^B}{\omega_K^3(k^2)} + \frac{a_8^B}{\omega_\eta^3(k^2)} \right], \tag{3.24}$$

$$G_M^B(Q^2)\big|_{VC} = \frac{1}{2(2\pi F)^2} \int_0^\infty dk\, k^4 F_{II}^2(k) G_M^p(Q^2)\big|_{LO}$$

$$\times \left[\frac{b_6^B}{\omega_\pi^3(k^2)} + \frac{b_7^B}{\omega_K^3(k^2)} + \frac{b_8^B}{\omega_\eta^3(k^2)} \right]. \tag{3.25}$$

(e) Meson-in-flight diagram (MF)

$$G_E^B(Q^2)\big|_{MF} \equiv 0, \tag{3.26}$$

$$G_M^B(Q^2)\big|_{MF} = \frac{m_B}{(2\pi F)^2} \int_0^\infty dk \int_{-1}^1 dx\, k^4(1 - x^2)$$

$$\times F_{II}(k)F_{II}(k_+) t_M^B(k^2, Q^2, x)\big|_{MF}, \tag{3.27}$$

where

$$t_M^B(k^2, Q^2, x)\big|_{MC} = b_9^B D_\pi(k^2, Q^2, x) + b_{10}^B D_K(k^2, Q^2, x). \tag{3.28}$$

Table 3.1 The constants a_i^B for the octet baryon charge form factors $G_E^B(Q^2)$.

	p	n	Σ^+	Σ^0	Σ^-	Λ	Ξ^0	Ξ^-
a_1	1	0	1	0	-1	0	0	-1
a_2	1	0	4/3	1/3	$-2/3$	1/3	2/3	$-1/3$
a_3	0	0	$-1/3$	$-1/3$	$-1/3$	$-1/3$	$-2/3$	$-2/3$
a_4	1	-1	2	0	-2	0	1	-1
a_5	2	1	1	0	-1	0	-1	-2
a_6	1	2	0	1	2	1	0	1
a_7	-2	-2	$-2/3$	$-2/3$	$-2/3$	$-2/3$	2/3	2/3
a_8	1/3	0	0	$-1/3$	$-2/3$	$-1/3$	$-2/3$	-1

The constants a_i^B and b_i^B are given in Table 3.1 and Table 3.2, respectively. It is found in the above analytical expressions that the contribution of the meson-in-flight diagram to the charge form factors of octet baryons vanish identically, that is, only four Feynman diagrams (a)-(d) in Figure 3.1 contribute to the charge form factors. For the magnetic form factors, however, the "meson-in-flight" diagram in Figure 3.1(e) contributes.

In the non-relativistic limit, the mean-square charge radius of a charged baryon is related to the baryon charge form factor as

$$\langle r_E^2 \rangle^B = -\frac{6}{G_E^B(0)} \frac{d}{dQ^2} G_E^B(Q^2) \bigg|_{Q^2=0}. \tag{3.29}$$

For the neutral baryons, the mean-square charge radius is defined by

$$\langle r_E^2 \rangle^B = -6 \frac{d}{dQ^2} G_E^B(Q^2) \bigg|_{Q^2=0}. \tag{3.30}$$

Table 3.2 The constants b_i^B for the octet baryon magnetic form factors $G_M^B(Q^2)$.

	p	n	Σ^+	Σ^0	Σ^-	Λ	Ξ^0	Ξ^-
b_1	1	$-2/3$	1	$1/3$	$-1/3$	$-1/3$	$-2/3$	$-1/3$
b_2	1	$-2/3$	$8/9$	$2/9$	$-4/9$	0	$-2/9$	$1/9$
b_3	0	0	$1/9$	$1/9$	$1/9$	$-1/3$	$-4/9$	$-4/9$
b_4	1	-1	$4/5$	0	$-4/5$	0	$-1/5$	$1/5$
b_5	$4/5$	$-1/5$	1	$3/5$	$1/5$	$-3/5$	-1	$-4/5$
b_6	$1/18$	$-2/9$	0	$-1/9$	$-2/9$	0	0	$1/18$
b_7	$1/9$	$1/9$	$5/27$	$5/27$	$5/27$	$-1/9$	$-5/27$	$-5/27$
b_8	$-1/18$	$1/27$	$-2/27$	$-1/27$	0	$-2/27$	$1/9$	$5/54$
b_9	1	-1	0	0	0	0	0	0
b_{10}	0	0	1	1	1	-1	-1	-1

In analogy, the mean-square magnetic radius is defined as

$$\langle r_M^2 \rangle^B = -\frac{6}{G_M^B(0)} \frac{d}{dQ^2} G_M^B(Q^2)\Big|_{Q^2=0}. \tag{3.31}$$

3.2 Quark Wave Function

The theoretical expressions in the above section reveal that the charge and magnetic form factors are mainly determined by the wave function of the quark core. In this work we fix the quark core wave function by adjusting our theoretical result of the proton charge form factor to experimental data, considering that the recent measurements of the proton charge form factor are in high precision, and that only four Feynman diagrams in the PCQM contribute to the proton charge form factor. For the sake of simplicity, we restrict our calculations to $SU(2)$ flavor.

Table 3.3 The normalized model parameters are determined by fitting theoretical results of the proton charge form factor to the experimental data.

n	A'_n	B'_n
0	0.21965608	0.13892063
1	−0.00817140	0.02905047
2	0.00072723	0.01024717
3	−0.01311738	0.00072182
4	−0.00853137	−0.00091915

We expand the quark wave functions $g(r)$ and $f(r)$ in the basis of Sturmian functions in Equation (2.15) and Equation (2.16), respectively. It is found that a basis of five Sturmian functions ($n = 0, 1, 2, 3, 4$) is good enough to let our theoretical result of the proton charge form factor fit to experimental data. The fitted model parameters for Sturmian function length parameter $b = 0.5$ GeV, and the expansion coefficients A'_n and B'_n are compiled in Table (3.3), where we redefine $A'_n = A_n b^{-1/2}$ and $B'_n = B_n b^{-3/2}$ to let the A'_n and B'_n be dimensionless.

Shown in Figures (3.2) and (3.3) are respectively the radial wave functions $g(r)$ and $f(r)$ for the quarks and the proton charge form factor $G_E^p(Q^2)$ derived with the fitted quark wave functions. It is seen in Figure (3.3) that the experimental data are well fitted up to the squared momentum transfer $Q^2 = 1$ GeV^2. The charge radius of proton derived with Equation (3.29) is also consistent with experimental data, as shown in Table 3.4.

Larger bases have been applied, but the fitted results of the quark wave function appear the same as the one with the five bases. Note that in the calculation quark wave functions are normalized according to $\int d^3\vec{x} u^\dagger(\vec{x}) u(\vec{x}) = 1$.
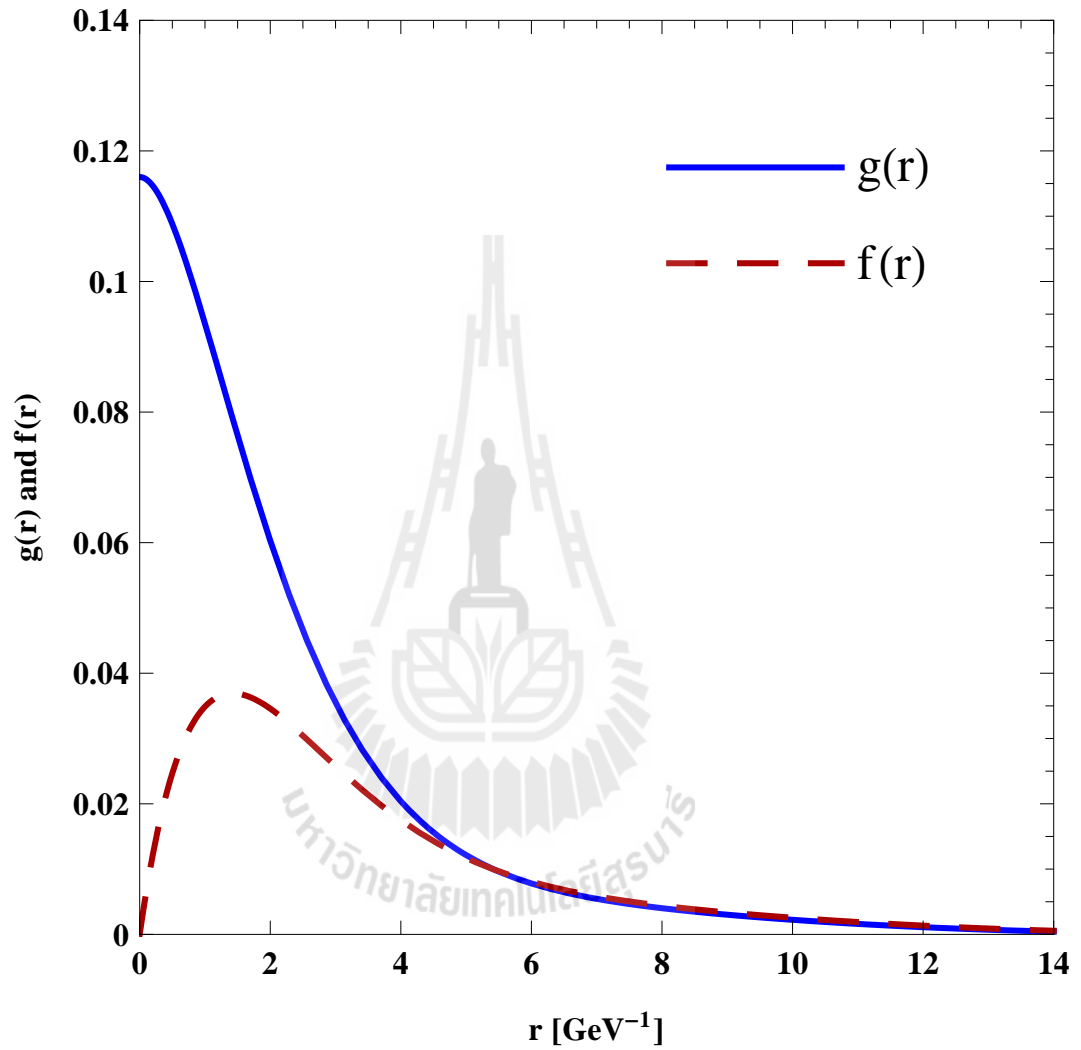
Figure 3.2 The normalized radial quark wave functions for the valence quark: solid line for the upper component g(r) and dashed line for the lower component f(r).
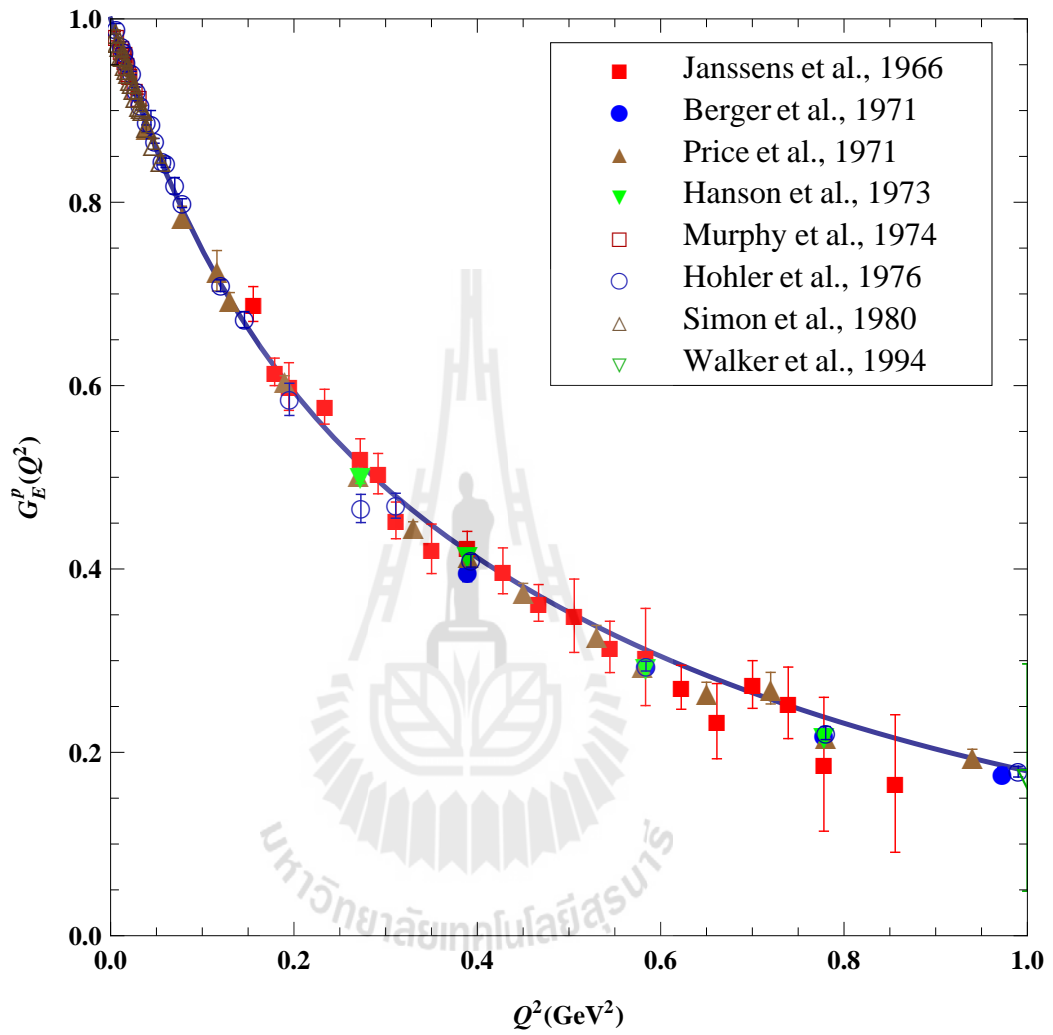
Figure 3.3 The fit of proton charge form factor compared to the measurements. The experimental data are taken from (Janssens et al., 1966; Berger et al., 1971; Price et al., 1971; Hanson et al., 1973; Murphy et al., 1974; Höhler et al., 1976; Simon et al., 1980; Walker et al., 1994).

Table 3.4 Numerical result for the proton mean-square charge radius $\langle r_E^2 \rangle^p$, and the experimental data are taken from (Beringer et al., 2012) (in units of fm^2).

	PCQM	Exp.
$\langle r_E^2 \rangle^p$	0.77	0.76 ± 0.02

3.3 Numerical Results

The quark wave function has been extracted by fitting the theoretical result of the proton charge form factor to experimental data in the framework of the SU(2) flavor symmetry. In this section, we study the electromagnetic properties of the octet baryons in the PCQM, applying the predetermined quark wave function. We extend the calculations to the SU(3) flavor symmetry, including kaon and η-meson cloud contributions as well.

Listed in Table 3.5 are the charge radii squared of the octet baryons, which are derived with Equations (3.29) and (3.30) for the charged and neutral baryons, respectively. It is found that the 3q-core (LO and CT diagrams) dominates the charge radii of the charged baryons (p, Σ^+, Σ^- and Ξ^-), contributing more than 90% to the total values. As shown in Table 3.5, the theoretical p and Σ^- charge radii are in good agreement with experimental values. The work predicts that the charge radii of Σ^+ and Ξ^- are contributed by a similar pattern, that is, about 90% from the 3q-core and meson cloud contributions and less than 10% from MC and VC diagrams. In Figure 3.4, we present the Q^2 dependence of the charge form factor of the charged baryons in the region $Q^2 \leq 1$ GeV^2, compared with experimental data. It is seen in Figure 3.4 that the theoretical charge form factors for the charged hyperons (Σ^+, Σ^- and Ξ^-) are consistent with experimental data.

However, the theoretical charge radii of neutral baryons (n, Σ^0, Λ and Ξ^0)

Table 3.5 Numerical results for the octet baryon mean-square charge radii $\langle r_E^2 \rangle^B$. The experimental data are taken from (Beringer et al., 2012) (in units of fm^2).

	3q LO+CT	Meson loops MC+VC	Total	Exp.
$\langle r_E^2 \rangle^p$	0.710	0.057	0.767	0.76 ± 0.09
$\langle r_E^2 \rangle^n$	0	-0.014	-0.014	-0.116 ± 0.002
$\langle r_E^2 \rangle^{\Sigma^+}$	0.701	0.080	0.781	—
$\langle r_E^2 \rangle^{\Sigma^0}$	-0.009	0.009	0	—
$\langle r_E^2 \rangle^{\Sigma^-}$	0.718	0.063	0.781	0.61 ± 0.21
$\langle r_E^2 \rangle^{\Lambda}$	-0.009	0.009	0	—
$\langle r_E^2 \rangle^{\Xi^0}$	-0.017	0.031	0.014	—
$\langle r_E^2 \rangle^{\Xi^-}$	0.727	0.040	0.767	—

listed in Table 3.5 are rather small. As seen, the neutron charge radii is much smaller than the experimental data, while the contributions to the charge radii of Σ^0 and Λ by various diagrams counteract each other to zero. As expected, the work also fails to reproduce the experimental data of the neutron form factor, as shown in Figure 3.5. The reason might be that the quark propagator is restricted to the ground-state only in our calculation. The meson cloud solely contributes to the neutral baryon charge form factors as the leading-order contribution of the 3q-core vanishes. One may propose that it is necessary to include excited-state quarks to investigate the neutral baryon charge form factors. More discussions and results on the neutron charge radius including the excited quark propagator are given in (Lyubovitskij et al., 2001a; Cheedket et al., 2004).
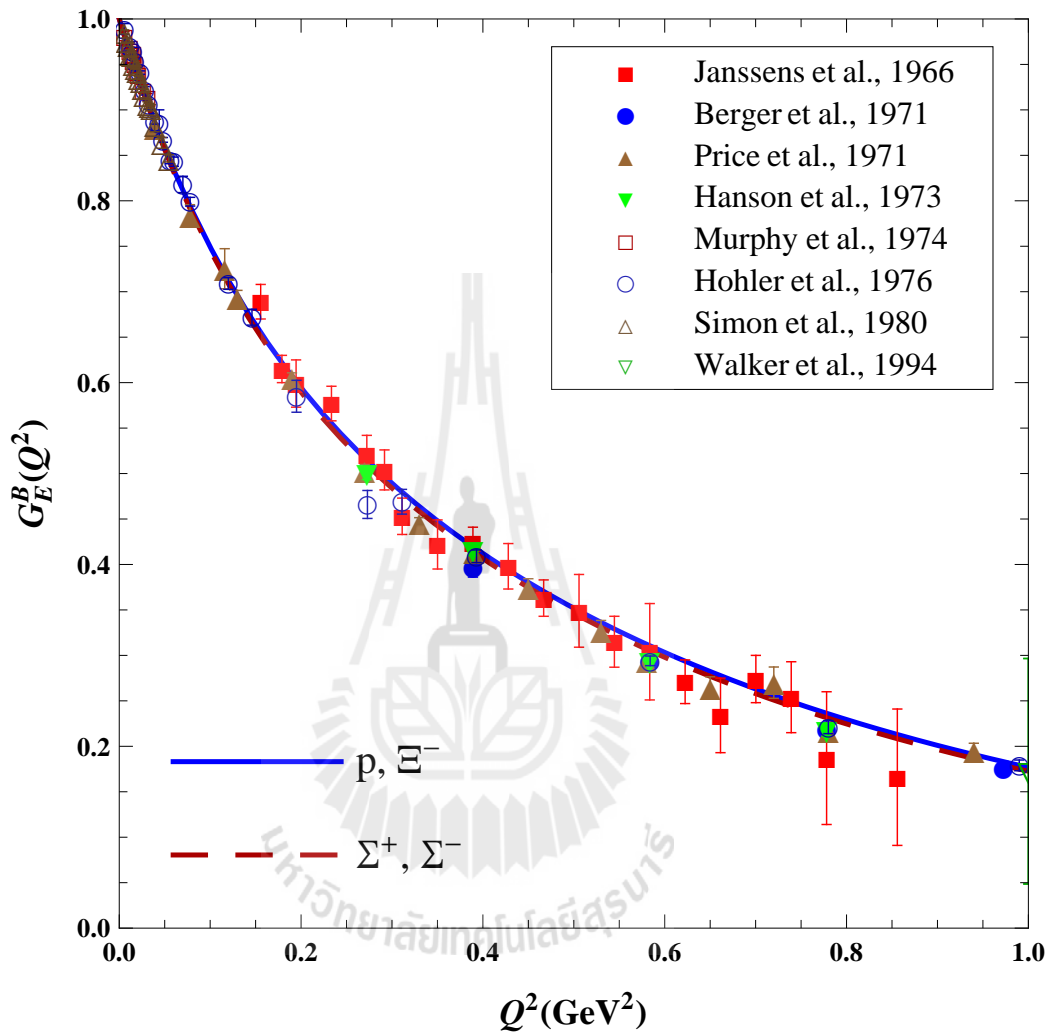
Figure 3.4 Charge form factors $G_E^B(Q^2)$ of charged baryons. The experimental data on proton charge form factor are taken from (Janssens et al., 1966; Berger et al., 1971; Price et al., 1971; Hanson et al., 1973; Murphy et al., 1974; Höhler et al., 1976; Simon et al., 1980; Walker et al., 1994).
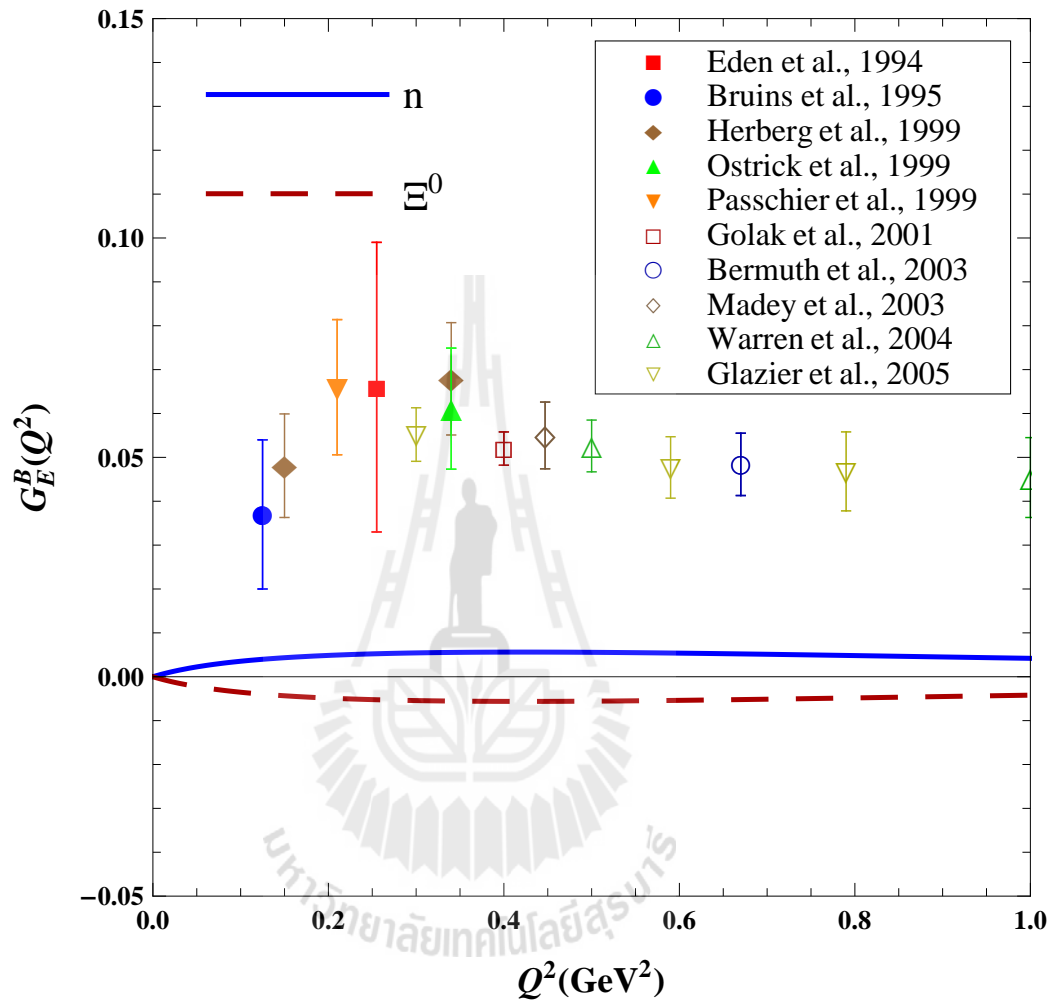
Figure 3.5 Charge form factors $G_E^B(Q^2)$ of neutral baryons. The experimental data on neutron charge form factor are taken from (Eden et al., 1994; Bruins et al., 1995; Herberg et al., 1999; Ostrick et al., 1999; Passchier et al., 1999; Golak et al., 2001; Bermuth et al., 2003; Madey et al., 2003; Warren et al., 2004; Glazier et al., 2005)

Table 3.6 Numerical results for the octet baryon magnetic moments μ_B with chiral mass $m_B = 1.039$ GeV. The experimental data are taken from (Beringer et al., 2012) (in units of the nucleon magneton μ_N).

	3q LO+CT	Meson loops MC+VC+MF	Total	Exp.
μ_p	2.290	0.445	2.735	2.793
μ_n	−1.527	−0.429	−1.956	−1.913
μ_{Σ^+}	2.299	0.238	2.537	2.458 ± 0.010
μ_{Σ^0}	0.773	0.065	0.838	—
μ_{Σ^-}	−0.754	−0.107	−0.861	$−1.160 \pm 0.025$
μ_Λ	−0.791	−0.076	−0.867	$−0.613 \pm 0.004$
μ_{Ξ^0}	−1.564	−0.126	−1.690	$−1.250 \pm 0.014$
μ_{Ξ^-}	−0.800	−0.040	−0.840	$−0.651 \pm 0.080$

In our evaluation of the charge form factor of octet baryons we have applied an ansatz that the predetermined quark wave function is the same for u, d, and s quarks. That is, we work in the SU(3) chiral symmetry limit. Therefore, baryon masses should be restricted to the same order in the calculation of the magnetic moments. We evaluate the magnetic moments with the baryon chiral mass $m_B = 1.039$ GeV (Scherer, 2003). The numerical results for the magnetic moments, which are the magnetic form factors in zero-recoil, and the magnetic radii of the octet baryons derived with Equation (3.31) are given respectively in Table 3.6 and Table 3.7. It is found that the theoretical results for the octet baryon magnetic moments are consistent with the experimental data, while the nucleon magnetic radii are a little bit larger than the experimental values. Note that meson cloud

Table 3.7 Numerical results for the octet baryon mean-square magnetic radii $\langle r_M^2 \rangle^B$. The experimental data are taken from (Beringer et al., 2012) (in units of fm^2).

|	3q	Meson loops	Total	Exp.
	LO+CT	MC+VC+MF		
$\langle r_M^2 \rangle^p$	0.748	0.161	0.909	0.74 ± 0.10
$\langle r_M^2 \rangle^n$	0.698	0.224	0.922	0.76 ± 0.02
$\langle r_M^2 \rangle^{\Sigma^+}$	0.810	0.075	0.885	—
$\langle r_M^2 \rangle^{\Sigma^0}$	0.824	0.027	0.851	—
$\langle r_M^2 \rangle^{\Sigma^-}$	0.783	0.168	0.951	—
$\langle r_M^2 \rangle^{\Lambda}$	0.815	0.037	0.852	—
$\langle r_M^2 \rangle^{\Xi^0}$	0.827	0.044	0.871	—
$\langle r_M^2 \rangle^{\Xi^-}$	0.851	−0.011	0.840	—

contributes around 20% to the total values of both the nucleon magnetic moments and radii, while the meson cloud contributions for hyperons are rather small except for the Σ^-.

It is noted that the constants b_4, b_6, and b_9 in Table 3.2 for hyperons, which are relevant to the π-meson cloud contribution, are smaller than those for the nucleon. This may indicate that the π-meson dominates the meson-cloud contribution to the octet baryon magnetic properties.

The Q^2 dependence of the magnetic form factors for the charged and neutral octet baryons are shown respectively in Figure 3.6 and Figure 3.7, which are normalized to one at zero-recoil. We also plot experimental data on the proton and neutron magnetic form factors in the corresponding figures. It is clear that
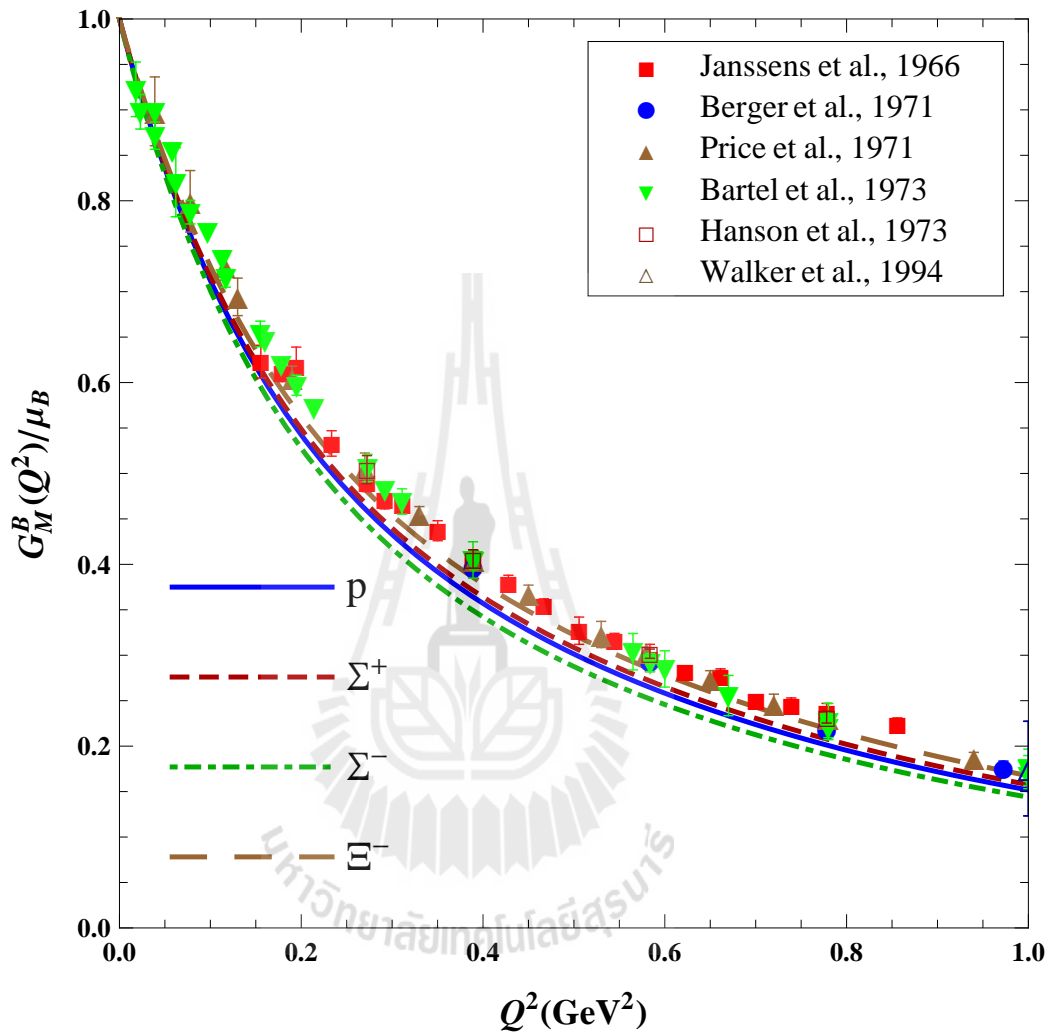
Figure 3.6 Normalized magnetic form factors $G_M^B(Q^2)/\mu_B$ of charged baryons. The experimental data on proton magnetic form factor are taken from (Janssens et al., 1966; Berger et al., 1971; Price et al., 1971; Bartel et al., 1973; Hanson et al., 1973; Walker et al., 1994).
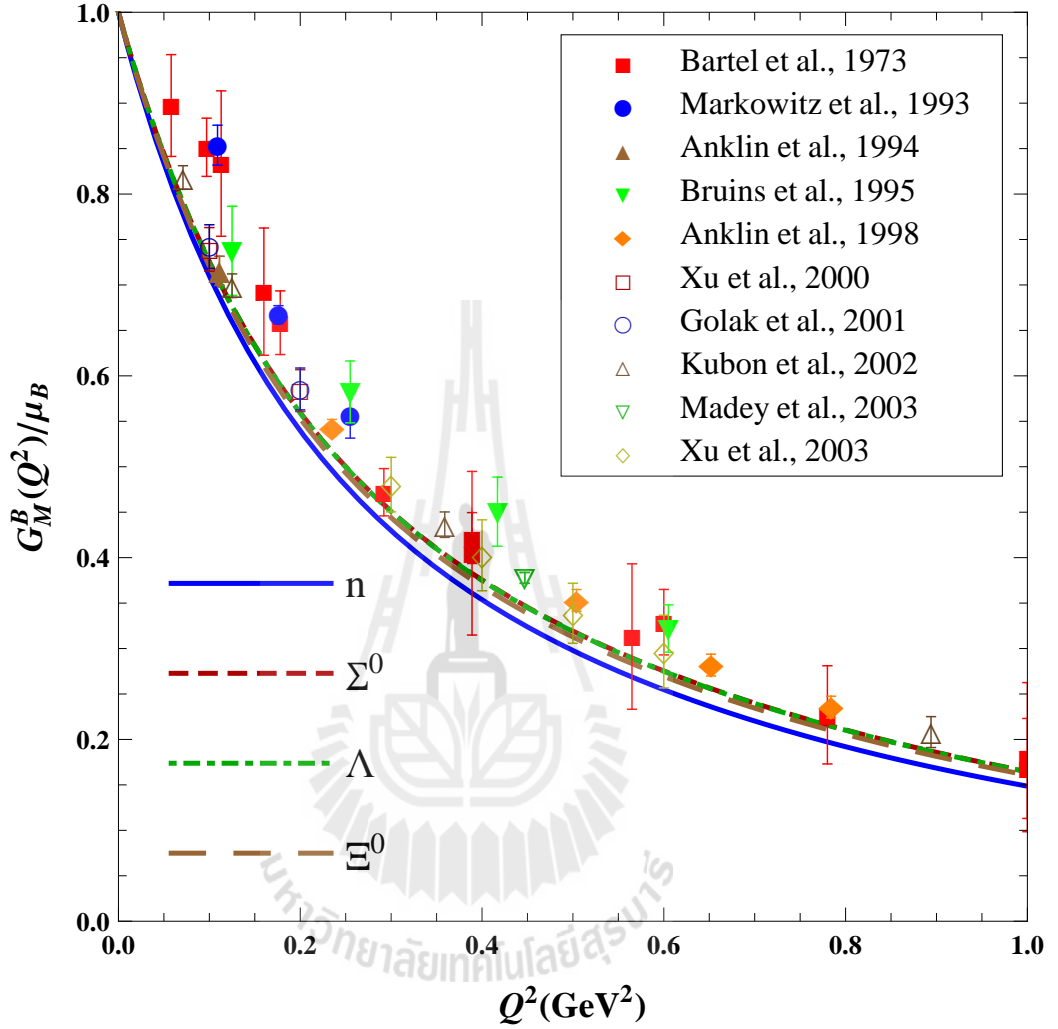
Figure 3.7 Normalized magnetic form factors $G_M^B(Q^2)/\mu_B$ of neutral baryons. The experimental data on neutron magnetic form factors are taken from (Bartel et al., 1973; Markowitz et al., 1993; Anklin et al., 1994; Bruins et al., 1995; Anklin et al., 1998; Xu et al., 2000; Golak et al., 2001; Kubon et al., 2002; Madey et al., 2003; Xu et al., 2003).

the nucleon magnetic form factors are fairly consistent with experimental data, and the magnetic form factors for hyperons behave the similar way.

The fact that the Q^2 dependence of the theoretical electromagnetic form factors in the region $Q^2 \leq 1 \, \mathrm{GeV}^2$ is consistent with experimental data implies that the predetermined quark wave function is reasonable in the PCQM. We expect that the determined quark wave function is applicable to the evaluation of the axial form factors of octet baryons.

CHAPTER IV

AXIAL FORM FACTORS

4.1 Axial Form Factors of Octet Baryons

Baryon axial form factors may be investigated through semileptonic decays $B_1 \to B_2 \ell \bar{\nu}$, such as $n \to p e^- \bar{\nu}_e$, $\Sigma^- \to \Sigma^0 e^- \bar{\nu}_e$, $\Xi^- \to \Xi^0 e^- \bar{\nu}_e$, etc. In the specific case of the neutron β decay, the matrix element of axial-vector current A_3^μ is given by

$$\langle p|A_3^\mu|p\rangle = G_A^N(Q^2)\bar{U}_p(p)\gamma^\mu\gamma_5\frac{\tau_3}{2}U_p(p), \tag{4.1}$$

or

$$\langle n|A_3^\mu|n\rangle = G_A^N(Q^2)\bar{U}_n(p)\gamma^\mu\gamma_5\frac{\tau_3}{2}U_n(p). \tag{4.2}$$

Therefore, we may express the axial form factor of baryons more generally as

$$\langle B|A_3^\mu|B\rangle = G_A^B(Q^2)\bar{U}_B(p)\gamma^\mu\gamma_5\frac{\tau_3}{2}U_B(p), \tag{4.3}$$

where $G_A^B(Q^2)$ is the axial form factor of baryons with the squared momentum transfer Q^2 which is carried out by axial-vector current A_3^μ, and $U_B(p)$ is the baryon spinors.

In the Breit frame, $G_A^B(Q^2)$ is set up as

$$\left\langle B_{s'}\left(\frac{\vec{q}}{2}\right)\middle|\int d^3\vec{x}\mathrm{e}^{\mathrm{i}\vec{q}\cdot\vec{x}}\vec{A}_3(x)\middle|B_s\left(-\frac{\vec{q}}{2}\right)\right\rangle = \chi_{B_{s'}}^\dagger\vec{\sigma}\frac{\tau_3}{2}\chi_{B_s}G_A^B(Q^2), \tag{4.4}$$

where χ_{B_s} and $\chi_{B_{s'}}^\dagger$ are the baryon spin wave functions in the initial and final states, $\vec{\sigma}$ is the baryon spin matrix and τ_3 is the third component of the SU(2) isospin matrix.

At zero recoil ($Q^2 = 0$) the axial form factor satisfies the condition:

$$G_A^B(0) = g_A^B, \tag{4.5}$$

where g_A^B is the axial charge of octet baryons.

In the PCQM, the axial form factor of octet baryons is given by

$$\chi_{B_{s'}}^\dagger \vec{\sigma}_B \frac{\tau_B^3}{2} \chi_{B_s} G_A^B(Q^2) = {}^B\langle\phi_0| \sum_{n=0}^2 \frac{i^n}{n!} \int \delta(t) d^4x d^4x_1 \cdots d^4x_n \mathrm{e}^{-iqx}$$

$$\times T[\mathcal{L}_I^W(x_1) \cdots \mathcal{L}_I^W(x_n) \vec{A}_3(x)]|\phi_0\rangle_c^B, \tag{4.6}$$

with the interaction Lagrangian $\mathcal{L}_I^W(x)$ given in Equation (2.11), and the axial-vector current A_I^μ taking the form

$$A_i^\mu = F\partial^\mu\Phi_i + \bar{\psi}\gamma^\mu\gamma^5\frac{\lambda_i}{2}\psi - \frac{f_{ijk}}{2F}\bar{\psi}\gamma^\mu\lambda_j\psi\Phi_k$$

$$+ \bar{\psi}(\hat{Z}-1)\gamma^\mu\gamma^5\frac{\lambda_i}{2}\psi + o(\Phi_i^2). \tag{4.7}$$

According to the interaction Lagrangian $\mathcal{L}_I^W(x)$ and the axial-vector current A_I^μ, the axial form factors of octet baryons are contributed by the following diagrams to the one-loop order: the three-quark core leading order diagram (Figure 4.1(a)), the three-quark core counterterm (Figure 4.1(b)), the self-energy diagram (Figures 4.1(c) and (d)), the exchange diagram (Figure 4.1(e)) and the vertex-correction diagram (Figure 4.1(f)). The corresponding analytical expressions of the axial form factors of octet baryons (detailed calculations are shown in Appendix E) are derived as follows:

(a) Three-quark leading order diagram (LO)

$$G_A^B(Q^2)\big|_{LO} = c_1^B 2\pi \int_0^\infty dr \int_0^\pi d\theta r^2 \sin\theta[g(r)^2 + f(r)^2\cos(2\theta)]e^{iQr\cos\theta}. \tag{4.8}$$
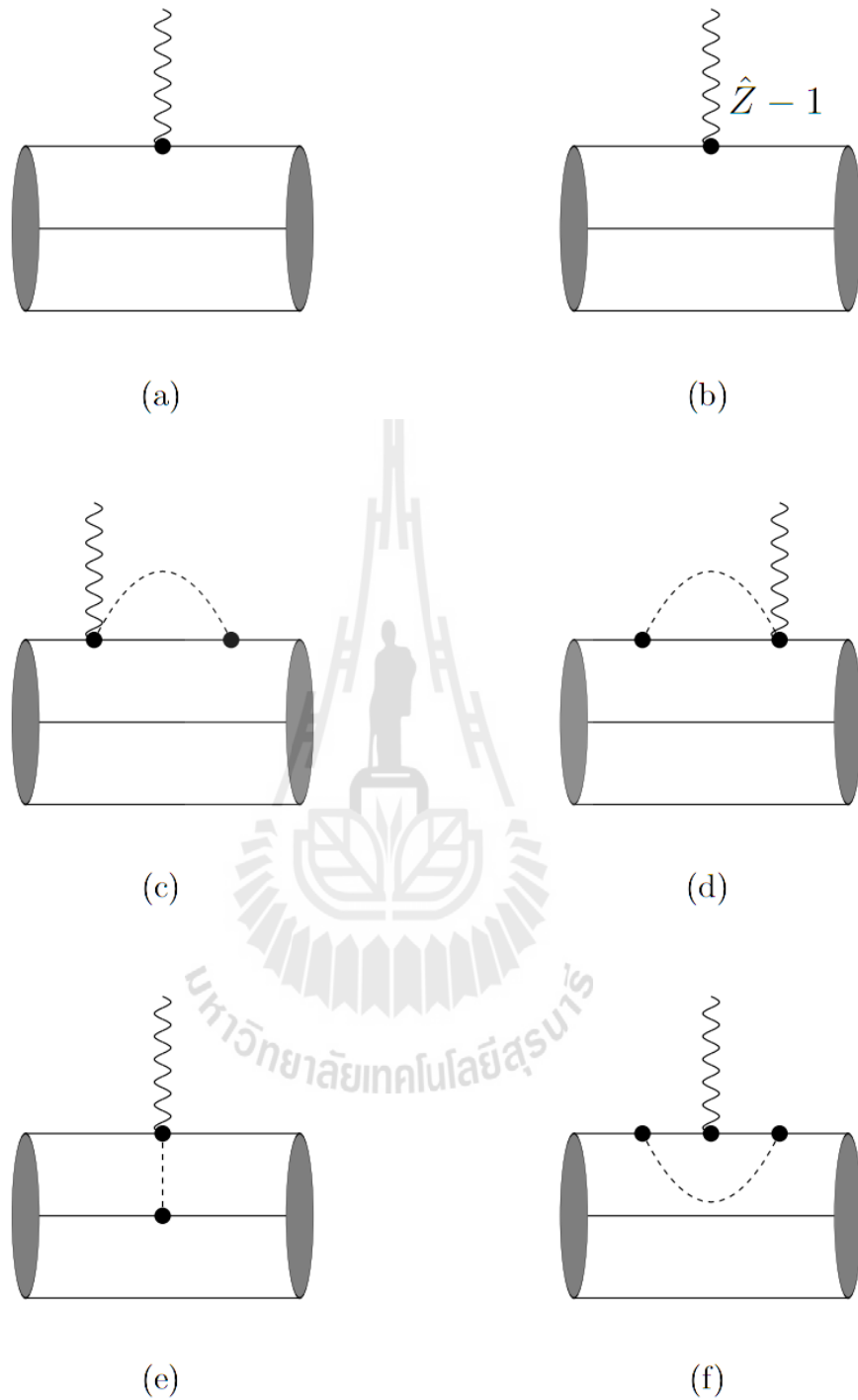
Figure 4.1 Diagrams contributing to the axial form factor of octet baryons : 3q-core leading order (a), 3q-core counterterm (b), self-energy (c and d), meson exchange (e), and vertex correction (f).

(b) Three-quark counterterm (CT):

$$G_A^B(Q^2)\big|_{CT} = (\hat{Z} - 1)G_A^B(Q^2)\big|_{LO}, \tag{4.9}$$

(c-d) Self-energy diagram I and II (SE)

$$
\begin{aligned}
G_A^B(Q^2)\big|_{SE} &= G_A^B(Q^2)\big|_{SE;I} + G_A^B(Q^2)|_{SE;II} \\
&= \frac{1}{(2\pi F)^2} \int_0^\infty dk \int_{-1}^1 dx\, k^4(1 - x^2)F_{II}(k)F_{III}(k_-) \\
&\quad \times \frac{1}{\sqrt{k_-^2}}\left[\frac{c_1^B}{\omega_\pi^2(k^2)} + \frac{c_2^B}{\omega_K^2(k^2)}\right].
\end{aligned}
\tag{4.10}
$$

where $G_A^B(Q^2)\big|_{SE;I} = G_A^B(Q^2)\big|_{SE;II}$, and the vertex function for the quark-pion-axial vector current $F_{III}(k)$ is given by

$$F_{III}(k) = -2i\pi \int_0^\infty dr \int_0^\pi d\theta\, r^2 g(r)f(r)\sin 2\theta\, e^{ikr\cos\theta}. \tag{4.11}$$

(e) Exchange diagram (EX)

$$
\begin{aligned}
G_A^B(Q^2)\big|_{EX} &= \frac{1}{4(2\pi F)^2} \int_0^\infty dk \int_{-1}^1 dx\, k^4(1 - x^2)F_{II}(k)F_{III}(k_-) \\
&\quad \times \frac{1}{\sqrt{k_-^2}}\left[\frac{c_3^B}{\omega_\pi^2(k^2)} + \frac{c_4^B}{\omega_K^2(k^2)}\right].
\end{aligned}
\tag{4.12}
$$

(f) Vertex-correction diagram (VC)

$$
\begin{aligned}
G_A^B(Q^2)\big|_{VC} &= \frac{1}{20(2\pi F)} \int_0^\infty dk\, k^4 F_{II}^2(k)G_A^N(Q^2)\big|_{LO} \\
&\quad \times \left[\frac{c_1^B}{\omega_\pi^3(k^2)} + \frac{c_5^B}{\omega_\eta^3(k^2)}\right].
\end{aligned}
\tag{4.13}
$$

The constants c_i^B in the above equations are given in Table 4.1.

Table 4.1 The constants c_i^B for the octet baryons axial form factors $G_A^B(Q^2)$.

	N	Σ	Ξ
c_1	$5/3$	$4/3$	$-1/3$
c_2	$5/6$	$2/3$	$-1/6$
c_3	8	0	0
c_4	0	4	-4
c_5	$-5/9$	$-4/9$	$1/9$

4.2 Numerical Results

The axial form factors of octet baryons are evaluated with the quark wave functions determined by fitting the theoretical result of the proton charge form factor to experimental data, as discussed in Chapter III. Note that there is no any free parameter in the study of the baryon axial form factors.

Presented in Table 4.2 are the numerical results from our calculations for the axial charge of octet baryons $B = N$, Σ, and Ξ. Except for the N, there is no direct experimental data for the axial charge, thus we have the lattice-QCD results (Erkol et al., 2010) shown in the table for comparison. The theoretical results shown in Table 4.2 reveal that the meson cloud plays an important role in the axial charge of octet baryons, contributing to 30%-40% of the total values. The theoretical nucleon axial charge is consistent with the experimental data and the theoretical Σ and Ξ axial charges are in good agreement with lattice QCD results.

Finally, we show the Q^2 dependence of the axial form factors of octet baryons in Figure 4.1, which are normalized to one at zero-recoil, with the experimental data for nucleon axial form factor plotted as well. As expected, the

Table 4.2 Numerical results for the octet baryon axial charges g_A^B. Lattice QCD results are taken from (Erkol et al., 2010), and the experimental data are taken from (Beringer et al., 2012).

	3q LO+CT	Meson loops SE+EX+VC	Total	Lattice	Exp.
g_A^N	0.823	0.478	1.301	1.314	1.269 ± 0.003
g_A^Σ	0.658	0.269	0.927	0.970	—
g_A^Ξ	-0.165	-0.118	-0.283	-0.299	—

theoretical axial form factors fall off smoothly as the momentum transfer Q^2 increase. It is also found that the theoretical result for the N axial form factor is in good agreement with experimental data, and the axial form factors for Σ and Ξ show a similar Q^2 dependence.

The fact that the theoretical results of the axial form factors and axial charges agree well with experimental data and lattice-QCD results indicates that our quark wave functions are reasonable in the PCQM.
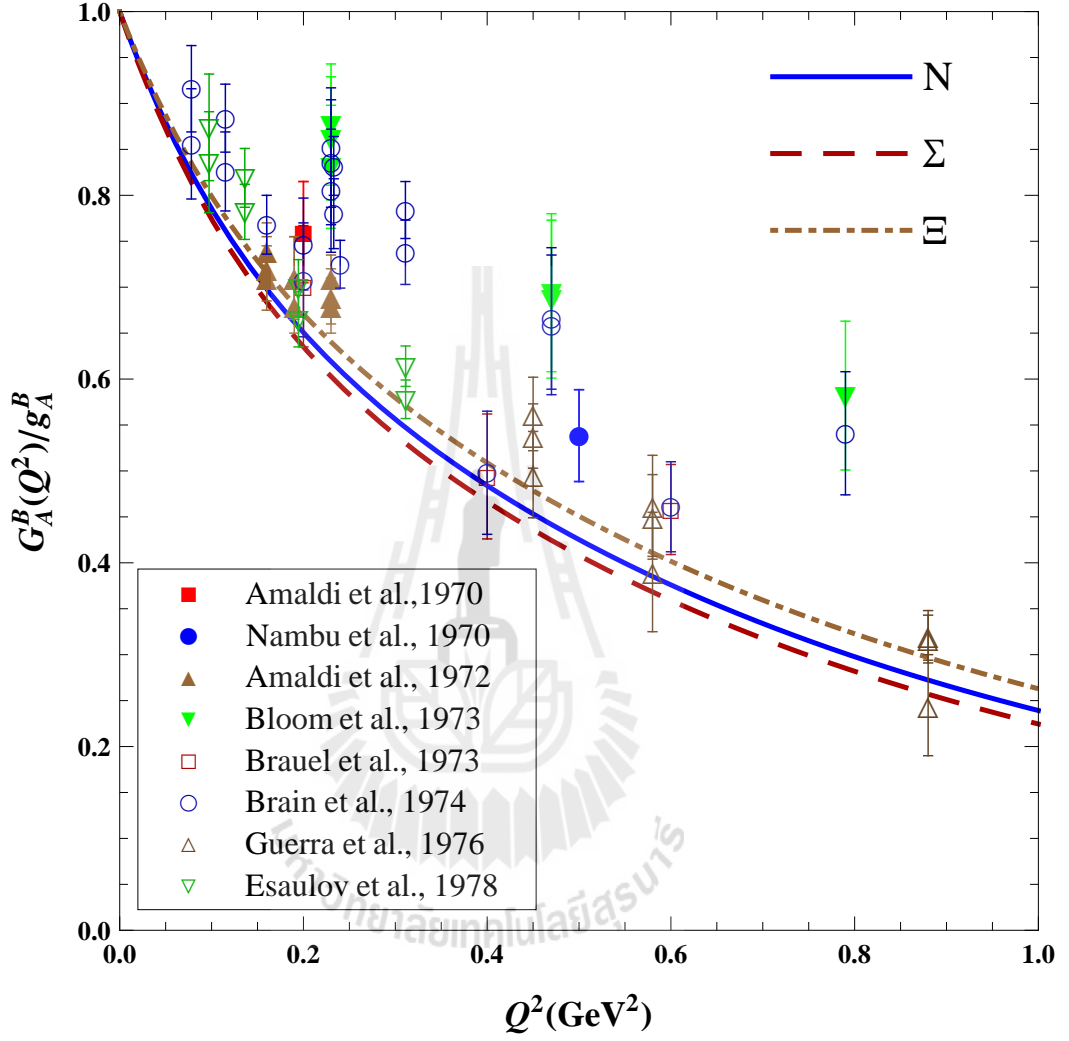
Figure 4.2 Normalized axial form factors $G_A^B(Q^2)/g_A^B$ of octet baryons. The experimental data on nucleon axial form factor are taken from (Amaldi et al., 1970; Nambu and Yoshimura, 1970; Amaldi et al., 1972; Bloom et al., 1973; Brauel et al., 1973; Read, 1974; Guerra et al., 1976; Esaulov et al., 1978).

CHAPTER V

CONCLUSIONS

In this work, we have studied the electromagnetic and axial form factors of octet baryons in the framework of the PCQM which, as a further development of chiral quark model with a perturbative treatment of the meson (π, K and η) cloud, is realized by the relativistic quark wave function and static potential for confinement as well as the chiral symmetry requirements. The quark wave function is not derived by solving the Dirac equation for a certain potential and also not proposed to be the Gaussian form usually employed by other works, but instead derived by fitting the theoretical result of the proton charge form factor to the existing experimental data. We have expanded the quark wave function in the complete basis of Sturmian functions, and found that a basis of five Sturmian functions is sufficient to reproduce the experimental data of the proton charge form factor.

The electromagnetic and axial form factors of octet baryons are investigated up to one-loop perturbation in the region $Q^2 \leq 1$ GeV^2 in the PCQM with the predetermined quark function. The charge and magnetic radii, the magnetic moments as well as the axial charge of the octet baryons are also evaluated. It is found that the theoretical results for all observables but the neutral baryon charge form factors are in good agreement with the experimental data. Therefore, one may conclude that the predetermined quark function reflects the physics suitable and reasonable for the PCQM.

The failure to reproduce the neutral baryon charge form factors may be

caused by the inclusion of only the ground-state quarks. The leading order 3q-core contribution to the neutral baryon charge form factors vanishes, that is, the neutral baryon charge form factors arise purely from the meson cloud. Therefore, it may be necessary to include the excited-state quarks to investigate the neutral baryon charge form factors as the leading-order contribution is fully suppressed.

The properties of decuplet baryons may also be studied in the PCQM with the predetermined quark wave function in the future work.
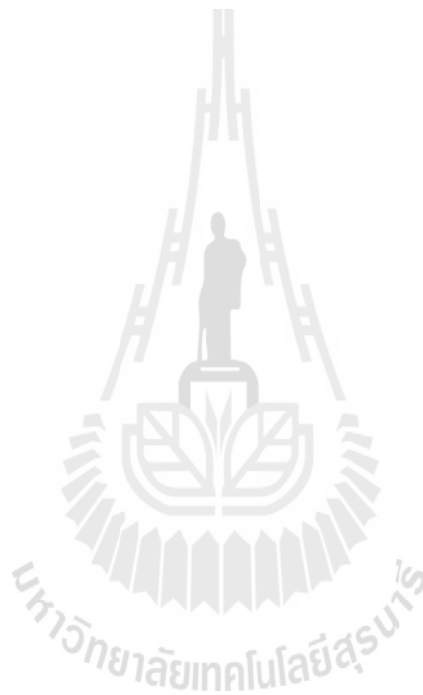
REFERENCES

REFERENCES

Ahrens, L. A. et al. (1987). Measurement of neutrino-proton and antineutrino-proton elastic scattering. **Phys. Rev. D** 35: 785–809.

Amaldi, E. et al. (1970). On pion electroproduction at 5 fm^{-2} near threshold. **Nuovo Cimento A** 67: 377–396.

Amaldi, E. et al. (1972). Axial-vector form-factor of the nucleon from a coincidence experiment on electroproduction at threshold. **Phys. Lett. B** 41: 216–220.

Andivahis, L. et al. (1994). Measurements of the electric and magnetic form factors of the proton from q^2=1.75 to 8.83 (gev/ c) ^{2}. **Phys. Rev. D** 50: 5491–5517.

Anklin, H. et al. (1994). Precision measurement of the neutron magnetic form factor. **Phys. Lett. B** 336: 313–318.

Anklin, H. et al. (1998). Precise measurements of the neutron magnetic form factor. **Phys. Lett. B** 428: 248–253.

Arnold, R. G. et al. (1986). Measurement of elastic electron scattering from the proton at high momentum transfer. **Phys. Rev. Lett.** 57: 174–177.

Arrington, J., Roberts, C. D., and Zanotti, J. M. (2007). Nucleon electromagnetic form factors. **J. Phys. G** 34: S23.

Bartel, W. et al. (1973). Measurement of proton and neutron electromagnetic form

factors at squared four-momentum transfers up to 3 $(\text{GeV/c})^2$. **Nucl. Phys. B** 58: 429–475.

Berger, C., Burkert, V., Knop, G., Langenbeck, B., and Rith, K. (1971). Electromagnetic form factors of the proton at squared four-momentum transfers between 10 and 50 fm^{-2}. **Phys. Lett. B** 35: 87–89.

Beringer, J. et al. (2012). Review of particle physics. **Phys. Rev. D** 86: 010001.

Bermuth, J. et al. (2003). The neutron charge form factor and target analyzing powers from ${}^3\text{He}(\vec{e},e'n)$ scattering. **Phys. Lett. B** 564: 199–204.

Bernard, V., Elouadrhiri, L., and Meißner, U. (2002). Axial structure of the nucleon. **J. Phys. G** 28: R1.

Bloom, E. D. et al. (1973). Measurements of inelastic electron scattering cross sections near the one-pion threshold. **Phys. Rev. Lett.** 30: 1186–1189.

Borkowski, F., Peuser, P., Simon, G., Walther, V., and Wendling, R. (1974). Electromagnetic form factors of the proton at low four-momentum transfer. **Nucl. Phys. A** 222: 269–275.

Borkowski, F., Simon, G., Walther, V., and Wendling, R. (1975). Electromagnetic form factors of the peoton at low four-momentum transfer (ii). **Nucl. Phys. B** 93: 461–478.

Bosted, P. E. et al. (1992). Measurements of the electric and magnetic form factors of the proton from q^2=1.75 to 8.83 (gev/ c) ^{2}. **Phys. Rev. Lett.** 68: 3841–3844.

Brauel, P. et al. (1973). π^+-electroproduction of hydrogen near threshold at

four-momentum transfers of 0.2, 0.4 and 0.6 $(\text{GeV}/c)^2$. **Phys. Lett. B** 45: 389–393.

Bruins, E. E. W. et al. (1995). Measurement of the neutron magnetic form factor. **Phys. Rev. Lett.** 75: 21–24.

Cheedket, S., Lyubovitskij, V., Gutsche, T., Faessler, A., Pumsa-ard, K., and Yan, Y. (2004). Electromagnetic form factors of the baryon octet in the perturbative chiral quark model. **Eur. Phys. J. A** 20: 317.

Chin, S. A. (1982). Many-body theory of confined quarks and excluded pions: A perturbative study of the chiral bag. **Nucl. Phys. A** 382: 355.

Chodos, A., Jaffe, R. L., Johnson, K., and Thorn, C. B. (1974a). Baryon structure in the bag theory. **Phys. Rev. D** 10: 2599.

Chodos, A., Jaffe, R. L., Johnson, K., Thorn, C. B., and Weisskopf, V. F. (1974b). New extended model of hadrons. **Phys. Rev. D** 9: 3471.

Close, F. E. (1979). An introduction to quarks and partons (5th ed.). Great Brirain: ST Edmundsbury Press.

Crawford, C. B. et al. (2007). Measurement of the proton's electric to magnetic form factor ratio from $^1\vec{h}(\vec{e},e'p)$. **Phys. Rev. Lett.** 98: 052301.

DeGrand, T., Jaffe, R. L., Johnson, K., and Kiskis, J. (1975). Masses and other parameters of the light hadrons. **Phys. Rev. D** 12: 2060.

Dib, C. et al. (2006). The neutron electric dipole form factor in the perturbative chiral quark model. **J. Phys. G** 32: 547.

Dong, Y. et al. (2006). Nucleon polarizabilities in the perturbative chiral quark model. **J. Phys. G** 32: 203–220.

Eden, T. et al. (1994). Electric form factor of the neutron from the ^{2}H($\vec{e}$,$e'\vec{n}$)^{1}H reaction at Q^2 = 0.255 (GeV/c)^2. **Phys. Rev. C** 50: R1749–R1753.

Erkol, G., Oka, M., and Takahashi, T. T. (2010). Axial charges of octet baryons in two-flavor lattice QCD. **Phys. Lett. B** 686: 36–40.

Esaulov, A., Pilipenko, A., and Titov, Y. (1978). Longitudinal and transverse contributions to the threshold cross-section slope of single-pion electro-production by a proton. **Nucl. Phys. B** 136: 511–532.

Eschrich, I. et al. (2001). Measurement of the Σ^- charge radius by Σ^--electron elastic scattering. **Phys. Lett. B** 522: 233–239.

Faessler, A., Thomas, G., Holstein, B., Lyubovitskij, V., Nicmorus, D., and Pumsa-ard, K. (2006a). Electromagnetic properties of nucleons and hyperons in a lorentz covariant quark model. **Proceedings HYP** 74: 335–338.

Faessler, A., Thomas, G., Holstein, B., Lyubovitskij, V., Nicmorus, D., and Pumsa-ard, K. (2006b). Light baryon magnetic moments and $n \to \delta\gamma$ transition in a lorentz covariant chiral quark approach. **Phys. Rev. D** 74: 074010.

Faessler, A., Thomas, G., Lyubovitskij, V., and Oonariya, C. (2008). Depenence of baryon octet properties on pseudoscalar meson masses in the pertrubative chiral quark model. **J. Phys. G** 35: 025005.

Faessler, A., Thomas, G., Lyubovitskij, V., and Pumsa-ard, K. (2005). Chiral dynamics of baryons in a covariant quark model. **Prog. Part. Nucl. Phys.** 55: 12.

Faessler, A., Thomas, G., Lyubovitskij, V., and Pumsa-ard, K. (2006c). Chiral dynamics of baryons in a lorentz covariant quark model. **Phys. Rev. D** 73: 114021.

Gayou, O. et al. (2002). Measurement of g_{E_p}/g_{M_p} in $\vec{e}p \to \vec{e}p$ to $q^2 = 5.6\text{gev}^2$. **Phys. Rev. Lett.** 88: 092301.

Glazier, D. et al. (2005). Measurement of the electric form factor of the neutron at Q^2=0.3-0.8$(\text{GeV}/c)^2$. **Eur. Phys. J. A** 24: 101–109.

Golak, J., Ziemer, G., Kamada, H., Witala, H., and Glöckle, W. (2001). Extraction of electromagnetic neutron form factors through inclusive and exclusive polarized electron scattering on a polarized ^{3}He target. **Phys. Rev. C** 63: 034006.

Guerra, A. D. et al. (1976). Threshold π^+ electroproduction at high-momentum transfer: A determination of the nucleon axial vector form factor. **Nucl. Phys. B** 107: 65–81.

Gutsche, T. and Robson, D. (1989). Positive and convergent self-energy in a chiral potential model. **Phys. Lett. B** 229: 333.

Hanson, K. M., Dunning, J. R., Goitein, M., Kirk, T., Price, L. E., and Wilson, R. (1973). Large-angle quasielastic electron-deuteron scattering. **Phys. Rev. D** 8: 753–778.

Herberg, C. et al. (1999). Determination of the neutron electric form factor in the D($e,e\vec{n}$)p reaction and the influence of nuclear binding. **Eur. Phys. J. A** 5: 131–135.

Höhler, G. et al. (1976). Analysis of electromagnetic nucleon form factors. **Nucl. Phys. B** 114: 505–534.

Janssens, T., Hofstadter, R., Hughes, E. B., and Yearian, M. R. (1966). Proton form factors from elastic electron-proton scattering. **Phys. Rev.** 142: 922–931.

Jones, M. K. et al. (2006). Proton G_E/G_M from beam-target asymmetry. **Phys. Rev. C** 74: 035201.

Khosonthongkee, K. et al. (2004). Axial form factor of the nucleon in the perturbative chiral quark model. **J. Phys. G** 30: 793.

Kubon, G. et al. (2002). Precise neutron magnetic form factors. **Phys. Lett. B** 524: 26–32.

Kustom, R. L., Lundquist, D. E., Novey, T. B., Yokosawa, A., and Chilton, F. (1969). Quasielastic neutrino scattering. **Phys. Rev. Lett.** 22: 1014–1017.

Lachniet, J. et al. (2009). Precise measurement of the neutron magnetic form factor G_M^n in the few-gev^2 region. **Phys. Rev. Lett.** 102: 192001.

Lyubovitskij, V., Gutsche, T., and Faessler, A. (2001a). Electromagnetic structure of the nucleon in the perturbative chiral quark model. **Phys. Rev. C** 64: 065203.

Lyubovitskij, V., Gutsche, T., Faessler, A., and Drukarev, E. (2001b). Sigma-term physics in the perturbative chiral quark model. **Phys. Rev. D** 63: 054026.

Lyubovitskij, V., Gutsche, T., Faessler, A., and Vinh Mau, R. (2001c). πn scattering and electromagnetic corrections in the perturbative chiral quark model. **Phys. Lett. B** 520: 204.

Lyubovitskij, V., Gutsche, T., Faessler, A., and Vinh Mau, R. (2002a). Electromagnetic couplings of the chiral perturbation theory lagrangian from the perturbative chiral quark model. **Phys. Rev. C** 65: 025202.

Lyubovitskij, V., Wang, P., Gutsche, T., and Faessler, A. (2002b). Strange necleon form factors in the perturbative chiral quark model. **Phys. Rev. C** 66: 055204.

Madey, R. et al. (2003). Measurements of G_E^n/G_M^n from the ^{2}H($\vec{e},e'\vec{n}$)^{1}H reaction to Q^2=1.45(GeV/c)^2. **Phys. Rev. Lett.** 91: 122002.

Markowitz, P. et al. (1993). Measurement of the magnetic form factor of the neutron. **Phys. Rev. C** 48: R5–R9.

Milbrath, B. D. et al. (1998). Comparison of polarization observables in electron scattering from the proton and deuteron. **Phys. Rev. Lett.** 80: 452–455.

Murphy, J. J., Shin, Y. M., and Skopik, D. M. (1974). Proton form factor from 0.15 to 0.79 fm^{-2}. **Phys. Rev. C** 9: 2125–2129.

Nambu, Y. and Yoshimura, M. (1970). Axial-vector form factor of nucleon determined from threshold electropion production. **Phys. Rev. Lett.** 24: 25–28.

Oset, E., Tegen, R., and Weise, W. (1984). Nucleon charge form factors and chiral quark models. **Nucl. Phys. A** 426: 456.

Ostrick, M. et al. (1999). Measurement of the neutron electric form factor $G_{E,n}$ in the quasifree ^{2}H($\vec{e},e'\vec{n}$)^{1}p reaction. **Phys. Rev. Lett.** 83: 276–279.

Passchier, I. et al. (1999). Charge form factor of the neutron from the reaction ^{2}H($\vec{e},e'n$)p. **Phys. Rev. Lett.** 82: 4988–4991.

Plaster, B. et al. (2006). Measurements of the neutron electric to magnetic form factor ratio g_{En}/g_{Mn} via the $^2h(\vec{e}, e'\vec{n})^1h$ reaction to $q^2 = 1.45\text{gev}/\text{c}^2$. **Phys. Rev. C** 73: 025205.

Platchkov, S. et al. (1990). The deuteron $a(q^2)$ structure function and the neutron electric form factor. **Nucl. Phys. B** 510: 740–758.

Price, L. E., Dunning, J. R., Goitein, M., Hanson, K., Kirk, T., and Wilson, R. (1971). Backward-angle electron-eroton elastic scattering and proton electromagnetic form factors. **Phys. Rev. D** 4: 45–53.

Pumsa-ard, K., Lyubovitskij, V., Gutsche, T., Faessler, A., and Cheedket, S. (2003). Electromagnetic nucleon-delta transition in the perturbative chiral quark model. **Phys. Rev. C** 68: 015205.

Read, B. J. (1974). Threshold electroproduction experiments and the axial vector form factor. **Nucl. Phys. B** 74: 482–492.

Ron, G. et al. (2011). Low-Q^2 measurements of the proton form factor ratio $\mu_p g_e/g_m$. **Phys. Rev. C** 84: 055204.

Rosenbluth, M. N. (1950). High energy elastic scattering of electrons on protons. **Phys. Rev.** 79: 615–619.

Rotenberg, M. (1970). Theory and application of sturmian functions. **Adv. At. Mol. Phys.** 6: 233–268.

Scherer, S. (2003). Introduction to chiral perturbation theory. **Adv. Nucl. Phys.** 27: 277–538.

Simon, G. G., Schmitt, C., Borkowski, F., and Walther, V. H. (1980). Absolute

electron-proton cross sections at low momentum transfer measured with a high pressure gas target system. **Nucl. Phys. A** 333: 381–391.

Suebka, P. and Yan, Y. (2004). Accurate evaluation of pionium wave functions. **Phys. Rev. C** 70: 034006.

Théberge, S., Thomas, A. W., and Miller, G. A. (1980). Pionic corrections to the mit bag model: the (3,3) resonance. **Phys. Rev. D** 22: 2838.

Thomas, A. W. (1984). Chiral symmetry and the bag model: A new stating point for nuclear physics. **Adv. Nucl. Phy.** 416: 1–137.

Thomas, A. W., Théberge, S., and Miller, G. A. (1981). Pionic corrections to the mit bag model: the (3,3) resonance. **Phys. Rev. D** 24: 216.

Walker, R. C. et al. (1994). Measurements of the proton elastic form factors for $1 \leq Q^2 \leq 3$ (GeV/c)^2 at SLAC. **Phys. Rev. D** 49: 5671–5689.

Warren, G. et al. (2004). Measurement of the electric form factor of the neutron at $q^2 = 0.5$ and 1.0 (GeV/c)^2. **Phys. Rev. Lett.** 92: 042301.

Wilson, K. G. (1974). Confinement of quarks. **Phys. Rev. D** 10: 2445–2459.

Xu, W. et al. (2000). Transverse asymmetry $A_{T'}$ from the quasielastic ^{3}He($\vec{e},e'$) process and the neutron magnetic form factor. **Phys. Rev. Lett.** 85: 2900–2904.

Xu, W. et al. (2003). Plane-wave impulse approximation extraction of the neutron magnetic form factor from quasielastic ^{3}He($\vec{e},e'$) at $Q^2 = 0.3$ to 0.6 (GeV/c)^2. **Phys. Rev. C** 67: 012201.

Yan, Y., Tegen, R., Gutsche, T., and Faessler, A. (1997). Sturmian function approach and $\overline{N}n$ bound states. **Phys. Rev. C** 56: 1596–1604.

Zhan, X. et al. (2011). High-precision measurement of the proton elastic form factor ratio $\mu_p g_e / g_m$ at low q^2. **Phys. Lett. B** 705: 59–64.

Zhu, H. et al. (2001). Measurement of the electric form factor of the neutron through $\vec{d}(\vec{e}, e'\text{n})\text{p}$ at $Q^2 = 0.5(\text{GeV}/c)^2$. **Phys. Rev. Lett.** 87: 081801.

APPENDICES

APPENDIX A

STURMIAN FUNCTIONS

The Sturmian function method was first used in atomic physics to evaluate the binding energy and the wave function of atoms. It was pointed out that the method is more powerful than the approach using harmonic oscillator and hydrogen wave functions. Subsequently, the method was applied to various physical problems such as electromagnetic collisions, binding energies of nuclei and bound and resonance states in special potentials. In Refs. (Suebka and Yan, 2004) and (Yan et al., 1997), the protonium and pionium problems have been successfully investigated based on the Sturmian functions. The Sturmian functions are very similar to the hydrogen wave functions, and are therefore, also named Coulomb-Sturmian functions. In coordinate state space the Sturmian functions $S_{nl}(r)$, which are used in the present work, satisfy the second order differential equation

$$\left(\frac{d^2}{dr^2} - \frac{l(l+1)}{r^2} + \frac{2b(n+l+1)}{r} - b^2 \right) S_{nl}(r) = 0, \tag{A.1}$$

which is quite similar to the radial Schödinger equation for hydrogen atom satisfied $u(r) = rR(r)$

$$\left(\frac{d^2}{dr^2} - \frac{l(l+1)}{r^2} + \frac{\lambda^2}{r} - k^2 \right) u(r) = 0. \tag{A.2}$$

By solving Eq.(A.1), one finds

$$S_{nl}(r) = \left[\frac{n!}{(n+2l+1)!} \right]^{\frac{1}{2}} (2br)^{l+1} e^{-br} L_n^{2l+1}(2br), \tag{A.3}$$

where $L_n^{2l+1}(x)$ are associated Laguerre polynomials defined as

$$L_n^k(x) = (-1)^k \frac{d^k}{dx^k} \left[L_{n+k}(x) \right]. \tag{A.4}$$

that is

$$L_n^{2l+1}(2br) = \sum_{m=0}^{n} (-1)^m \frac{(n+2l+1)!}{(n-m)!(2l+1+m)!m!} (2br)^m. \tag{A.5}$$

The Sturmian functions are orthogonal and form a completes set with respect to the weight function $1/r$, which follows from the corresponding $1/r$ potential term in Equation (A.3)

$$\int_0^\infty r^2 dr \frac{S_{nl}(r)}{r} \frac{1}{r} \frac{S_{n'l}(r)}{r} = \delta_{nn'}. \tag{A.6}$$

Because almost all bound-state hydrogen state functions are close to zero energy, the innermost zeros of the functions are insensitive to the principle quantum number (see Figure A.1). This accounts for that the bound hydrogen functions do not form a complete set; the continuum is needed to analyze the region between the origin and the limiting first zero. Unlike hydrogen functions, the first node of the Sturmian functions continues to move closer to the origin with increasing the principle number n as shown in Figure A.2. This is the key point why a short-ranged nuclear force can easily be taken into account for $\bar{N}N$ atomic state problem by using complete sets of the Sturmian functions (Yan et al., 1997).
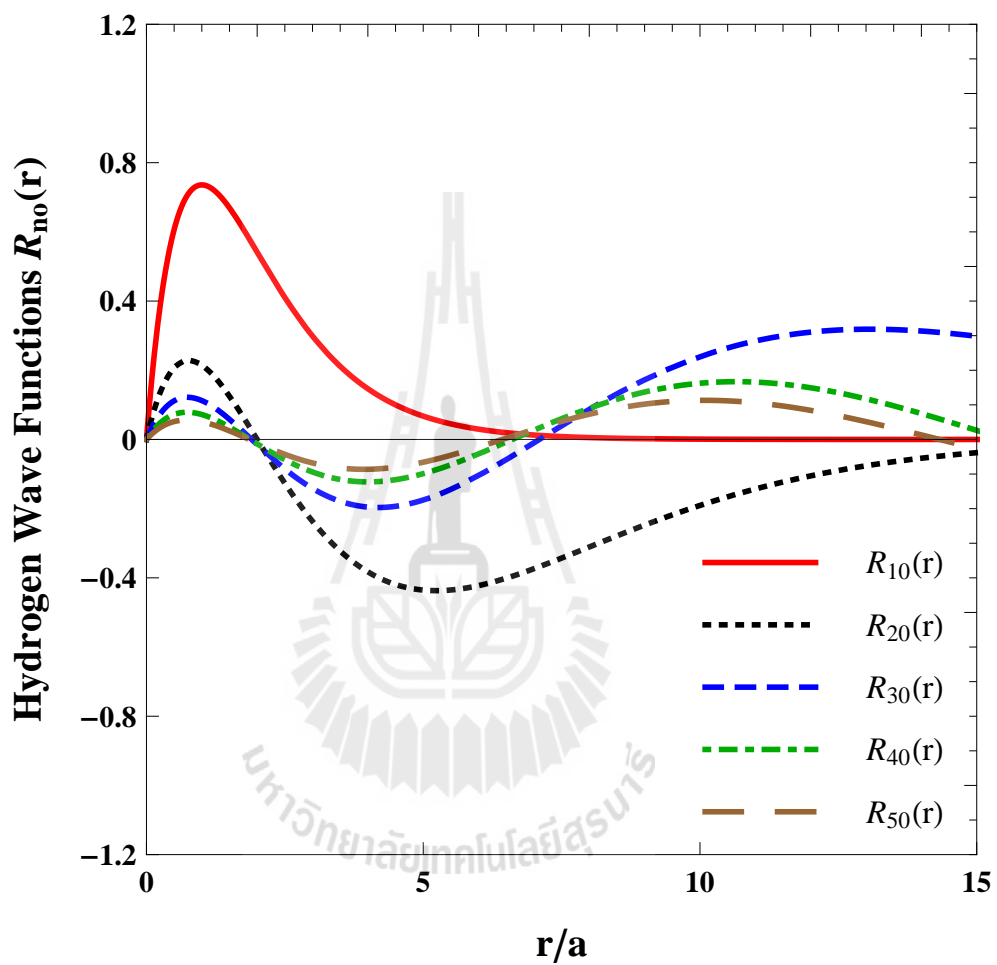
Figure A.1 The $l = 0$ hydrogen wave functions for $n = 1$, 2, 3, 4 and 5. The innermost zeros of the functions are insensitive to the principle quantum number n.
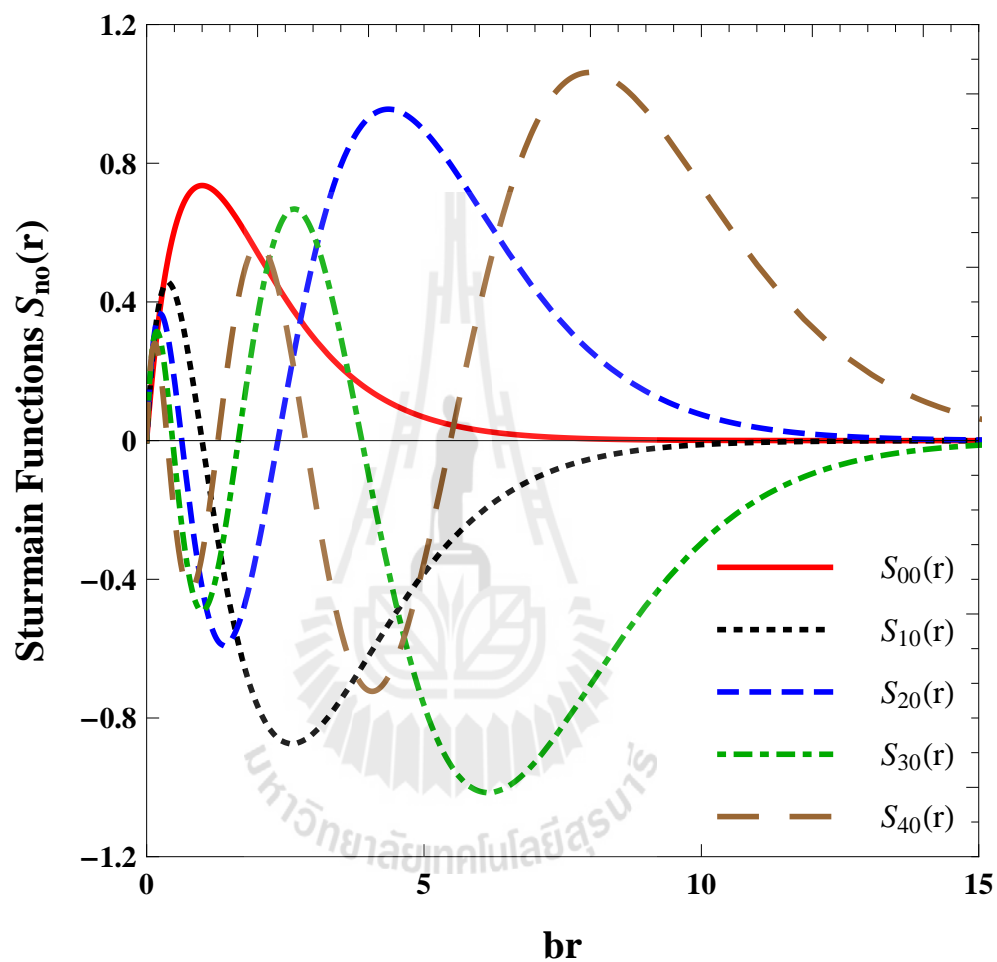
Figure A.2 The $l = 0$ Sturmian functions for $n = 0, 1, 2, 3$ and 4. Unlike hydrogen functions, the first nodes continue to move to the origin with increasing n.

APPENDIX B

GELL-MANN AND LOW THEOREM

The Gell-Mann and Low theorem was proved by Murray Gell-Mann and Francis E. Low in 1951. It is a theorem in quantum field theory that allows one to relate the ground (or vacuum) state of an interacting system to the ground state of the corresponding non-interacting theory. We consider a system described by the Hamiltonian H which might be written as

$$H = H_0 + H_I, \tag{B.1}$$

where H_0 and H_I are respectively the free and interaction parts of the Hamiltonian. Let $|\psi_0\rangle$ and $|n\rangle$ be the eigenstates of the free and full Hamiltonian, respectively. One has

$$H|n\rangle = E^{(n)}|n\rangle,$$

$$H_0|\psi_0\rangle = E_0|\psi_0\rangle, \tag{B.2}$$

hence

$$
\begin{aligned}
e^{-\mathrm{i}Ht}|\psi_0\rangle &= \sum_n e^{-\mathrm{i}E^{(n)}t}|n\rangle\langle n|\psi_0\rangle \\
&= e^{-\mathrm{i}Et}|\psi\rangle\langle\psi|\psi_0\rangle + \sum_{n\neq 0} e^{-\mathrm{i}E^{(n)}t}|n\rangle\langle n|\psi_0\rangle,
\end{aligned} \tag{B.3}
$$

here we have rewritten ground eigenstate $|0\rangle$ and ground eigenvalue $E^{(0)}$ in the above equation respectively as $|\psi\rangle$ and E, that is

$$H|\psi\rangle = E|\psi\rangle. \tag{B.4}$$

Multiplying the above equation by $e^{iE_0 t}$, one derives

$$e^{iE_0 t} e^{iHt}|\psi_0\rangle = e^{i(E-E_0)t}|\psi\rangle\langle\psi|\psi_0\rangle + \sum_{n\neq 0} e^{-i(E^{(n)}-E_0)t}|n\rangle\langle n|\psi_0\rangle. \tag{B.5}$$

Since $E^{(n)} > E$ for all $n \neq 0$, we can get rid of all the $n \neq 0$ terms in the series by sending t to ∞ in a slightly imaginary direction $t \to \infty(1 - i\varepsilon)$. Then the exponential factor $e^{-i(E-E_0)t}$ dies slowest and we have

$$\begin{aligned}
|\psi\rangle &= \lim_{t\to\infty(1-i\varepsilon)} \frac{e^{iH(-t)}e^{-iH_0(-t)}|\psi_0\rangle}{e^{-i(E-E_0)t}\langle\psi|\psi_0\rangle} \\
&= \lim_{t\to\infty(1-i\varepsilon)} \frac{U(0,-t)|\psi_0\rangle}{e^{-i(E-E_0)t}\langle\psi|\psi_0\rangle}.
\end{aligned} \tag{B.6}$$

here we have used

$$U(t_0, t) = e^{iH(t-t_0)}e^{-iH_0(t-t_0)}. \tag{B.7}$$

In the same way, we can derive

$$\langle\psi| = \lim_{t\to\infty(1-i\varepsilon)} \frac{\langle\psi_0|U(t,0)}{e^{-i(E-E_0)t}\langle\psi_0|\psi\rangle}. \tag{B.8}$$

Now we evaluate the expectation value of the operator $O(x) \equiv O(x^0, \vec{x})$ in the state $|\psi\rangle$

$$\begin{aligned}
\langle\psi|O(x^0, \vec{x})|\psi\rangle &= \lim_{t\to\infty(1-i\varepsilon)} \frac{\langle\psi_0|U(t,0)U^\dagger(x^0,0)O_I(x)U(x^0,0)U(0,-t)|\psi_0\rangle}{e^{-i(E-E_0)t}\langle\psi_0|\psi\rangle e^{-i(E-E_0)t}\langle\psi|\psi_0\rangle} \\
&= \lim_{t\to\infty(1-i\varepsilon)} \frac{\langle\psi_0|U(t,x^0)O_I(x)U(x^0,-t)|\psi_0\rangle}{e^{-2i(E-E_0)t}|\langle\psi_0|\psi\rangle|^2}.
\end{aligned} \tag{B.9}$$

To get rid of the denominator in the equation, one may divide it by 1 in the form

$$1 = \langle\psi|\psi\rangle = \lim_{t\to\infty(1-i\varepsilon)} \frac{\langle\psi_0|U(t,0)U(0,-t)|\psi_0\rangle}{e^{-2i(E-E_0)t}|\langle\psi_0|\psi\rangle|^2}. \tag{B.10}$$

Then finally we derive

$$\langle\psi|O(x^0,\vec{x})|\psi\rangle = \lim_{t\to\infty(1-i\varepsilon)} \frac{\langle\psi_0|U(t,x^0)O_I(x)U(x^0,-t)|\psi_0\rangle}{\langle\psi_0|U(t,-t)|\psi_0\rangle}. \tag{B.11}$$

The above equation holds for a product of arbitrarily many operators, for example, for two operators

$$\langle\psi|T[O(x)P(x)]|\psi\rangle = \lim_{t\to\infty(1-i\varepsilon)} \frac{\langle\psi_0|T\{O_I(x)P_I(x)\exp[-i\int_{-t}^{t}dzH_I(z)]\}|\psi_0\rangle}{\langle\psi_0|T\{\exp[-i\int_{-t}^{t}dzH_I(z)]\}|\psi_0\rangle}. \tag{B.12}$$

APPENDIX C

CALCULATION OF THE DIAGRAMS FOR

THE CHARGE FORM FACTOR

In the framework of the PCQM, the charge form factors of octet baryons in the Breit frame are defined by

$$\chi_{B'_s}^\dagger \chi_{B_s} G_E^B(Q^2) = {}^B\langle\phi_0| \sum_{n=0}^{2} \frac{i^n}{n!} \int \delta(t) d^4x d^4x_1 \cdots d^4x_n e^{-iq\cdot x}$$

$$\times T[\mathcal{L}_I^W(x_1) \cdots \mathcal{L}_I^W(x_n) j^0(x)]|\phi_0\rangle_c^B, \qquad (C.1)$$

where χ_{B_s} and $\chi_{B'_s}^\dagger$ are the baryon spin wavefunctions in the initial and final states. We assume they are spin-up states, so

$$\chi_{B'_s}^\dagger \chi_{B_s} = 1. \qquad (C.2)$$

In calculation, the upper and lower component quark wave functions are expanded into a completed basis of Sturmian functions in Equations (2.15) and (2.16). We employ the fermion and boson Feymann propagators as following:

$$\overbrace{\psi(x)\bar\psi(y)} = \langle\phi_0|T\{\psi(x)\bar\psi(y)\}|\phi_0\rangle$$

$$= u_0(\vec{x})u_0(\vec{y}) \exp[-i\mathcal{E}_0(x_0 - y_0)]\theta(x_0 - y_0), \qquad (C.3)$$

$$\overbrace{\Phi_i(x)\Phi_j(y)} = \langle 0|T\{\Phi_i(x)\Phi_j(y)\}|0\rangle$$

$$= \delta_{ij} \int \frac{d^4k}{(2\pi)^4 i} \frac{\exp[-ik(x - y)]}{M_\Phi^2 - k^2 - i\epsilon}, \qquad (C.4)$$

here the fermion propagator is restricted on the ground state only.

C.1 Leading Order Diagram (LO)

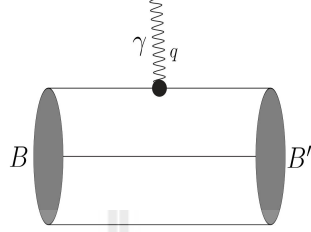**Figure C.1** Leading order diagram.

$$
\begin{aligned}
G_E^B(Q^2)\big|_{LO} &= {}^B\langle\phi_0|\mathcal{Q}\int\delta(t)d^4xe^{-\mathrm{i}qx}j_\psi^0(x)|\phi_0\rangle^B \\[2mm]
&= {}^B\langle\phi_0|\mathcal{Q}\int\delta(t)d^4xe^{-\mathrm{i}qx}\bar\psi(x)\gamma^0\psi(x)|\phi_0\rangle^B \\[2mm]
&= {}^B\langle\phi_0|b_0^\dagger\mathcal{Q}\int d^3xe^{\mathrm{i}\vec{q}\cdot\vec{x}}\bar u_0(x)\gamma^0 u_0(x)b_0|\phi_0\rangle^B \\[2mm]
&= a_1^B G_E^p(Q^2)\big|_{3q}^{LO},
\end{aligned}
\tag{C.5}
$$

where

$$
G_E^p(Q^2)\big|_{LO} = 2\pi\int_0^\infty dr\int_0^\pi d\theta r^2\sin\theta[g(r)^2+f(r)^2]e^{\mathrm{i}Qr\cos\theta},
\tag{C.6}
$$

$$
\begin{aligned}
a_1^B &= {}^B\langle\phi_0|b_0^\dagger\chi_{f'}\sum_{i=1}^3\mathcal{Q}(i)\chi_f b_0|\phi_0\rangle^B \\[2mm]
&= \langle B\uparrow|\sum_{i=1}^3\mathcal{Q}(i)|B\uparrow\rangle.
\end{aligned}
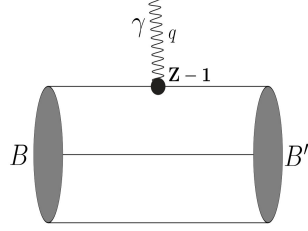\tag{C.7}
$$

C.2 Counterterm Diagram (CT)

Figure C.2 Counterterm diagram.

$$
\begin{aligned}
G_E^B(Q^2)\Big|_{CT} &= {}^B\langle\phi_0|\mathcal{Q}\int\delta(t)d^4xe^{-iqx}\delta j_\psi^0(x)|\phi_0\rangle^B \\[2mm]
&= {}^B\langle\phi_0|\mathcal{Q}\int\delta(t)d^4xe^{-iqx}\bar{\psi}(x)(Z-1)\gamma^0\psi(x)|\phi_0\rangle^B \\[2mm]
&= \Big[a_2^B(\hat{Z}-1)+a_3^B(Z_s-1)\Big]G_E^p(Q^2)\big|_{3q}^{LO},
\end{aligned}
\tag{C.8}
$$

where

$$
\begin{aligned}
a_2^B &= {}^B\langle\phi_0|b_0^\dagger\chi_{f'}\sum_{i=1}^3\hat{\mathcal{Q}}(i)\chi_f b_0|\phi_0\rangle^B \\[2mm]
&= \langle B\uparrow|\sum_{i=1}^3\hat{\mathcal{Q}}(i)|B\uparrow\rangle,
\end{aligned}
\tag{C.9}
$$

$$
\begin{aligned}
a_3^B &= {}^B\langle\phi_0|b_0^\dagger\chi_{f'}\sum_{i=1}^3\mathcal{Q}_s(i)\chi_f b_0|\phi_0\rangle^B \\[2mm]
&= \langle B\uparrow|\sum_{i=1}^3\mathcal{Q}_s(i)|B\uparrow\rangle,
\end{aligned}
\tag{C.10}
$$

$$\hat{\mathcal{Q}} \;=\; \begin{pmatrix} 2/3 & 0 & 0 \\ 0 & -1/3 & 0 \\ 0 & 0 & 0 \end{pmatrix}, \tag{C.11}$$

$$\mathcal{Q}_s \;=\; \begin{pmatrix} 0 & 0 & 0 \\ 0 & 0 & 0 \\ 0 & 0 & -1/3 \end{pmatrix}. \tag{C.12}$$
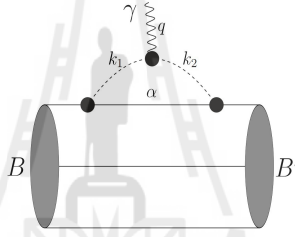
C.3   Meson Cloud Diagram (MC)

Figure C.3 Meson Cloud Diagram.

$$G_E^B(Q^2)\Big|_{MC}^{\alpha}$$

$$= \;\; {}^B\langle\phi_0|\frac{\mathrm{i}^2}{2!}\int \delta(t)d^4x\,d^4x_1\,d^4x_2\,e^{-\mathrm{i}qx}T\Big[\mathcal{L}_I^W(x_1)\mathcal{L}_I^W(x_2)j_\Phi^0(x)\Big]|\phi_0\rangle^B$$

$$= \;\; 4\,{}^B\langle\phi_0|\frac{-1}{2}\int \delta(t)d^4x\,d^4x_1\,d^4x_2\,e^{-\mathrm{i}qx}$$

$$\times N\Big\{\Big[\frac{1}{2F}\partial_\mu\Phi_i\bar\psi\gamma^\mu\gamma^5\lambda_i\psi\Big]_{x_1}\Big[(f_{3kl}+\frac{f_{8kl}}{\sqrt{3}})\Phi_k\frac{\partial}{\partial t}\Phi_l\Big]_x\Big[\frac{1}{2F}\partial_\nu\Phi_j\bar\psi\gamma^\nu\gamma^5\lambda_j\psi\Big]_{x_2}\Big\}$$

$$\times|\phi_0\rangle^B$$

$$= \;\; \frac{-i}{2F^2(2\pi)^8}\,{}^B\langle\phi_0|b_0^\dagger\int d^3x_1\,d^3x_2\,d^4k_1\,d^4k_2\frac{e^{-i\vec{k}_1\cdot\vec{x}_1}}{M_\Phi^2-k_1^2-i\epsilon}\frac{e^{-i\vec{k}_2\cdot\vec{x}_2}}{M_\Phi^2-k_2^2-i\epsilon}$$

$$\times(f_{3ij}+\frac{f_{8ij}}{\sqrt{3}})\bar{u}_0(x_1)\gamma^\mu k_{1\mu}\gamma^5\lambda_i u_\alpha(x_1)\bar{u}_\alpha(x_2)\gamma^\nu k_{2\nu}\gamma^5 k_2^0\lambda_j u_0(x_2)$$

$$\times \int dt\, dt_1 dt_2\, \delta t\, \Theta(t_1 - t_2) e^{-iqt} e^{-i\varepsilon_0(t_2 - t_1)} e^{-i\varepsilon_\alpha(t_1 - t_2)} e^{-ik_1^0(t_1 - t)} e^{-ik_2^0(t - t_2)}$$

$$\times \int d^3x\, e^{-i(\vec{k}_1 - \vec{k}_2 - \vec{q})\cdot\vec{x}} b_0 |\phi_0\rangle^B$$

$$= -\frac{(f_{3ij} + \frac{f_{8ij}}{\sqrt{3}})}{2F^2(2\pi)^4} {}^B\langle\phi_0|b_0^\dagger \int d^3x_1 d^3x_2 d^3k_1 d^3k_2\, \delta(\vec{k}_1 - \vec{k}_2 - \vec{q})$$

$$\times \int dk_1^0 dk_2^0 \frac{\delta(k_1^0 - k_2^0)}{[\omega_\Phi(k_1^2) - (k_1^0)^2 - i\epsilon][\omega_\Phi(k_2^2) - (k_2^0)^2 - i\epsilon][\Delta\varepsilon_\alpha + k_1^0 - i\epsilon]}$$

$$\times \Big[(k_2^0)^3 \bar{u}_0(x_1)\gamma^0\gamma^5\lambda_i u_\alpha(x_1)\bar{u}_\alpha(x_2)\gamma^0\gamma^5\lambda_j u_0(x_2)$$

$$-(k_2^0)^2 \bar{u}_0(x_1)\gamma^0\gamma^5\lambda_i u_\alpha(x_1)\bar{u}_\alpha(x_2)\vec{\gamma}\cdot\vec{k}_2\gamma^5\lambda_j u_0(x_2)$$

$$-(k_2^0)^2 \bar{u}_0(x_1)\vec{\gamma}\cdot\vec{k}_1\gamma^5\lambda_i u_\alpha(x_1)\bar{u}_\alpha(x_2)\gamma^0\gamma^5\lambda_j u_0(x_2)$$

$$+k_2^0 \bar{u}_0(x_1)\vec{\gamma}\cdot\vec{k}_1\gamma^5\lambda_i u_\alpha(x_1)\bar{u}_\alpha(x_2)\vec{\gamma}\cdot\vec{k}_2\gamma^5\lambda_j u_0(x_2)\Big] b_0 |\phi_0\rangle^B$$

$$= \frac{i}{4F^2(2\pi)^3} {}^B\langle\phi_0|b_0^\dagger \int d^3k_2 \frac{f_{3ij} + \frac{f_{8ij}}{\sqrt{3}}}{[\omega_\Phi(k_2'^2) + \omega_\Phi(k_2^2)][\omega_\Phi(k_2'^2) + \Delta\varepsilon_\alpha][\omega_\Phi(k_2^2) + \Delta\varepsilon_\alpha]}$$

$$\times \Big\{ \Big[\omega_\Phi(k_2'^2)\omega_\Phi(k_2^2) + (\omega_\Phi(k_2'^2) + \omega_\Phi(k_2^2))\Delta\varepsilon_\alpha\Big]$$

$$\times \int d^3x_1 \bar{u}_0(x_1)\gamma^0\gamma^5\lambda_i u_\alpha(x_1)e^{i\vec{k}_2'\cdot\vec{x}_1} \int d^3x_2 \bar{u}_\alpha(x_2)\gamma^0\gamma^5\lambda_j u_0(x_2)e^{-i\vec{k}_2\cdot\vec{x}_2}$$

$$-\Delta\varepsilon_\alpha \int d^3x_1 \bar{u}_0(x_1)\gamma^0\gamma^5\lambda_i u_\alpha(x_1)e^{i\vec{k}_2'\cdot\vec{x}_1} \int d^3x_2 \bar{u}_\alpha(x_2)\vec{\gamma}\cdot\vec{k}_2\gamma^5\lambda_j u_0(x_2)e^{-i\vec{k}_2\cdot\vec{x}_2}$$

$$-\Delta\varepsilon_\alpha \int d^3x_1 \bar{u}_0(x_1)\vec{\gamma}\cdot\vec{k}_2'\gamma^5\lambda_i u_\alpha(x_1)e^{i\vec{k}_2'\cdot\vec{x}_1} \int d^3x_2 \bar{u}_\alpha(x_2)\gamma^0\gamma^5\lambda_j u_0(x_2)e^{-i\vec{k}_2\cdot\vec{x}_2}$$

$$-\int d^3x_1 \bar{u}_0(x_1)\vec{\gamma}\cdot\vec{k}_2'\gamma^5\lambda_i u_\alpha(x_1)e^{i\vec{k}_2'\cdot\vec{x}_1} \int d^3x_2 \bar{u}_\alpha(x_2)\vec{\gamma}\cdot\vec{k}_2\gamma^5\lambda_j u_0(x_2)e^{-i\vec{k}_2\cdot\vec{x}_2}\Big\}$$

$$\times b_0 |\phi_0\rangle^B$$

$$= \frac{i}{4F^2(2\pi)^3} {}^B\langle\phi_0|b_0^\dagger \chi_c^\dagger \chi_f^\dagger \chi_s^\dagger \int d^3k_2$$

$$\times \frac{1}{[\omega_\Phi(k_2'^2) + \omega_\Phi(k_2^2)][\omega_\Phi(k_2'^2) + \Delta\varepsilon_\alpha][\omega_\Phi(k_2^2) + \Delta\varepsilon_\alpha]}$$

$$\times \Big\{ \big[\omega_\Phi(k_2'^2)\omega_\Phi(k_2^2) + (\omega_\Phi(k_2'^2) + \omega_\Phi(k_2^2))\Delta\varepsilon_\alpha\big] F_{I\alpha}(k_2') F_{I\alpha}^\dagger(k_2)$$

$$-\Delta\varepsilon_\alpha F_{I\alpha}(k_2') F_{II\alpha}^\dagger(k_2) - \Delta\varepsilon_\alpha F_{II\alpha}(k_2') F_{I\alpha}^\dagger(k_2) - F_{II\alpha}(k_2') F_{II\alpha}^\dagger(k_2) \Big\}$$

$$\times (f_{3ij} + \frac{f_{8ij}}{\sqrt{3}})[(\vec{\sigma} \cdot \vec{k}_2')\lambda_i]_{0,\alpha}[(\vec{\sigma} \cdot \vec{k}_2)\lambda_j]_{\alpha,0} \chi_s \chi_f \chi_c b_0 |\phi_0\rangle^B \qquad \text{(C.13)}$$

where $\Delta\varepsilon_\alpha = \varepsilon_\alpha - \varepsilon_0$, $\vec{k}_2' = \vec{k}_1 + \vec{q}$ and $\omega_\Phi(k^2) = \sqrt{M_\Phi^2 + k^2}$,

$$\int d^3x \bar{u}_0(x)\gamma^0\gamma^5\lambda_i u_\alpha(x)e^{i\vec{k}\cdot\vec{x}} = F_{I\alpha}(k)\chi_c^\dagger\chi_f^\dagger\chi_s^\dagger[\vec{\sigma} \cdot \vec{k}\lambda_i]_{0,\alpha}\chi_s\chi_f\chi_c, \qquad \text{(C.14)}$$

$$\int d^3x_1 \bar{u}_0(x)\vec{\gamma} \cdot \vec{k}\gamma^5\lambda_i u_\alpha(x)e^{i\vec{k}\cdot\vec{x}} = F_{II\alpha}(k)\chi_c^\dagger\chi_f^\dagger\chi_s^\dagger[\vec{\sigma} \cdot \vec{k}\lambda_i]_{0,\alpha}\chi_s\chi_f\chi_c, \qquad \text{(C.15)}$$

with

$$F_{I\alpha}(k) = \int_0^\infty dr r[g_0(r)f_\alpha(r) - f_0(r)g_\alpha(r)]\frac{\partial}{\partial k}\int_\Omega d\Omega e^{ikr\cos\theta}\mathcal{C}_\alpha Y_{l_\alpha 0}(\theta,\phi),$$

$$\text{(C.16)}$$

$$F_{II\alpha}(k) = \int_0^\infty dr r^2[g_0(r)g_\alpha(r) - f_0(r)f_\alpha(r)]\int_\Omega d\Omega e^{ikr\cos\theta}\mathcal{C}_\alpha Y_{l_\alpha 0}(\theta,\phi)$$

$$-2i\frac{\partial}{\partial k}\int_0^\infty dr r f_0(r)f_\alpha(r)\int_\Omega d\Omega \cos\theta e^{ikr\cos\theta}\mathcal{C}_\alpha Y_{l_\alpha 0}(\theta,\phi). \qquad \text{(C.17)}$$

We define $x = \cos\theta = \frac{\vec{q}\cdot\vec{k}_2}{|\vec{q}||\vec{k}_2|}$, $k = |\vec{k}_2|$, $Q = |\vec{q}|$ and

$$k_\pm = |\vec{q} \pm \vec{k}_2| = \sqrt{k^2 + Q^2 \pm 2kQx}, \qquad \text{(C.18)}$$

$$\int d^3k_2 = \int_0^\infty dk k^2 \int_{-1}^1 dx \int_0^{2\pi} d\phi. \qquad \text{(C.19)}$$

We obtain the expression of $G_E^B(Q^2)\big|_{MC}^\alpha$ as

$$G_E^B(Q^2)\big|_{MC}^\alpha = -\frac{1}{2(2\pi F)^2}\int_0^\infty dk \int_{-1}^1 dx k^2(k^2 + kQx)$$

$$\times \Bigg\{ \Big[\omega_\Phi(k_+^2)\omega_\Phi(k^2) + (\omega_\Phi(k_+^2) + \omega_\Phi(k_2^2))\Delta\varepsilon_\alpha \Big] F_{I\alpha}(k_+)F_{I\alpha}^\dagger(k)$$

$$-\Delta\varepsilon_\alpha F_{I\alpha}(k_+)F_{II\alpha}^\dagger(k) - \Delta\varepsilon_\alpha F_{II\alpha}(k_+)F_{I\alpha}^\dagger(k) - F_{II\alpha}(k_+)F_{II\alpha}^\dagger(k) \Bigg\}$$

$$\times \frac{^B\langle\phi_0|b_0^\dagger\chi_c^\dagger\chi_f^\dagger\chi_s^\dagger\frac{-i}{2}(f_{3ij} + \frac{f_{8ij}}{\sqrt{3}})\lambda_i\lambda_j\chi_s\chi_f\chi_c b_0|\phi_0\rangle^B}{[\omega_\Phi(k_+^2) + \omega_\Phi(k^2)][\omega_\Phi(k_+^2) + \Delta\varepsilon_\alpha][\omega_\Phi(k^2) + \Delta\varepsilon_\alpha]}. \tag{C.20}$$

In our calculation, the quark propagator is restricted on the ground state only, i.e. $\alpha = 0$. Hence, we have $\Delta\varepsilon_\alpha = 0$, $F_{I0}(k^2) = 0$ and

$$F_{II}(k) = 2\pi \int_0^\infty dr \int_0^\pi d\theta r^2 (g_0(r)^2 + f_0(r)^2\cos 2\theta)\sin\theta e^{ikr\cos\theta}, \tag{C.21}$$

Finally

$$G_E^B(Q^2)\big|_{MC} = \frac{1}{2(2\pi F)^2} \int_0^\infty dk \int_{-1}^1 dx k^2(k^2 + kQx)F_{II}(k)F_{II}(k_+)$$
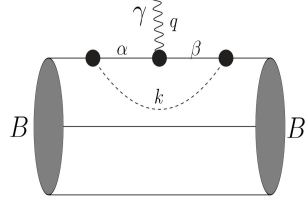
$$\times [a_4^B C_\pi(k^2, Q^2, x) + a_5^B C_K(k^2, Q^2, x)], \tag{C.22}$$

where

$$C_\Phi(k^2, Q^2, x) = \frac{1}{\omega_\Phi(k^2)\omega_\Phi(k_+^2)[\omega_\Phi(k^2) + \omega_\Phi(k_+^2)]}, \tag{C.23}$$

$$a_4^B = \sum_{i,j=1}^3 {}^B\langle\phi_0|b_0^\dagger\chi_{f'}^\dagger - \frac{i}{2}(f_{3ij} + \frac{f_{8ij}}{\sqrt{3}})\lambda_i\lambda_j\chi_f b_0|\phi_0\rangle^B$$

$$= \sum_{i,j=1}^3 \langle B| \sum_{k=1}^3 -\frac{i}{2}(f_{3ij} + \frac{f_{8ij}}{\sqrt{3}})\lambda_i(k)\lambda_j(k)|B\rangle, \tag{C.24}$$

$$a_5^B = \sum_{i,j=4}^7 \langle B| \sum_{k=1}^3 -\frac{i}{2}(f_{3ij} + \frac{f_{8ij}}{\sqrt{3}})\lambda_i(k)\lambda_j(k)|B\rangle. \tag{C.25}$$

C.4   Vertex Correction Diagram (VC)

Figure C.4 Vertex Correction Diagram.

$$G_E^B(Q^2)\Big|_{VC}^{\alpha}$$

$$= {}^B\langle\phi_0|\frac{\mathrm{i}2}{2!}\int\delta(t)d^4xd^4x_1d^4x_2e^{-\mathrm{i}qx}T\Big[\mathcal{L}_I^W(x_1)\mathcal{L}_I^W(x_2)j_\psi^0(x)\Big]|\phi_0\rangle^B$$

$$= 2\,{}^B\langle\phi_0|\frac{-1}{2}\int\delta(t)d^4xd^4x_1d^4x_2e^{-\mathrm{i}qx}$$

$$\times N\Big\{\Big[\frac{1}{2F}\partial_\mu\Phi_i\bar{\psi}\gamma^\mu\gamma^5\lambda_i\psi\Big]_{x_1}\Big[\bar{\psi}\gamma^0\mathcal{Q}\psi\Big]_x\Big[\frac{1}{2F}\partial_\nu\Phi_j\bar{\psi}\gamma^\nu\gamma^5\lambda_j\psi\Big]_{x_2}\Big\}|\phi_0\rangle^B$$

$$= \frac{i}{4F^2(2\pi)^4}\,{}^B\langle\phi_0|b_0^\dagger\int d^3xd^3x_1d^3x_2d^4ke^{i\vec{q}\cdot\vec{x}}\frac{e^{i\vec{k}\cdot(\vec{x}_1-\vec{x}_2)}}{M_\Phi^2-k^2-i\epsilon}$$

$$\times\bar{u}_0(x_1)\gamma^\mu k_\mu\gamma^5\lambda_i u_\alpha(x_1)\bar{u}_\alpha(x)\gamma^0\mathcal{Q}u_\beta(x)\bar{u}_\beta(x_2)\gamma^\nu k_\nu\gamma^5\lambda_i u_0(x_2)$$

$$\times\int dtdt_1dt_2\delta t\Theta(t_1-t)\Theta(t-t_2)e^{-iqt}e^{-i\varepsilon_0(t_2-t_1)}e^{-i\varepsilon_\alpha(t_1-t)}$$

$$\times e^{-i\varepsilon_\beta(t-t_2)}e^{-ik_0(t_1-t_2)}b_0|\phi_0\rangle^B$$

$$= \frac{-i}{4F^2(2\pi)^4}\,{}^B\langle\phi_0|b_0^\dagger d^3xd^3x_1d^3x_2d^3ke^{i\vec{q}\cdot\vec{x}}e^{i\vec{k}\cdot(\vec{x}_1-\vec{x}_2)}$$

$$\times\int dk_0\frac{1}{[\omega_\Phi(k^2)-(k_0)^2-i\epsilon][k_0+\Delta\varepsilon_\alpha-i\eta][k_0+\Delta\varepsilon_\beta-i\eta]}$$

$$\times\bar{u}_0(x_1)(\gamma^0 k_0-\vec{\gamma}\cdot\vec{k})\gamma^5\lambda_i u_\alpha(x_1)\bar{u}_\alpha(x)\gamma^0\mathcal{Q}u_\beta(x)$$

$$\times\bar{u}_\beta(x_2)(\gamma^0 k_0-\vec{\gamma}\cdot\vec{k})\gamma^5\lambda_i u_0(x_2)b_0|\phi_0\rangle^B$$

$$
= \left. \frac{G_E^p(Q^2)\big|_{LO}^{\alpha}}{8F^2(2\pi)^3} \right. {}^B\langle\phi_0|b_0^\dagger\chi_c^\dagger\chi_f^\dagger\chi_s^\dagger \int d^3k \frac{1}{\omega_\Phi(k^2)[\omega_\Phi(k^2)+\Delta\varepsilon_\alpha]^2}
$$

$$
\times\Big[\omega_\Phi^2(k^2)F_{I\alpha}(k)F_{I\alpha}^\dagger(k) - \omega_\Phi(k^2)F_{I\alpha}(k)F_{II\alpha}^\dagger(k) - \omega_\Phi(k^2)F_{II\alpha}(k)F_{I\alpha}^\dagger(k)
$$

$$
+F_{II\alpha}(k)F_{II\alpha}^\dagger(k)\Big][(\vec{\sigma}\cdot\vec{k})\lambda_i]_{0,\alpha}\mathcal{Q}_{\alpha\alpha}[(\vec{\sigma}\cdot\vec{k})\lambda_i]_{\alpha,0}\chi_s\chi_f\chi_c b_0|\phi_0\rangle^B, \qquad (C.26)
$$

where

$$
\int d^3x\, \bar{u}_\alpha(x)\gamma^0\mathcal{Q}u_\beta(x)e^{i\vec{q}\cdot\vec{x}} = \delta_{\alpha\beta}G_E^p(Q^2)\big|_{LO}^{\alpha}\chi_c^\dagger\chi_f^\dagger\chi_s^\dagger\mathcal{Q}_{\alpha\beta}\chi_s\chi_f\chi_c. \qquad (C.27)
$$

Finally, we have

$$
G_E^B(Q^2)\big|_{VC}^{\alpha}
$$

$$
= \frac{1}{4(2\pi F)^2}G_E^p(Q^2)\big|_{LO}^{\alpha}\int dk\,k^4\Big[\omega_\Phi^2(k^2)F_{I\alpha}(k)F_{I\alpha}^\dagger(k)
$$

$$
-\omega_\Phi(k^2)F_{I\alpha}(k)F_{II\alpha}^\dagger(k) - \omega_\Phi(k^2)F_{II\alpha}(k)F_{I\alpha}^\dagger(k) + F_{II\alpha}(k)F_{II\alpha}^\dagger(k)\Big]
$$

$$
\times\frac{{}^B\langle\phi_0|b_0^\dagger\chi_c^\dagger\chi_f^\dagger\chi_s^\dagger\lambda_i\mathcal{Q}\lambda_i\chi_s\chi_f\chi_c b_0|\phi_0\rangle^B}{\omega_\Phi(k^2)[\omega_\Phi(k^2)+\Delta\varepsilon_\alpha]^2}. \qquad (C.28)
$$

For the case $\alpha = 0$, we obtain

$$
G_E^B(Q^2)\big|_{VC} = \frac{1}{4(2\pi F)^2}G_E^p(Q^2)\big|_{LO}\int_0^\infty dk\,k^4 F_{II}^2(k)
$$

$$
\times\left[\frac{a_6^B}{\omega_\pi^3(k^2)} + \frac{a_7^B}{\omega_K^3(k^2)} + \frac{a_8^B}{\omega_\eta^3(k^2)}\right], \qquad (C.29)
$$

where

$$
a_6^B = {}^B\langle\phi_0|b_0^\dagger\chi_c^\dagger\chi_f^\dagger\chi_s^\dagger\lambda_i\mathcal{Q}\lambda_i\chi_s\chi_f\chi_c b_0|\phi_0\rangle^B
$$

$$
= \sum_{i=1}^3\langle B|\sum_{k=1}^3[\lambda_i\mathcal{Q}\lambda_i]^{(k)}|B\rangle
$$

$$a_7^B = \sum_{i=4}^{7} \langle B| \sum_{k=1}^{3} [\lambda_i \mathcal{Q} \lambda_i]^{(k)} |B\rangle,$$

$$a_8^B = \langle B| \sum_{k=1}^{3} [\lambda_8 \mathcal{Q} \lambda_8]^{(k)} |B\rangle. \tag{C.30}$$

APPENDIX D

CALCULATION OF THE DIAGRAMS FOR

THE MAGNETIC FORM FACTOR

The diagrams contributing to the magnetic form factor are the same ones as for the case of the charge form factor and the meson-in-flight diagram in addition.

D.1 Leading Order Diagram (LO)

$$
\chi^\dagger_{B'_s} \frac{i\vec{\sigma}\times\vec{q}}{m_B+m'_B} \chi_{B_s} G^B_M(Q^2)\Big|_{LO}
$$

$$
= \quad {}^B\langle\phi_0|\mathcal{Q}\int \delta(t)d^4x e^{-\mathrm{i}qx}\vec{j}_\psi(x)|\phi_0\rangle^B
$$

$$
= \quad {}^B\langle\phi_0|b_0^\dagger\mathcal{Q}\int d^3x e^{\mathrm{i}\vec{q}\cdot\vec{x}}u_0^\dagger(x)\gamma^0\vec{\gamma}u_0(x)b_0|\phi_0\rangle^B
$$

$$
= \quad 2\frac{\partial}{\partial q}\int d^3x e^{\mathrm{i}\vec{q}\cdot\vec{x}}\frac{g(r)f(r)}{r}\,{}^B\langle\phi_0|b_0^\dagger\chi^\dagger_{c'}\chi^\dagger_{f'}\chi^\dagger_{s'}\mathcal{Q}(\vec{\sigma}\times\hat{q})\chi_s\chi_f\chi_c b_0|\phi_0\rangle^B \quad \text{(D.1)}
$$

here we restrict initial and final spin states to be in the same states, and define $\hat{q}=\hat{j}$, $\vec{\sigma}\times\hat{q}=-\sigma_3\hat{i}+\sigma_1\hat{k}$, we have

$$
\chi^\dagger_{c'}\chi^\dagger_{f'}\chi^\dagger_{s'}\mathcal{Q}(\vec{\sigma}\times\hat{q})\chi_s\chi_f\chi_c = -\chi^\dagger_{c'}\chi^\dagger_{f'}\chi^\dagger_{s'}\mathcal{Q}\sigma_3\chi_s\chi_f\chi_c\hat{i} \quad \text{(D.2)}
$$

and

$$
\chi^\dagger_{B'_s}\frac{i\vec{\sigma}\times\vec{q}}{m_B+m'_B}\chi_{B_s} = -\frac{Q}{2m_B}\chi^\dagger_{B'_s}\sigma_3\chi_{B_s}\hat{i}. \quad \text{(D.3)}
$$

Finally, the leading order of magnetic form factor can be obtained as

$$
G^B_M(Q^2)\Big|_{LO} = b_1^B\frac{m_B}{m_N}G^p_M(Q^2)\Big|_{LO}, \quad \text{(D.4)}
$$

where

$$G_M^p(Q^2)\big|_{LO} = \frac{4\pi i m_N}{Q} \int_0^\infty dr \int_0^\pi d\theta r^2 \sin(2\theta) g(r) f(r) e^{iQr\cos\theta}, \quad \text{(D.5)}$$

$$b_1^B = {}^B\langle\phi_0|b_0^\dagger \chi_{c'}^\dagger \chi_{f'}^\dagger \chi_{s'}^\dagger \mathcal{Q}\sigma_3 \chi_s \chi_f \chi_c|\phi_0\rangle^B$$

$$= \langle B\uparrow|\sum_{k=1}^3 [\mathcal{Q}\sigma_3]^{(k)}|B\uparrow\rangle. \quad \text{(D.6)}$$

D.2 Counterterm Diagram (CT)

$$\chi_{B_s'}^\dagger \frac{i\vec{\sigma}\times\vec{q}}{m_B+m_B'}\chi_{B_s} G_E^B(Q^2)\big|_{CT}$$

$$= {}^B\langle\phi_0|\mathcal{Q}\int \delta(t) d^4x e^{-iqx} \delta\vec{j}_\psi(x)|\phi_0\rangle^B$$

$$= {}^B\langle\phi_0|b_0^\dagger \mathcal{Q}\int d^3x e^{i\vec{q}\cdot\vec{x}} u_0^\dagger(x)(Z-1)\gamma^0\vec{\gamma}u_0(x)b_0|\phi_0\rangle^B, \quad \text{(D.7)}$$

then

$$G_E^B(Q^2)\big|_{CT} = \left[b_2^B(\hat{Z}-1)+b_3^B(Z_s-1)\right]\frac{m_B}{m_N}G_M^p(Q^2)\big|_{LO}, \quad \text{(D.8)}$$

where

$$b_2^B = {}^B\langle\phi_0|b_0^\dagger \chi_{c'}^\dagger \chi_{f'}^\dagger \chi_{s'}^\dagger \sum_{k=1}^3 [\hat{\mathcal{Q}}\sigma_3]^{(k)}\chi_s \chi_f \chi_c b_0|\phi_0\rangle^B$$

$$= \langle B\uparrow|\sum_{k=1}^3 [\hat{\mathcal{Q}}\sigma_3]^{(k)}|B\uparrow\rangle, \quad \text{(D.9)}$$

$$b_3^B = \langle B\uparrow|\sum_{k=1}^3 [\mathcal{Q}_s\sigma_3]^{(k)}|B\uparrow\rangle. \quad \text{(D.10)}$$

D.3 Meson Cloud Diagram (MC)

$G_M^B(Q^2)\big|_{MC}^\alpha$

$$= {}^B\langle\phi_0|\frac{\mathrm{i}^2}{2!}\int \delta(t)d^4x d^4x_1 d^4x_2 e^{-\mathrm{i}qx} T\big[\mathcal{L}_I^W(x_1)\mathcal{L}_I^W(x_2)\vec{j}_\Phi(x)\big]|\phi_0\rangle^B$$

$$= 4\,{}^B\langle\phi_0|\frac{-1}{2}\int \delta(t)d^4x d^4x_1 d^4x_2 e^{-\mathrm{i}qx}$$

$$\times N\Big\{\Big[\frac{1}{2F}\partial_\mu\Phi_i\bar{\psi}\gamma^\mu\gamma^5\lambda_i\psi\Big]_{x_1}\Big[(f_{3kl}+\frac{f_{8kl}}{\sqrt{3}})\Phi_k(-\vec{\nabla}\Phi_l)\Big]_x\Big[\frac{1}{2F}\partial_\nu\Phi_j\bar{\psi}\gamma^\nu\gamma^5\lambda_j\psi\Big]_{x_2}\Big\}$$

$$\times|\phi_0\rangle^B$$

$$= \frac{-i}{2F^2(2\pi)^8}\,{}^B\langle\phi_0|b_0^\dagger\int d^3x_1 d^3x_2 d^4k_1 d^4k_2 \frac{e^{-i\vec{k}_1\cdot\vec{x}_1}}{M_\Phi^2-k_1^2-i\epsilon}\frac{e^{-i\vec{k}_2\cdot\vec{x}_2}}{M_\Phi^2-k_2^2-i\epsilon}$$

$$\times(f_{3kl}+\frac{f_{8kl}}{\sqrt{3}})\bar{u}_0(x_1)\gamma^\mu k_{1\mu}\gamma^5\lambda_i u_\alpha(x_1)\bar{u}_\alpha(x_2)\gamma^\nu k_{2\nu}\gamma^5\vec{k}_2\lambda_j u_0(x_2)$$

$$\times\int dt\, dt_1\, dt_2\,\delta t\,\Theta(t_1-t_2)e^{-iq_0 t}e^{-i\varepsilon_0(t_2-t_1)}e^{-i\varepsilon_\alpha(t_1-t_2)}e^{-ik_1^0(t_1-t)}e^{-ik_2^0(t-t_2)}$$

$$\times\int d^3x\, e^{-i(\vec{k}_1-\vec{k}_2-\vec{q})\cdot\vec{x}}b_0|\phi_0\rangle^B$$

$$= -\frac{(f_{3ij}+\frac{f_{8ij}}{\sqrt{3}})}{2F^2(2\pi)^4}\,{}^B\langle\phi_0|b_0^\dagger\int d^3x_1 d^3x_2 d^3k_1 d^3k_2\vec{k}_2\delta(\vec{k}_1-\vec{k}_2-\vec{q})$$

$$\times\int dk_1^0 dk_2^0 \frac{\delta(k_1^0-k_2^0)}{[\omega_\Phi(k_1^2)-(k_1^0)^2-i\epsilon][\omega_\Phi(k_2^2)-(k_2^0)^2-i\epsilon][\Delta\varepsilon_\alpha+k_1^0-i\eta]}$$

$$\times\Big[(k_2^0)^2\bar{u}_0(x_1)\gamma^0\gamma^5\lambda_i u_\alpha(x_1)\bar{u}_\alpha(x_2)\gamma^0\gamma^5\lambda_j u_0(x_2)$$

$$-k_2^0\bar{u}_0(x_1)\gamma^0\gamma^5\lambda_i u_\alpha(x_1)\bar{u}_\alpha(x_2)\vec{\gamma}\cdot\vec{k}_2\gamma^5\lambda_j u_0(x_2)$$

$$-k_2^0\bar{u}_0(x_1)\vec{\gamma}\cdot\vec{k}_1\gamma^5\lambda_i u_\alpha(x_1)\bar{u}_\alpha(x_2)\gamma^0\gamma^5\lambda_j u_0(x_2)$$

$$+\bar{u}_0(x_1)\vec{\gamma}\cdot\vec{k}_1\gamma^5\lambda_i u_\alpha(x_1)\bar{u}_\alpha(x_2)\vec{\gamma}\cdot\vec{k}_2\gamma^5\lambda_j u_0(x_2)\Big]b_0|\phi_0\rangle^B$$

$$
= \frac{i}{4F^2(2\pi)^3} \, {}^B\langle\phi_0|b_0^\dagger \int d^3k_2 \vec{k}_2 \frac{f_{3ij} + \frac{f_{8ij}}{\sqrt{3}}}{\omega_\Phi(k_2'^2)\omega_\Phi(k_2^2)[\omega_\Phi(k_2'^2) + \Delta\varepsilon_\alpha][\omega_\Phi(k_2^2) + \Delta\varepsilon_\alpha]}
$$

$$
\times \Bigg\{ -\frac{\Delta\varepsilon_\alpha \omega_\Phi(k_2^2)\omega_\Phi(k_2'^2)}{\omega_\Phi(k_2'^2) + \omega_\Phi(k_2^2)} \int d^3x_1 \bar{u}_0(x_1)\gamma^0\gamma^5\lambda_i u_\alpha(x_1) e^{i\vec{k}_2'\cdot\vec{x}_1}
$$

$$
\times \int d^3x_2 \bar{u}_\alpha(x_2)\gamma^0\gamma^5\lambda_j u_0(x_2) e^{-i\vec{k}_2\cdot\vec{x}_2} - \frac{\omega_\Phi(k_2'^2)\omega_\Phi(k_2^2)}{\omega_\Phi(k_2'^2) + \omega_\Phi(k_2^2)}
$$

$$
\times \int d^3x_1 \bar{u}_0(x_1)\gamma^0\gamma^5\lambda_i u_\alpha(x_1) e^{i\vec{k}_2'\cdot\vec{x}_1} \int d^3x_2 \bar{u}_\alpha(x_2)\vec{\gamma}\cdot\vec{k}_2\gamma^5\lambda_j u_0(x_2) e^{-i\vec{k}_2\cdot\vec{x}_2}
$$

$$
- \frac{\omega_\Phi(k_2'^2)\omega_\Phi(k_2^2)}{\omega_\Phi(k_2'^2) + \omega_\Phi(k_2^2)} \int d^3x_1 \bar{u}_0(x_1)\vec{\gamma}\cdot\vec{k}_2'\gamma^5\lambda_i u_\alpha(x_1) e^{i\vec{k}_2'\cdot\vec{x}_1}
$$

$$
\times \int d^3x_2 \bar{u}_\alpha(x_2)\gamma^0\gamma^5\lambda_j u_0(x_2) e^{-i\vec{k}_2\cdot\vec{x}_2} + \frac{\omega_\Phi(k_2'^2) + \omega_\Phi(k_2^2) + \Delta\varepsilon_\alpha}{\omega_\Phi(k_2'^2) + \omega_\Phi(k_2^2)}
$$

$$
\times \int d^3x_1 \bar{u}_0(x_1)\vec{\gamma}\cdot\vec{k}_2'\gamma^5\lambda_i u_\alpha(x_1) e^{i\vec{k}_2'\cdot\vec{x}_1} \int d^3x_2 \bar{u}_\alpha(x_2)\vec{\gamma}\cdot\vec{k}_2\gamma^5\lambda_j u_0(x_2) e^{-i\vec{k}_2\cdot\vec{x}_2} \Bigg\}
$$

$$
\times b_0|\phi_0\rangle^B
$$

$$
= \frac{i}{4F^2(2\pi)^3} \, {}^B\langle\phi_0|b_0^\dagger \chi_c^\dagger \chi_f^\dagger \chi_s^\dagger \int d^3k_2 \vec{k}_2
$$

$$
\times \frac{1}{\omega_\Phi(k_2'^2)\omega_\Phi(k_2^2)[\omega_\Phi(k_2'^2) + \Delta\varepsilon_\alpha][\omega_\Phi(k_2^2) + \Delta\varepsilon_\alpha]}
$$

$$
\times \Bigg\{ -\frac{\Delta\varepsilon_\alpha \omega_\Phi(k_2^2)\omega_\Phi(k_2'^2)}{\omega_\Phi(k_2'^2) + \omega_\Phi(k_2^2)} F_{I\alpha}(k_2') F_{I\alpha}^\dagger(k_2)
$$

$$
+ \frac{\omega_\Phi(k_2'^2)\omega_\Phi(k_2^2)}{\omega_\Phi(k_2'^2) + \omega_\Phi(k_2^2)} F_{I\alpha}(k_2') F_{II\alpha}^\dagger(k_2) + \frac{\omega_\Phi(k_2'^2)\omega_\Phi(k_2^2)}{\omega_\Phi(k_2'^2) + \omega_\Phi(k_2^2)} F_{II\alpha}(k_2') F_{I\alpha}^\dagger(k_2)
$$

$$
+ \frac{\omega_\Phi(k_2'^2) + \omega_\Phi(k_2^2) + \Delta\varepsilon_\alpha}{\omega_\Phi(k_2'^2) + \omega_\Phi(k_2^2)} F_{II\alpha}(k_2') F_{II\alpha}^\dagger(k_2) \Bigg\}
$$

$$
\times (f_{3ij} + \frac{f_{8ij}}{\sqrt{3}})[(\vec{\sigma}\cdot\vec{k}_2')\lambda_i]_{0,\alpha}[(\vec{\sigma}\cdot\vec{k}_2)\lambda_j]_{\alpha,0}\chi_s\chi_f\chi_c b_0|\phi_0\rangle^B
$$

$$
= -\frac{5i}{12(2\pi F)^2} \int_0^\infty dk \int_{-1}^1 dx\, k^4(1-x^2)
$$

$$\times \left\{ -\frac{\Delta\varepsilon_\alpha \omega_\Phi(k_2^2)\omega_\Phi(k_2'^2)}{\omega_\Phi(k_2'^2)+\omega_\Phi(k_2^2)} F_{I\alpha}(k_2') F_{I\alpha}^\dagger(k_2) \right.$$

$$+\frac{\omega_\Phi(k_2'^2)\omega_\Phi(k_2^2)}{\omega_\Phi(k_2'^2)+\omega_\Phi(k_2^2)} F_{I\alpha}(k_2') F_{II\alpha}^\dagger(k_2) + \frac{\omega_\Phi(k_2'^2)\omega_\Phi(k_2^2)}{\omega_\Phi(k_2'^2)+\omega_\Phi(k_2^2)} F_{II\alpha}(k_2') F_{I\alpha}^\dagger(k_2)$$

$$\left. +\frac{\omega_\Phi(k_2'^2)+\omega_\Phi(k_2^2)+\Delta\varepsilon_\alpha}{\omega_\Phi(k_2'^2)+\omega_\Phi(k_2^2)} F_{II\alpha}(k_2') F_{II\alpha}^\dagger(k_2) \right\}$$

$$\times \frac{{}^B\langle\phi_0|b_0^\dagger\chi_c^\dagger\chi_f^\dagger\chi_s^\dagger \frac{-3i}{10}(f_{3ij}+\frac{f_{8ij}}{\sqrt{3}})\lambda_i\lambda_j\sigma_3\chi_s\chi_f\chi_c b_0|\phi_0\rangle^B}{\omega_\Phi(k_+^2)\omega_\Phi(k^2)[\omega_\Phi(k_+^2)+\Delta\varepsilon_\alpha][\omega_\Phi(k^2)+\Delta\varepsilon_\alpha]}, \tag{D.11}$$

When the quark propagator is restricted on the ground state, we obtain

$$G_M^B(Q^2)\big|_{MC} = \frac{5}{6(2\pi F)^2}\int_0^\infty dk \int_{-1}^1 dx\, k^4(1-x^2)$$

$$\times F_{II}(k)F_{II}(k_+)[b_4^B D_\pi(k^2,Q^2,x)+b_5^B D_K(k^2,Q^2,x)], \tag{D.12}$$

where

$$D_\Phi(k^2,Q^2,x) = \frac{1}{\omega_\Phi^2(k_+^2)\omega_\Phi^2(k^2)}, \tag{D.13}$$

$$b_4^B = \sum_{i,j=1}^3 {}^B\langle\phi_0|b_0^\dagger\chi_{f'}^\dagger\chi_{s'}^\dagger -\frac{3i}{10}(f_{3ij}+\frac{f_{8ij}}{\sqrt{3}})\lambda_i\lambda_j\sigma_3\chi_s\chi_f b_0|\phi_0\rangle^B$$

$$= \sum_{i,j=1}^3 \langle B\uparrow|\sum_{k=1}^3 [-\frac{3i}{10}(f_{3ij}+\frac{f_{8ij}}{\sqrt{3}})\lambda_i\lambda_j\sigma_3]^{(k)}|B\uparrow\rangle, \tag{D.14}$$

$$b_5^B = \sum_{i,j=4}^7 \langle B\uparrow|\sum_{k=1}^3 [-\frac{3i}{10}(f_{3ij}+\frac{f_{8ij}}{\sqrt{3}})\lambda_i\lambda_j\sigma_3]^{(k)}|B\uparrow\rangle. \tag{D.15}$$

D.4 Vertex Correction Diagram (VC)

$$G_M^B(Q^2)\big|_{VC}^{\alpha\beta}$$

$$= {}^B\langle\phi_0|\frac{\mathrm{i}^2}{2!}\int \delta(t)d^4x\,d^4x_1\,d^4x_2\,e^{-\mathrm{i}qx}T\Big[\mathcal{L}_I^W(x_1)\mathcal{L}_I^W(x_2)\vec{j}_\psi(x)\Big]|\phi_0\rangle^B$$

$$= 2\,{}^B\langle\phi_0|\frac{-1}{2}\int \delta(t)d^4x\,d^4x_1\,d^4x_2\,e^{-\mathrm{i}qx}$$

$$\times N\left\{\Big[\frac{1}{2F}\partial_\mu\Phi_i\bar\psi\gamma^\mu\gamma^5\lambda_i\psi\Big]_{x_1}\Big[\bar\psi\vec\gamma\mathcal{Q}\psi\Big]_x\Big[\frac{1}{2F}\partial_\nu\Phi_j\bar\psi\gamma^\nu\gamma^5\lambda_j\psi\Big]_{x_2}\right\}|\phi_0\rangle^B$$

$$= \frac{i}{4F^2(2\pi)^4}\,{}^B\langle\phi_0|b_0^\dagger\int d^3x\,d^3x_1\,d^3x_2\,d^4k\,e^{i\vec q\cdot\vec x}\frac{e^{i\vec k\cdot(\vec x_1-\vec x_2)}}{M_\Phi^2-k^2-i\epsilon}$$

$$\times \bar u_0(x_1)\gamma^\mu k_\mu\gamma^5\lambda_i u_\alpha(x_1)\bar u_\alpha(x)\vec\gamma\mathcal{Q}u_\beta(x)\bar u_\beta(x_2)\gamma^\nu k_\nu\gamma^5\lambda_i u_0(x_2)$$

$$\times \int dt\,dt_1\,dt_2\,\delta t\,\Theta(t_1-t)\Theta(t-t_2)e^{-iqt}e^{-i\varepsilon_0(t_2-t_1)}e^{-i\varepsilon_\alpha(t_1-t)}$$

$$\times e^{-i\varepsilon_\beta(t-t_2)}e^{-ik_0(t_1-t_2)}b_0|\phi_0\rangle^B$$

$$= \frac{-i}{4F^2(2\pi)^4}\,{}^B\langle\phi_0|b_0^\dagger d^3x\,d^3x_1\,d^3x_2\,d^3k\,e^{i\vec q\cdot\vec x}e^{i\vec k\cdot(\vec x_1-\vec x_2)}$$

$$\times \int dk_0\frac{1}{[\omega_\Phi(k^2)-(k_0)^2-i\epsilon][k_0+\Delta\varepsilon_\alpha-i\eta][k_0+\Delta\varepsilon_\beta-i\eta]}$$

$$\times \bar u_0(x_1)(\gamma^0 k_0-\vec\gamma\cdot\vec k)\gamma^5\lambda_i u_\alpha(x_1)\bar u_\alpha(x)\vec\gamma\mathcal{Q}u_\beta(x)$$

$$\times \bar u_\beta(x_2)(\gamma^0 k_0-\vec\gamma\cdot\vec k)\gamma^5\lambda_i u_0(x_2)b_0|\phi_0\rangle^B$$

$$= \frac{G_M^p(Q^2)\big|_{LO}^\alpha}{8F^2(2\pi)^3}\,{}^B\langle\phi_0|b_0^\dagger\chi_c^\dagger\chi_f^\dagger\chi_s^\dagger\int d^3k\frac{1}{\omega_\Phi(k^2)[\omega_\Phi(k^2)+\Delta\varepsilon_\alpha]^2}$$

$$\times \Big[\omega_\Phi^2(k^2)F_{I\alpha}(k)F_{I\alpha}^\dagger(k)-\omega_\Phi(k^2)F_{I\alpha}(k)F_{II\alpha}^\dagger(k)-\omega_\Phi(k^2)F_{II\alpha}(k)F_{I\alpha}^\dagger(k)$$

$$+F_{II\alpha}(k)F_{II\alpha}^\dagger(k)\Big]\lambda_i\mathcal{Q}_{\alpha\alpha}\lambda_i(\vec\sigma\cdot\vec k)(\vec\sigma\times\vec k)(\vec\sigma\cdot\vec k)\chi_s\chi_f\chi_c b_0|\phi_0\rangle^B$$

$$= \frac{q\hat{i}}{4(2\pi F)^2} G_M^p(Q^2)\big|_{LO}^\alpha \int_0^\infty dk k^4 \Big[\omega_\Phi^2(k^2) F_{I\alpha}(k) F_{I\alpha}^\dagger(k) - \omega_\Phi(k^2) F_{I\alpha}(k) F_{II\alpha}^\dagger(k)$$

$$-\omega_\Phi(k^2) F_{II\alpha}(k) F_{I\alpha}^\dagger(k) + F_{II\alpha}(k) F_{II\alpha}^\dagger(k) \Big]$$

$$\times \frac{{}^B\langle \phi_0 | b_0^\dagger \chi_c^\dagger \chi_f^\dagger \chi_s^\dagger \lambda_i \mathcal{Q}_{\alpha\alpha} \lambda_i \sigma_3 \chi_s \chi_f \chi_c b_0 | \phi_0 \rangle^B}{\omega_\Phi(k^2)[\omega_\Phi(k^2) + \Delta\varepsilon_\alpha]^2}, \tag{D.16}$$

where

$$\int d^3 x \bar{u}_\alpha(x) \vec{\gamma} u_\beta(x) e^{i\vec{q}\cdot\vec{x}} = \delta_{\alpha\beta} G_E^p(Q^2)\big|_{LO}^\alpha. \tag{D.17}$$

For the case $\alpha = 0$, we obtain

$$G_M^B(Q^2)\big|_{VC} = \frac{1}{2(2\pi F)^2} G_M^p(Q^2)\big|_{LO} \int_0^\infty dk k^4 F_{II}^2(k^2)$$

$$\times \left[\frac{b_6^B}{\omega_\pi^3(k^2)} + \frac{b_7^B}{\omega_K^3(k^2)} + \frac{b_8^B}{\omega_\eta^3(k^2)} \right]. \tag{D.18}$$

where

$$a_6^B = {}^B\langle \phi_0 | b_0^\dagger \chi_c^\dagger \chi_f^\dagger \chi_s^\dagger \lambda_i \mathcal{Q} \lambda_i \sigma_3 \chi_s \chi_f \chi_c b_0 | \phi_0 \rangle^B$$

$$= \sum_{i=1}^3 \langle B\uparrow | \sum_{k=1}^3 [\lambda_i \mathcal{Q} \lambda_i \sigma_3]^{(k)} | B\uparrow \rangle,$$

$$a_7^B = \sum_{i=4}^7 \langle B\uparrow | \sum_{k=1}^3 [\lambda_i \mathcal{Q} \lambda_i \sigma_3]^{(k)} | B\uparrow \rangle,$$

$$a_8^B = \langle B\uparrow | \sum_{k=1}^3 [\lambda_8 \mathcal{Q} \lambda_8 \sigma_3]^{(k)} | B\uparrow \rangle. \tag{D.19}$$

D.5 Meson-in-Flight Diagram (MF)

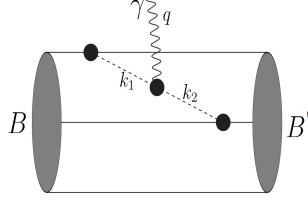**Figure D.1** Meson-in-Flight Diagram.

$G_E^B(Q^2)\big|_{MF}$

$$= {}^B\langle\phi_0|\frac{i^2}{2!}\int \delta(t)d^4x\,d^4x_1\,d^4x_2\,e^{-iqx}T\big[\mathcal{L}_I^W(x_1)\mathcal{L}_I^W(x_2)\vec{j}_\Phi(x)\big]|\phi_0\rangle^B$$

$$= 2\,{}^B\langle\phi_0|\frac{-1}{2}\int \delta(t)d^4x\,d^4x_1\,d^4x_2\,e^{-iqx}$$

$$\times N\Big\{\Big[\frac{1}{2F}\partial_\mu\overbrace{\Phi_i\bar\psi\gamma^\mu\gamma^5\lambda_i\psi}\Big]_{x_1}\Big[\overbrace{(f_{3kl}+\frac{f_{8kl}}{\sqrt{3}})\Phi_k}(-\vec\nabla\Phi_l)\Big]_x\Big[\frac{1}{2F}\partial_\nu\overbrace{\Phi_j\bar\psi\gamma^\nu\gamma^5\lambda_j\psi}\Big]_{x_2}\Big\}$$

$$\times|\phi_0\rangle^B$$

$$= \frac{-i}{4F^2(2\pi)^8}\,{}^B\langle\phi_0|b_0^{m\dagger}b_0^{n\dagger}\int d^3x_1\,d^3x_2\,d^4k_1\,d^4k_2\,\vec k_2\frac{e^{i\vec k_1\cdot\vec x_1}}{M_\Phi^2-k_1^2-i\epsilon}\frac{e^{-i\vec k_2\cdot\vec x_2}}{M_\Phi^2-k_2^2-i\epsilon}$$

$$\times(f_{3ij}+\frac{f_{8ij}}{\sqrt{3}})\bar u_0(x_1)\gamma^\mu k_{1\mu}\gamma^5\lambda_i u_0(x_1)\bar u_0(x_2)\gamma^\nu k_{2\nu}\gamma^5\lambda_j u_0(x_2)$$

$$\times\int dt\,dt_1\,dt_2\,\delta t\,e^{-iqt}e^{-ik_1^0(t_1-t)}e^{-ik_2^0(t-t_2)}\int d^3x\,e^{-i(-\vec k_1-\vec k_2-\vec q)\cdot\vec x}b_0^n b_0^m|\phi_0\rangle^B$$

$$= -\frac{(f_{3ij}+\frac{f_{8ij}}{\sqrt{3}})}{2F^2(2\pi)^4}\,{}^B\langle\phi_0|b_0^{m\dagger}b_0^{n\dagger}\int d^3x_1\,d^3x_2\,d^3k_1\,d^3k_2\,\vec k_2\,\delta(\vec k_1-\vec k_2-\vec q)$$

$$\times\int dk_2^0\frac{1}{[\omega_\Phi(k_1^2)-(k_1^0)^2-i\epsilon][\omega_\Phi(k_2^2)-(k_2^0)^2-i\epsilon][k_1^0-i\epsilon]}$$

$$\times\Big[(k_2^0)^2\bar u_0(x_1)\gamma^0\gamma^5\lambda_i u_0(x_1)\bar u_0(x_2)\gamma^0\gamma^5\lambda_j u_0(x_2)$$

$$-k_2^0\bar u_0(x_1)\gamma^0\gamma^5\lambda_i u_0(x_1)\bar u_0(x_2)\vec\gamma\cdot\vec k_2\gamma^5\lambda_j u_0(x_2)$$

$$-k_2^0 \bar{u}_0(x_1)\vec{\gamma} \cdot \vec{k}_1 \gamma^5 \lambda_i u_0(x_1) \bar{u}_0(x_2) \gamma^0 \gamma^5 \lambda_j u_0(x_2)$$

$$+\bar{u}_0(x_1)\vec{\gamma} \cdot \vec{k}_1 \gamma^5 \lambda_i u_0(x_1) \bar{u}_0(x_2)\vec{\gamma} \cdot \vec{k}_2 \gamma^5 \lambda_j u_0(x_2)\Big] b_0^n b_0^m |\phi_0\rangle^B$$

$$= -\frac{i}{4F^2(2\pi)^3}{}^B\langle\phi_0| b_0^{m\dagger} b_0^{n\dagger} \chi_c^{m\dagger} \chi_c^{n\dagger} \chi_f^{m\dagger} \chi_f^{n\dagger} \chi_s^{m\dagger} \chi_s^{n\dagger} \int d^3k_2 \vec{k}_2 F_{II}(k_2') F_{II}(k_2)$$

$$\times \frac{(f_{3ij} + \frac{f_{8ij}}{\sqrt{3}})[(\vec{\sigma} \cdot \vec{k}_2')\lambda_i][(\vec{\sigma} \cdot \vec{k}_2)\lambda_j]}{\omega_\Phi^2(k_2'^2)\omega_\Phi^2(k_2^2)} \chi_s^n \chi_s^m \chi_f^n \chi_f^m \chi_c^n \chi_c^m b_0^n b_0^m |\phi_0\rangle^B$$

$$= \frac{-iq}{2(2\pi F)^2} \int_0^\infty dk \int_{-1}^1 dx k^4 (1-x^2) F_{II}(k_2') F_{II}(k_2)$$

$$\times {}^B\langle\phi_0| b_0^{m\dagger} b_0^{n\dagger} \chi_c^{m\dagger} \chi_c^{n\dagger} \chi_f^{m\dagger} \chi_f^{n\dagger} \chi_s^{m\dagger} \chi_s^{n\dagger} \frac{1}{4}(f_{3ij} + \frac{f_{8ij}}{\sqrt{3}})$$

$$\times \frac{[\lambda_i \sigma_1]^{(k)} [\lambda_j \sigma_2]^{(l)}}{\omega_\Phi^2(k_2'^2)\omega_\Phi^2(k_2^2)} \chi_s^n \chi_s^m \chi_f^n \chi_f^m \chi_c^n \chi_c^m b_0^n b_0^m |\phi_0\rangle^B, \tag{D.20}$$

Finally, we have

$$G_M^B(Q^2)\big|_{MF} = \frac{m_B}{(2\pi F)^2} \int_0^\infty dk \int_{-1}^1 dx k^4 (1-x^2) F_{II}(k) F_{II}(k_+)$$

$$\times [b_9^B D_\pi(k^2, Q^2, x) + b_{10}^B D_K(k^2, Q^2, x)], \tag{D.21}$$

where

$$b_9^B = \sum_{i,j=1}^3 \langle B\uparrow | \sum_{\substack{k,l=1\\k\neq l}}^3 [\lambda_i \sigma_1]^{(k)} [\lambda_j \sigma_2]^{(l)} | B\uparrow\rangle, \tag{}$$

$$b_{10}^B = \sum_{i,j=4}^7 \langle B\uparrow | \sum_{\substack{k,l=1\\k\neq l}}^3 [\lambda_i \sigma_1]^{(k)} [\lambda_j \sigma_2]^{(l)} | B\uparrow\rangle. \tag{D.22}$$

APPENDIX E

CALCULATION OF THE DIAGRAMS FOR

THE AXIAL FORM FACTOR

In the PCQM, the axial form factor of the baryon octet is given by

$$
\chi_{B_{s'}}^{\dagger} \vec{\sigma}_B \frac{\tau_B^3}{2} \chi_{B_s} G_A^B(Q^2) = {}^B\langle\phi_0| \sum_{n=0}^{2} \frac{i^n}{n!} \int \delta(t) d^4x d^4x_1 \cdots d^4x_n \mathrm{e}^{-\mathrm{i}qx}
$$

$$
\times T[\mathcal{L}_I^W(x_1) \cdots \mathcal{L}_I^W(x_n) \vec{A}_3(x)]|\phi_0\rangle_c^B, \qquad (E.1)
$$

where χ_{B_s} and $\chi_{B_{s'}}^{\dagger}$ are the baryon spin wavefunctions in the initial and final states, $\vec{\sigma}$ is the spin matrix and τ_3 is the third component of the SU(2) isospin matrix. On the baryon level

$$
\chi_{B_{s'}}^{\dagger} \vec{\sigma}_B \frac{\tau_B^3}{2} \chi_{B_s} = \frac{1}{2}. \qquad (E.2)
$$

E.1   Leading Order Diagram (LO)
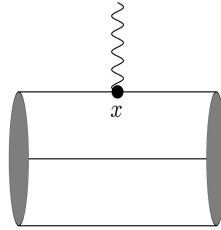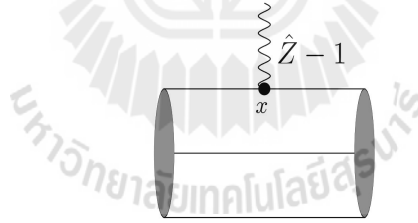

Figure E.1 Leading order Diagram.

$$
G_A^B(Q^2)\big|_{LO}
$$

$$
= 2 {}^B\langle\phi_0| \int \delta(x) d^4x e^{iqx} \bar{\psi}(x)\gamma^3\gamma^5 \frac{\lambda_3}{2} \psi(x)|\phi_0\rangle^B
$$

$$= {}^B\langle\phi_0|b_0^\dagger \int d^3x e^{i\vec{q}\cdot\vec{x}} u_0^\dagger(x)\gamma^0\gamma^3\gamma^5\lambda_3 u_0(x)b_0|\phi_0\rangle^B$$

$$= 2\pi \int_0^\infty dr \int_0^\pi d\theta r^2\sin\theta[g(r)^2 + f(r)^2\cos(2\theta)]e^{iQr\cos\theta}$$

$$\times {}^B\langle\phi_0|b_0^\dagger\chi_{c'}^\dagger\chi_{f'}^\dagger\chi_{s'}^\dagger(\sigma_3\lambda_3)\chi_s\chi_f\chi_c b_0|\phi_0\rangle^B$$

$$= c_1^B 2\pi \int_0^\infty dr \int_0^\pi d\theta r^2\sin\theta[g(r)^2 + f(r)^2\cos(2\theta)]e^{iQr\cos\theta} \tag{E.3}$$

where

$$c_1^B = \langle\phi_0|b_0^\dagger\chi_{c'}^\dagger\chi_{f'}^\dagger\chi_{s'}^\dagger(\sigma_3\lambda_3)\chi_s\chi_f\chi_c b_0|\phi_0\rangle^B$$

$$= {}^B\langle B\uparrow|\sum_{k=1}^3[\sigma_3\lambda_3]^{(k)}|B\uparrow\rangle. \tag{E.4}$$

E.2 Counterterm Diagram (CT)

Figure E.2 Counterterm Diagram.

$$G_A^B(Q^2)\big|_{CT}$$

$$= 2\,{}^B\langle\phi_0|\int \delta(x)d^4x e^{iqx}\bar{\psi}(x)(\hat{Z}-1)\gamma^3\gamma^5\frac{\lambda_3}{2}\psi(x)|\phi_0\rangle^B$$

$$= (\hat{Z}-1)G_A^B(Q^2)\big|_{LO}. \tag{E.5}$$
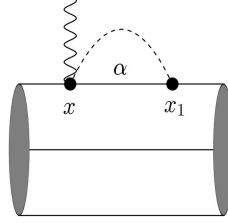
E.3 Self-Energy Diagram I (SE;I)

Figure E.3 Self-energy Diagram I.

$$G_A^B(Q^2)\big|_{SE;I}^{\alpha}$$

$$= 2\,{}^B\langle\phi_0|i\int\delta(t)d^4xd^4x_1e^{-iqx}$$

$$\times N\left\{\left[\frac{1}{2F}\partial_\mu\Phi_m\bar{\psi}\gamma^\mu\gamma^5\lambda_m\psi\right]_{x_1}\left[-\frac{f_{3ij}}{2F}\bar{\psi}\gamma^3\lambda_i\psi\Phi_j\right]_x\right\}|\phi_0\rangle^B$$

$$= \frac{2if_{3ij}}{4F^2(2\pi)^4}\,{}^B\langle\phi_0|b_0^\dagger\int d^3xd^3x_1d^4ke^{i\vec{q}\cdot\vec{x}}\frac{e^{i\vec{k}\cdot(\vec{x}_1-\vec{x})}}{M_\Phi^2-k^2-i\epsilon}$$

$$\times\bar{u}_0(x_1)\gamma^\mu k_\mu\gamma^5\lambda_j u_\alpha(x_1)\bar{u}_\alpha(x)\gamma^3\lambda_i u_0(x)$$

$$\times\int dtdt_1\delta t\Theta(t_1-t)e^{-iq_0t}e^{-i\varepsilon_0(t-t_1)}e^{-i\varepsilon_\alpha(t_1-t)}e^{-ik^0(t_1-t)}b_0|\phi_0\rangle^B$$

$$= \frac{f_{3ij}}{2F^2(2\pi)^4}\,{}^B\langle\phi_0|b_0^\dagger\int d^3xd^3x_1d^3ke^{i\vec{q}\cdot\vec{x}}e^{i\vec{k}\cdot(\vec{x}_1-\vec{x})}$$

$$\times\int dk_0\frac{1}{[\omega_\Phi(k^2)-k_0^2+i\epsilon][\Delta\varepsilon_\alpha+k_0-i\eta]}$$

$$\times\bar{u}_0(x_1)(\gamma^0k_0-\vec{\gamma}\cdot\vec{k})\gamma^5\lambda_j u_\alpha(x_1)\bar{u}_\alpha(x)\gamma^3\lambda_i u_0(x)b_0|\phi_0\rangle^B$$

$$= \frac{i}{4F^2(2\pi)^3}\,{}^B\langle\phi_0|b_0^\dagger\chi_c^\dagger\chi_f^\dagger\chi_s^\dagger\int d^3k\frac{f_{3ij}}{\omega_\Phi(k^2)[\omega_\Phi(k^2)+\Delta\varepsilon_\alpha]}$$

$$\times\left[\omega_\Phi(k^2)F_{I\alpha}(k)-F_{II\alpha}(k)\right][(\vec{\sigma}\cdot\vec{k})\lambda_j]_{0,\alpha}\left\{\frac{F_{III\alpha}(|\vec{q}-\vec{k}|)}{|\vec{q}-\vec{k}|}[\epsilon_{3mn}k_m\sigma_n\lambda_i]_{\alpha,0}\right.$$

$$+ \frac{F_{IV\alpha}(|\vec{q} - \vec{k}|)}{|\vec{q} - \vec{k}|}[\sqrt{Q^2} - k_3 + i\epsilon_{3mn}\sigma_m k_n \lambda_i]_{\alpha,0}\bigg\}\chi_s\chi_f\chi_c b_0|\phi_0\rangle^B, \qquad (E.6)$$

where

$$\int d^3x\, \bar{u}_\alpha(x)\gamma^3\lambda_i u_0(x)e^{i(\vec{q}-\vec{k})\cdot\vec{x}} = \frac{F_{III\alpha}(|\vec{q} - \vec{k}|)}{|\vec{q} - \vec{k}|}[\epsilon_{3mn}k_m\sigma_n\lambda_i]_{\alpha,0}$$

$$+ \frac{F_{IV\alpha}(|\vec{q} - \vec{k}|)}{|\vec{q} - \vec{k}|}[\sqrt{Q^2} - k_3 + i\epsilon_{3mn}\sigma_m k_n \lambda_i]_{\alpha,0},$$

$$(E.7)$$

with

$$F_{III\alpha}(k) = -2i\frac{\partial}{\partial k}\int_0^\infty dr\, r g_0(r)f_\alpha(r)\int_\Omega d\Omega \mathcal{C}_\alpha Y_{l_\alpha 0}(\theta,\phi)e^{ikx\cos\theta}, \qquad (E.8)$$

$$F_{IV\alpha}(k) = \frac{\partial}{\partial k}\int_0^\infty dr\, r[g_\alpha(r)f_0(r) - g_0(r)f_\alpha(r)]\int_\Omega d\Omega \mathcal{C}_\alpha Y_{l_\alpha 0}(\theta,\phi)e^{ikx\cos\theta}.$$

$$(E.9)$$

Finally, we get

$$G_A^B(Q^2)\Big|_{SE;I}^\alpha$$

$$= \frac{1}{2(2\pi F)^2}\int_0^\infty dk\, k^3\frac{\omega_\Phi(k^2)F_{I\alpha}(k) - F_{II\alpha}(k)}{\omega_\Phi(k^2)[\omega_\Phi(k^2) + \Delta\varepsilon_\alpha]}$$

$$\times \int_{-1}^1 dx\bigg\{\frac{ik(1-x^2)F_{III\alpha}(k_-)}{\sqrt{k_-^2}} + \frac{F_{IV\alpha}(k_-)}{\sqrt{k_-^2}}[\sqrt{Q^2}x + k(1-2x^2)]\bigg\}$$

$$\times {}^B\langle\phi_0|b_0^\dagger\chi_c^\dagger\chi_f^\dagger\chi_s^\dagger\frac{i}{2}f_{3ij}\lambda_j\lambda_i\sigma_3\chi_s\chi_f\chi_c b_0|\phi_0\rangle^B \qquad (E.10)$$

For $\alpha = 0$

$$F_{III}(k) = -2i\pi\int_0^\infty dr\int_0^\pi d\theta\, r^2 g(r)f(r)\sin 2\theta\, e^{ikr\cos\theta}, \qquad (E.11)$$

$$F_{IV}(k) = 0. \qquad (E.12)$$

Hence

$$G_A^B(Q^2)|_{SE;I} = \frac{1}{(2\pi F)^2} \int_0^\infty dk \int_{-1}^1 dx k^4 (1-x^2) F_{II}(k^2) F_{III}(k_-^2)$$

$$\times \frac{1}{\sqrt{k_-^2}} \left[\frac{c_1^B}{\omega_\pi^2(k^2)} + \frac{c_2^B}{\omega_K^2(k^2)} \right], \tag{E.13}$$

where

$$c_1^B = \sum_{i,j=1}^3 {}^B\langle \phi_0 | b_0^\dagger \chi_c^\dagger \chi_f^\dagger \chi_s^\dagger \frac{i}{2} f_{3ij} \lambda_j \lambda_i \sigma_3 \chi_s \chi_f \chi_c b_0 | \phi_0 \rangle^B$$

$$= \langle B\uparrow | \sum_{k=1}^3 [\sigma_3 \lambda_3]^{(k)} | B\uparrow \rangle, \tag{E.14}$$

$$c_2^B = \sum_{i,j=4}^7 \langle B\uparrow | \sum_{k=1}^3 [\frac{i}{2} f_{3ij} \lambda_j \lambda_i \sigma_3]^{(k)} | B\uparrow \rangle. \tag{E.15}$$
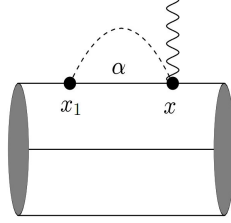
E.4   Self-Energy Diagram II (SE;II)

Figure E.4 Self-energy Diagram II.

$$
G_A^B(Q^2)\Big|_{SE;II}^{\alpha}
$$

$$
= \; 2\,{}^B\langle\phi_0|i\int\delta(t)d^4x\,d^4x_1 e^{-iqx}
$$

$$
\times N\bigg\{\bigg[-\frac{f_{3ij}}{2F}\bar{\psi}\gamma^3\lambda_i\psi\,\overline{\Phi_j}\bigg]_x\bigg[\frac{1}{2F}\partial_\mu\Phi_m\bar{\psi}\gamma^\mu\gamma^5\lambda_m\psi\bigg]_{x_1}\bigg\}|\phi_0\rangle^B
$$

$$
= \; \frac{2if_{3ij}}{4F^2(2\pi)^4}\,{}^B\langle\phi_0|b_0^\dagger\int d^3x\,d^3x_1 d^4k\,e^{i\vec{q}\cdot\vec{x}}\frac{e^{i\vec{k}\cdot(\vec{x}_1-\vec{x})}}{M_\Phi^2-k^2-i\epsilon}
$$

$$
\times\bar{u}_0(x)\gamma^\mu k_\mu\gamma^5\lambda_j u_\alpha(x)\bar{u}_\alpha(x_1)\gamma^3\lambda_i u_0(x_1)
$$

$$
\times\int dt\,dt_1\delta t\,\Theta(t-t_1)e^{-iq_0 t}e^{-i\varepsilon_0(t_1-t)}e^{-i\varepsilon_\alpha(t-t_1)}e^{-ik_0(t-t_1)}b_0|\phi_0\rangle^B
$$

$$
= \; \frac{f_{3ij}}{2F^2(2\pi)^4}\,{}^B\langle\phi_0|b_0^\dagger\int d^3x\,d^3x_1 d^3k\,e^{i\vec{q}\cdot\vec{x}}e^{i\vec{k}\cdot(\vec{x}-\vec{x}_1)}
$$

$$
\times\int dk_0\frac{1}{[\omega_\Phi(k^2)-k_0^2-i\epsilon][\Delta\varepsilon_\alpha+k_0-i\eta]}
$$

$$
\times\bar{u}_0(x)(\gamma^0 k_0-\vec{\gamma}\cdot\vec{k})\gamma^5\lambda_j u_\alpha(x)\bar{u}_\alpha(x_1)\gamma^3\lambda_i u_0(x_1)b_0|\phi_0\rangle^B
$$

$$
= \; \frac{i}{4F^2(2\pi)^3}\,{}^B\langle\phi_0|b_0^\dagger\chi_c^\dagger\chi_f^\dagger\chi_s^\dagger\int d^3k\frac{f_{3ij}}{\omega_\Phi(k^2)[\omega_\Phi(k^2)+\Delta\varepsilon_\alpha]}
$$

$$
\times\bigg\{\frac{F_{III\alpha}(|\vec{q}+\vec{k}|)}{|\vec{q}+\vec{k}|}[\epsilon_{3mn}k_m\sigma_n\lambda_i]_{0,\alpha}
$$

$$-\frac{F_{IV\alpha}(|\vec{q}+\vec{k}|)}{|\vec{q}+\vec{k}|}[\sqrt{Q^2}+k_3+i\epsilon_{3mn}\sigma_m k_n \lambda_i]_{0,\alpha}\Big\}$$

$$\times \Big[\omega_\Phi(k^2)F_{I\alpha}^\dagger(k)-F_{II\alpha}^\dagger(k)\Big][(\vec{\sigma}\cdot\vec{k})\lambda_j]_{\alpha,0}\chi_s\chi_f\chi_c b_0|\phi_0\rangle^B. \tag{E.16}$$

It is similar to $G_A^B(Q^2)\big|_{SE;I}^\alpha$, we can obtain

$G_A^B(Q^2)\big|_{SE;II}^\alpha$

$$= \frac{1}{2(2\pi F)^2}\int_0^\infty dk k^3 \frac{\omega_\Phi(k^2)F_{I\alpha}^\dagger(k)-F_{II\alpha}^\dagger(k)}{\omega_\Phi(k^2)[\omega_\Phi(k^2)+\Delta\varepsilon_\alpha]}$$

$$\times \int_{-1}^1 dx \Big\{\frac{ik(1-x^2)F_{V\alpha}(k_+)}{\sqrt{k_+^2}}+\frac{F_{IV\alpha}(k_+)}{\sqrt{k_+^2}}[\sqrt{Q^2}x+k)]\Big\}$$

$$\times {}^B\langle\phi_0|b_0^\dagger\chi_c^\dagger\chi_f^\dagger\chi_s^\dagger\frac{i}{2}f_{3ij}\lambda_j\lambda_i\sigma_3\chi_s\chi_f\chi_c b_0|\phi_0\rangle^B, \tag{E.17}$$

where

$$F_{V\alpha}(k)=-2i\frac{\partial}{\partial k}\int_0^\infty dr r g_\alpha(r)f_0(r)\int_\Omega d\Omega \mathcal{C}_\alpha Y_{l\alpha 0}(\theta,\phi)e^{ikx\cos\theta}. \tag{E.18}$$

When we restrict the quark propagator to the ground state,

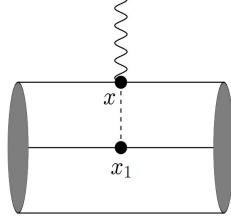$$G_A^B(Q^2)\big|_{SE;I}=G_A^B(Q^2)\big|_{SE;II}. \tag{E.19}$$

E.5 Exchange Diagram (EX)

Figure E.5 Exchange Diagram.

$$G_A^B(Q^2)\big|_{EX}$$

$$= 2\,^B\langle\phi_0|i\int\delta(t)d^4xd^4x_1e^{-iqx}$$

$$\times N\left\{\left[\frac{1}{2F}\partial_\mu\overbrace{\Phi_m\bar\psi\gamma^\mu\gamma^5\lambda_m\psi}\right]_{x_1}\left[-\frac{f_{3ij}}{2F}\bar\psi\gamma^3\lambda_i\psi\Phi_j\right]_x\right\}|\phi_0\rangle^B$$

$$= \frac{if_{3ij}}{2F^2(2\pi)^4}\,^B\langle\phi_0|b_0^\dagger(x_1)b_0^\dagger(x)\int d^3xd^3x_1d^4ke^{i\vec q\cdot\vec x}\frac{e^{i\vec k\cdot(\vec x_1-\vec x)}}{M_\Phi^2-k^2-i\epsilon}$$

$$\times\bar u_0(x_1)\gamma^\mu k_\mu\gamma^5\lambda_ju_0(x_1)\bar u_0(x)\gamma^3\lambda_iu_0(x)$$

$$\times\int dtdt_1\delta te^{-iq_0t}e^{-ik_0(t_1-t)}b_0(x)b_0(x_1)|\phi_0\rangle^B \tag{E.20}$$

Here, there is no quark propagator contribution to $G_A^B(Q^2)\big|_{EX}$, i.e., the ground state gives contribution only. Equation (E.20) is similar to Equation (E.6) when $\alpha = 0$.

$$G_A^B(Q^2)\big|_{EX} = \frac{1}{4(2\pi F)^2}\int_0^\infty dk\int_{-1}^1 dxk^4(1-x^2)F_{II}(k^2))F_{III}(k_-^2)$$

$$\times\frac{1}{\sqrt{k_-^2}}\left[\frac{c_3^B}{\omega_\pi^2(k^2)}+\frac{c_4^B}{\omega_K^2(k^2)}\right]. \tag{E.21}$$

where

$$c_3^B = \sum_{i,j,m,n=1}^{3} \langle B\uparrow | \sum_{\substack{k,l=1\\k\neq l}}^{3} f_{3ij}\epsilon_{3mn}[\sigma_m\lambda_j]^{(k)}[\sigma_n\lambda_i]^{(l)}|B\uparrow\rangle, \qquad \text{(E.22)}$$

$$c_4^B = \sum_{i,j,m,n=4}^{7} \langle B\uparrow | \sum_{\substack{k,l=1\\k\neq l}}^{3} f_{3ij}\epsilon_{3mn}[\sigma_m\lambda_j]^{(k)}[\sigma_n\lambda_i]^{(l)}|B\uparrow\rangle. \qquad \text{(E.23)}$$
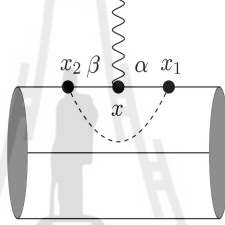
E.6 Vertex Correction Diagram (VC)

Figure E.6 Vertex Correction Diagram.

$$G_A^B(Q^2)\Big|_{VC}^{\alpha\beta}$$

$$= 4\,^B\langle\phi_0|\frac{-1}{2}\int\delta(t)d^4x d^4x_1 d^4x_2 e^{-iqx}$$

$$\times N\left\{\left[\frac{1}{2F}\partial_\mu\Phi_i\bar\psi\gamma^\mu\gamma^5\lambda_i\psi\right]_{x_1}\left[\bar\psi\gamma^3\gamma^5\frac{\lambda_3}{2}\psi\right]_x\left[\frac{1}{2F}\partial_\nu\Phi_j\bar\psi\gamma^\nu\gamma^5\lambda_j\psi\right]_{x_2}\right\}|\phi_0\rangle^B$$

$$= \frac{i}{8F^2(2\pi)^4}\,^B\langle\phi_0|b_0^\dagger\int d^3x d^3x_1 d^3x_2 d^4k e^{i\vec{q}\cdot\vec{x}}\frac{e^{i\vec{k}\cdot(\vec{x}_1-\vec{x}_2)}}{M_\Phi^2-k^2-i\epsilon}$$

$$\times\bar u_0(x_1)\gamma^\mu k_\mu\gamma^5\lambda_i u_\alpha(x_1)\bar u_\alpha(x)\gamma^3\gamma^5\lambda_3 u_\beta(x)\bar u_\beta(x_2)\gamma^\nu k_\nu\gamma^5\lambda_i u_0(x_2)$$

$$\times\int dt dt_1 dt_2\delta t\Theta(t_1-t)\Theta(t-t_2 e^{-iq_0 t}e^{-i\varepsilon_0(t_2-t_1)}e^{-i\varepsilon_\alpha(t_1-t)}$$

$$\times e^{-i\varepsilon_\beta(t-t_2)}e^{-ik_0(t_1-t_2)}b_0|\phi_0\rangle^B$$

$$= \frac{-i}{8F^2(2\pi)^4} {}^B\langle\phi_0|b_0^\dagger d^3x d^3x_1 d^3x_2 d^3k e^{i\vec{q}\cdot\vec{x}}e^{i\vec{k}\cdot(\vec{x}_1-\vec{x}_2)}$$

$$\times \int dk_0 \frac{1}{[\omega_\Phi(k^2)-(k_0)^2-i\epsilon][k_0+\Delta\varepsilon_\alpha-i\eta][k_0+\Delta\varepsilon_\beta-i\eta]}$$

$$\times\bar{u}_0(x_1)(\gamma^0 k_0-\vec{\gamma}\cdot\vec{k})\gamma^5\lambda_i u_\alpha(x_1)\bar{u}_\alpha(x)\gamma^3\gamma^5\lambda_3 u_\beta(x)$$

$$\times\bar{u}_\beta(x_2)(\gamma^0 k_0-\vec{\gamma}\cdot\vec{k})\gamma^5\lambda_i u_0(x_2)b_0|\phi_0\rangle^B$$

$$= -\frac{3G_A^N(Q^2)\big|_{LO}^\alpha}{40F^2(2\pi)^3} {}^B\langle\phi_0|b_0^\dagger\chi_c^\dagger\chi_f^\dagger\chi_s^\dagger \int d^3k \frac{1}{\omega_\Phi(k^2)[\omega_\Phi(k^2)+\Delta\varepsilon_\alpha]^2}$$

$$\times\Big[\omega_\Phi^2(k^2)F_{I\alpha}(k)F_{I\alpha}^\dagger(k) - \omega_\Phi(k^2)F_{I\alpha}(k)F_{II\alpha}^\dagger(k) - \omega_\Phi(k^2)F_{II\alpha}(k)F_{I\alpha}^\dagger(k)$$

$$+F_{II\alpha}(k)F_{II\alpha}^\dagger(k)\Big]\lambda_i\lambda_3\lambda_i \int_\Omega d\Omega(\vec{\sigma}\cdot\vec{k})\sigma_3(\vec{\sigma}\cdot\vec{k})\chi_s\chi_f\chi_c b_0|\phi_0\rangle^B, \quad\text{(E.24)}$$

where

$$\int d^3x \bar{u}_\alpha(x)\gamma^3\gamma^5\lambda_3 u_\beta(x)e^{i\vec{q}\cdot\vec{x}} = \frac{3}{5}\delta_{\alpha\beta}G_A^N(Q^2)\big|_{LO}^\alpha \chi_c^\dagger\chi_f^\dagger\chi_s^\dagger[\sigma_3\lambda_3]_{\alpha\beta}\chi_s\chi_f\chi_c. \quad\text{(E.25)}$$

Finally, we have
$$G_A^B(Q^2)\big|_{VC}^\alpha$$

$$= \frac{1}{20(2\pi F)^2}G_A^N(Q^2)\big|_{LO}^\alpha \int dk k^4\Big[\omega_\Phi^2(k^2)F_{I\alpha}(k)F_{I\alpha}^\dagger(k)$$

$$-\omega_\Phi(k^2)F_{I\alpha}(k)F_{II\alpha}^\dagger(k) - \omega_\Phi(k^2)F_{II\alpha}(k)F_{I\alpha}^\dagger(k) + F_{II\alpha}(k)F_{II\alpha}^\dagger(k)\Big]$$

$$\times\frac{{}^B\langle\phi_0|b_0^\dagger\chi_c^\dagger\chi_f^\dagger\chi_s^\dagger\lambda_i\lambda_3\lambda_i\sigma_3\chi_s\chi_f\chi_c b_0|\phi_0\rangle^B}{\omega_\Phi(k^2)[\omega_\Phi(k^2)+\Delta\varepsilon_\alpha]^2}. \quad\text{(E.26)}$$

For the ground state $\alpha=0$, we obtain

$$G_A^B(Q^2)|_{VC} = \frac{1}{20(2\pi F)}G_A^N(Q^2)|_{LO} \int_0^\infty dk k^4 F_{II}^2(k^2)$$

$$\times\left[\frac{c_1^B}{\omega_\pi^3(k^2)} + \frac{c_5^B}{\omega_\eta^3(k^2)}\right], \quad\text{(E.27)}$$

where

$$
\begin{aligned}
c_1^B &= {}^B\langle\phi_0|b_0^\dagger\chi_c^\dagger\chi_f^\dagger\chi_s^\dagger\lambda_i\lambda_3\lambda_i\sigma_3\chi_s\chi_f\chi_c b_0|\phi_0\rangle^B \\[2mm]
&= \sum_{i=1}^{3}\langle B\uparrow|\sum_{k=1}^{3}[\lambda_i\lambda_3\lambda_i\sigma_3]^{(k)}|B\uparrow\rangle \\[2mm]
&= \langle B\uparrow|\sum_{k=1}^{3}[\lambda_3\sigma_3]^{(k)}|B\uparrow\rangle,
\end{aligned}
\tag{E.28}
$$

$$
c_5^B = \langle B\uparrow|\sum_{k=1}^{3}[\lambda_8\lambda_3\lambda_8\sigma_3]^{(k)}|B\uparrow\rangle.
\tag{E.29}
$$

CURRICULUM VITAE

NAME: Xuyang Liu   **GENDER**: Male

NATIONALITY: Chinese   **DATE OF BIRTH**: March 04, 1982

EDUCATIONS:

- M. Sc. Department of Physics, Guizhou University, China, 2008.

- B. Sc. Department of Physics, Bohai University, China, 2005.

PUBLICATIONS

[1] X. Liu, G. Wei, X. Cao and H. Bai, **"Spin Symmetry for Dirac Equation with the Trigonometric Pöschl-Teller Potential"**, Int. J. Theor. Phys.(2010) 49:343-348.

[2] G. Wei, X. Duan and X. Liu, **"Algebraic Approach to Spin Symmetry for the Dirac Equation with the Trigonometric Scarf Potential"**, Int. J. Mod. Phys. A(2010) 25:1649-1659.

[3] X. Liu, G. Wei and C. Long, **"Arbitrary Wave Relativistic Bound State Solutions for the Eckart Potential"**, Int. J. Theor. Phys.(2009) 48:463-470.

[4] G. Wei, X. Liu and W. Chen, **"The Relativistic Scattering States of the Hulthén Potential with an Improved New Approximate Scheme to the Centrifugal Term"**, Int. J. Theor. Phys.(2009) 48:1649-1658.

[5] G. Wei and X. Liu, **"The relativistic bound states of the hyperbolical potential with the centrifugal term"**, Phys. Scr.(2008) 78:065009.